

# Exploring a simple sector of the Einstein-Maxwell landscape

César Asensio\* and Antonio Seguí†

*Departamento de Física Teórica, Universidad de Zaragoza*

September 21, 2018

## Abstract

We explore the four dimensional Einstein-Maxwell landscape as a toy model in which we can formulate a sphere compactification stabilized by an electromagnetic field. Replacing the compactification sphere by  $J$  spheres, we obtain a simple sector of the  $(2J + 2)$ -dimensional Einstein-Maxwell landscape. In this toy model, we analyze some properties which are very difficult to uncover in the string theory landscape, including: complete moduli stabilization, stability conditions, and state counting. We also show how to construct anthropic states in this model. A detailed comparison between the main features of this landscape and the Bousso-Polchinski landscape is given. We finally speculate on the impact of these phenomena in the string theory landscape.

## 1 Introduction

As a candidate of a theory-of-everything, string theory has led to many striking results. Among them we find the string theory landscape [1, 2], a very complicated structure of vacuum states of the theory which raises its own questions and problems. All models of this landscape are rich and complex, and the existence of this landscape is almost beyond doubt [3]. When deriving cosmological models in a landscape we are led to the notion of multiverse [4], a quantum ensemble of different classical cosmological models. The multiverse shows very appealing features, such as inflation, which is needed to remedy the difficulties of older cosmological models [5, 6, 7, 8, 9], and it is generally believed that the cosmological constant [10, 11] and the coincidence problems can be solved with realistic models of the multiverse [12, 13]. Nevertheless, the multiverse has its own problems, which will be described briefly.

---

\*casencha@unizar.es

†seguí@unizar.es

The huge amount of possible universes present in the landscape [14, 15, 16, 17] should be complemented with a probability distribution which can explain why we are living in this particular universe. The standard rule of assigning probabilities as proportional to  $e^{-S}$  for some euclidean action  $S$  breaks down in this context because the classical action of a cosmological model is divergent due to the infinite spacetime volume. To extract some useful information, the action should be regularized, but there are many different ways of regulating an infinite volume because no cut-off procedure is invariant under a coordinate change. Different regularization procedures can lead to different probability distributions predicting different universes. This is known as the measure problem [4, 18], which consists in giving an unambiguous definition of the relative probabilities in a given landscape model. So far, the measures derived from first principles need the AdS/CFT correspondence [19] and similar ideas as a key ingredient [20, 21], which has a stringy origin, and thus the whole picture is slowly evolving towards a unified formalism of the multiverse derived from string theory.

When a multiverse model is used to explain, for example, the smallness of the observed cosmological constant ( $\lambda_{\text{obs}} \approx 10^{-120}$  in Planck units) [22, 23], theory should bring a probability distribution of  $\lambda$  values. This probability distribution should take into account the number of states of the landscape, but also its relative probability computed using a measure as stated above. This measure is derived from a mechanism by which states are populated in the landscape, for example, by some form of Euclidean Quantum Gravity, with its own difficulties as commented in the previous paragraph, or by eternal inflation, which populates all states in the landscape in a stochastic fashion. When considering the distribution of  $\lambda$  values conditioned on those states which support some form of observers (like us) [24, 25, 2], one needs to add an anthropic factor to the probability which should be provided to complete the prediction. Therefore, there are three parts which contribute to the final probability: the distribution of the states in the landscape (also known as the *prior* part), the cosmological measure (which needs a mechanism for populating the landscape), and the anthropic factor (which incorporates the condition for the existence of observers, such as galaxy formation).

Another problem is the vast complexity of the landscape. Extracting a four-dimensional cosmology from string theory requires choosing a compactification of the remaining dimensions. Each possible choice of compactification describes a sector of the entire landscape, and the number and properties of the states in different sectors can be very different. This diversity can be explored by considering different sectors separately. Thus, simplified models of some sectors of the landscape have been built, and they constitute a very important tool to understand the full implications of the string theory landscape. The reader can consult [26, 27] for a review of several models of the string theory landscape. For our purposes only the simplest models are needed. Among these models we should mention:

- The Kachru-Kalosh-Linde-Trivedi (KKLT) mechanism [28, 29, 30] is a supersymmetric string model with many stabilized AdS vacua which are lifted to dS by quantum effects. This landscape model gives inflationary states represented by brane-antibrane pairs evolving in Klebanov-Strassler throats in the compactification manifold. The

model has no classical dS vacua, and thus its more controversial aspect is the quantum nature of the lifting from AdS to dS, which is uncontrollable by its very nature.

- The Bousso-Polchinski (BP) model [1] is a simplified vacuum sector of M theory compactified from eleven to four dimensions with quantized four-form fluxes and M5 branes wrapped around three-cycles in the seven-dimensional compactification manifold. The volumes of the three-cycles are the moduli of the model, and gives a fundamental charge  $q_i$  which determines the cosmological constant of the 3+1 cosmological part of the eleven-dimensional metric by the formula

$$\lambda = \Lambda + \frac{1}{2} \sum_{i=1}^J q_i^2 n_i^2. \quad (1)$$

Here, each  $n_i$  is the number of flux units stored in the  $i^{\text{th}}$  three-cycle, and  $\Lambda$  is a bare, negative cosmological constant, a parameter of the model. Equation (1) provides a very elegant mechanism to deal with the cosmological constant problem. By choosing a large number  $J$  of three-cycles, we can choose the integers  $n_i$  to approximately cancel the  $\Lambda$  contribution, thus obtaining a huge landscape of AdS and dS vacua containing states with very low values of the effective cosmological constant  $\lambda$ , also known as the *discretuum*. Calabi-Yau compactifications typically have a large amount of three-cycles, so that realistic values of the cosmological constant can be obtained without any fine-tuning of the model parameters.

On one hand, unlike the KKLT mechanism, the BP model does not rely on quantum effects for producing dS states. On the other hand, BP moduli are frozen from the very beginning, and thus no stabilization mechanism analogous to KKLT is included in the BP model.

While there are some extensions of the KKLT scenario where the structure of states in the landscape has been elucidated by means of numerical searches [31], a very appealing feature of the BP landscape is that the closed expression (1) leads to analytically tractable counting problems. Thus, relative probabilities of different states can be computed based on combinatorics, but this leads to the conclusion that the number of states with realistic  $\lambda$  values are a very sparse minority, thus opening the door to anthropic arguments [24, 25, 2].

If we combine the computation of probabilities by naive state counting with the lack of stability analysis, we find another curious property of the BP landscape. Under a large number of three-cycles  $J$ , flux space is a very high-dimensional space. Such spaces have very counterintuitive geometric features: for example, the opposite vertexes of a unit hypercube are separated by a distance  $\sqrt{J}$ , which can be interpreted (in Planck units) as a huge energy scale. Another consequence of this elongation of diagonal distances is that the vast majority of lattice nodes inside a sphere in flux space are located on hyperplanes, that is, they always have at least one vanishing component. In fact, we have seen that as  $J$  grows, the dimension of the most populated hyperplanes is distributed in a narrow Gaussian window around a typical value  $\alpha^* J$  with  $\alpha^* < 1$  [32]. But as the KKLT mechanism shows, flux quantum numbers cannot vanish in stable states. Of course, the lack of a stabilization mechanism in the BP model prevents us from directly excluding those states from the

model; if they were excluded, the states with very low  $\lambda$  values could even disappear. This “ $\alpha^*$ -problem” of the BP model is only present for large  $J$ , but a large  $J$  is certainly needed to solve the cosmological constant problem.

Thus, looking for a scenario where we can closely examine this  $\alpha^*$ -problem, we are led to consider a model with the following properties:

- It should be exactly solvable.
- It should have many moduli.
- It should have a stabilization mechanism.

The simplest landscape with the first and third requirements is the Einstein-Maxwell landscape, considered in a plethora of papers as a toy model landscape [33, 34, 35, 36]. This landscape has compactifications of the form (A)dS<sub>2</sub> × S<sup>4</sup> or (A)dS<sub>4</sub> × S<sup>2</sup> having a single modulus, namely, the radius of the compactification sphere. We have added many moduli by considering compactifications of the form

$$(A)dS_2 \times \prod_{i=1}^J S^2, \tag{2}$$

and thus the moduli are the radii of the  $J$  spheres. We call this sector *multi-sphere* Einstein-Maxwell compactification. We will see that dS states with low quantum numbers are always unstable, and thus they should be excluded from the landscape. This legitimates the  $\alpha^*$ -problem as an objection against naive counting arguments in the BP landscape.

The stability of states in multi-sphere compactifications has been studied previously [37], [38], [39]. In particular, in [39] it is shown that compactifications of the form AdS <sub>$p$</sub>  × S <sup>$n$</sup>  × S <sup>$q-n$</sup>  are unstable for  $q < 9$  but they are stable for  $q \geq 9$ . In contrast, the multi-sphere model (2) gives always stable AdS<sub>2</sub> states. This example emphasizes the importance of the dimensionality in determining stability.

We have chosen the cosmological part in the multi-sphere model to be 1+1 instead of 3+1 for simplicity. On one hand, these cosmologies are unrealistic, and they have the peculiarities of two-dimensional dilatonic gravities. On the other hand, there is no theory predicting how observers form in a 1+1 universe, and no quantum measure defined on this multiverse, and therefore the prediction of the cosmological constant relies on the state counting problem only. It is also a good candidate for studying the measure problem in future papers.

The paper is organized as follows. In section 2, we give a detailed description of the single-modulus compactification (A)dS<sub>2</sub> × S<sup>2</sup> in the Einstein-Maxwell theory, together with the stabilization mechanism and the state counting. In section 3 we consider the multi-sphere model and its stabilization mechanism in detail, and give a very detailed account of the (A)dS<sub>2</sub> × S<sup>2</sup> × S<sup>2</sup> sector of the six-dimensional Einstein-Maxwell theory. Section 4 is devoted to counting the states in the model. In section 5 we show how anthropic states can be constructed in this model. In section 6 we summarize the differences found between the

multi-sphere Einstein-Maxwell sector and the Bousso-Polchinski landscape, and in section 7 we speculate on some consequences that those phenomena can have on the string theory landscape. The last section 8 summarizes our conclusions.

## 2 One-flux compactification in the four-dimensional Einstein-Maxwell theory

### 2.1 The one-flux four-dimensional Einstein Maxwell landscape

By a compactification in four-dimensional gravity we understand a solution of the Einstein field equations of the form

$$ds^2 = e^{2\phi(x,t)}(-dt^2 + dx^2) + e^{2\psi(u,v)}(du^2 + dv^2). \quad (3)$$

This is a particular expression of a Kantowski-Sachs cosmology [40, 41]. The metric splits in a  $(t, x)$ -spacetime part, which we will identify with a two-dimensional cosmological solution, and a  $(u, v)$ -surface  $\mathcal{K}$ , the compact part.

The Einstein field equations are, in units with  $G = c = 1$ ,

$$R_{\mu\nu} = 8\pi \left( T_{\mu\nu} - \frac{1}{2} T g_{\mu\nu} \right). \quad (4)$$

The stress-energy tensor has two contributions, the first comes from the electromagnetic field and the second from a vacuum energy density:

$$\begin{aligned} T_{\mu\nu} &= T_{\mu\nu}^{(M)} + T_{\mu\nu}^{(\Lambda)}, \\ T_{\mu\nu}^{(M)} &= \frac{1}{4\pi} \left( F_{\mu\rho} F_{\nu}{}^{\rho} - \frac{1}{4} F^2 g_{\mu\nu} \right) \\ T_{\mu\nu}^{(\Lambda)} &= -\frac{\Lambda}{8\pi} g_{\mu\nu}. \end{aligned} \quad (5)$$

The symbol  $F^2 = F_{\mu\nu} F^{\mu\nu}$  is the electromagnetic Lagrangian density, and  $\Lambda$  is the cosmological constant of the four-dimensional theory.

The stress-energy tensor of the Maxwell field is traceless, so we have

$$T = T^{(\Lambda)} = -\frac{\Lambda}{2\pi}. \quad (6)$$

We will assume a magnetic monopole configuration for the electromagnetic field:

$$\mathbf{F} = \frac{Q}{V} e^{2\psi(u,v)} du \wedge dv, \quad (7)$$

where the boldface is used to denote differential forms. Here the constant  $Q$  is the magnetic charge of the monopole, and  $V$  is the volume of the compactification manifold, so that

$$V = \text{vol } \mathcal{K} = \int_{\mathcal{K}} e^{2\psi(u,v)} du \wedge dv \quad (8)$$

and we have

$$\int_{\mathcal{K}} \mathbf{F} = Q. \quad (9)$$

In matrix notation, the Maxwell field is

$$(F_{\mu\nu}) = \begin{pmatrix} 0 & E_x & E_u & E_v \\ -E_x & 0 & -B_v & B_u \\ -E_u & B_v & 0 & -B_x \\ -E_v & -B_u & B_x & 0 \end{pmatrix} = \begin{pmatrix} 0 & 0 & 0 & 0 \\ 0 & 0 & 0 & 0 \\ 0 & 0 & 0 & -B_x \\ 0 & 0 & B_x & 0 \end{pmatrix}, \quad B_x = \frac{Q}{V} e^{2\psi(u,v)}. \quad (10)$$

This configuration solves Maxwell equations in curved spacetime

$$\nabla_{\nu} F^{\mu\nu} = \frac{1}{\sqrt{-g}} \partial_{\nu} (\sqrt{-g} F^{\mu\nu}) = 0 \quad (11)$$

and the non-vanishing components of the corresponding stress-energy tensor are

$$\begin{aligned} T_{tt}^{(M)} &= \frac{1}{8\pi} B_x^2 e^{2\phi-4\psi} = \frac{1}{8\pi} \left(\frac{Q}{V}\right)^2 e^{2\phi}, \\ T_{xx}^{(M)} &= -\frac{1}{8\pi} B_x^2 e^{2\phi-4\psi} = -\frac{1}{8\pi} \left(\frac{Q}{V}\right)^2 e^{2\phi}, \\ T_{uu}^{(M)} &= T_{vv}^{(M)} = \frac{1}{8\pi} B_x^2 e^{-2\psi} = \frac{1}{8\pi} \left(\frac{Q}{V}\right)^2 e^{2\psi}. \end{aligned} \quad (12)$$

The contribution of the cosmological constant is

$$T_{\mu\nu}^{(\Lambda)} - \frac{1}{2} T^{(\Lambda)} g_{\mu\nu} = \frac{\Lambda}{8\pi} g_{\mu\nu}. \quad (13)$$

Finally, the Ricci tensor has the following nonzero components:

$$\begin{aligned} R_{tt} &= -R_{xx} = -\phi_{tt} + \phi_{xx}, \\ R_{uu} &= -R_{vv} = -\psi_{uu} - \psi_{vv}, \end{aligned} \quad (14)$$

where the subscripts in  $\phi_{xx}$  etc. represent partial derivatives. Einstein equations coincide in the  $tt$  and  $xx$  components, and in the  $uu$  and  $vv$  components also:

$$\begin{aligned} -\phi_{tt} + \phi_{xx} &= \left[ -\Lambda + \left(\frac{Q}{V}\right)^2 \right] e^{2\phi}, \\ -\psi_{uu} - \psi_{vv} &= \left[ \Lambda + \left(\frac{Q}{V}\right)^2 \right] e^{2\psi}, \end{aligned} \quad (15)$$

Thus,  $\phi$  and  $\psi$  are uncoupled and satisfy Liouville equations of  $-+$  and  $++$  signatures respectively.

The Liouville equation states that the Gaussian curvature of the corresponding surface is constant. We will call these two constants  $\lambda$  and  $K$ :

$$\begin{aligned} (\phi_{tt} - \phi_{xx})e^{-2\phi} &= \Lambda - \left(\frac{Q}{V}\right)^2 = \lambda, \\ -(\psi_{uu} + \psi_{vv})e^{-2\psi} &= \Lambda + \left(\frac{Q}{V}\right)^2 = K. \end{aligned} \tag{16}$$

Thus, a solution of the  $-+$  Liouville equation  $\phi(t, x)$  represents a two-dimensional space-time of constant curvature  $\lambda$ , which is de Sitter (dS<sub>2</sub>) if  $\lambda > 0$ , Minkowski (M<sub>2</sub>) if  $\lambda = 0$  and anti-de Sitter (AdS<sub>2</sub>) if  $\lambda < 0$ . Therefore,  $\lambda$  can be interpreted as the cosmological constant of the dimensionally reduced cosmological model. On the other hand,  $\psi$  represents a compact surface of constant curvature  $K$ . We can choose  $K$  positive, and then the surface will be a sphere of radius  $1/\sqrt{K}$ .

The positivity of the constant  $K$  is equivalent to zero genus by the Gauss-Bonnet formula, which also relates volume with curvature:

$$\frac{1}{2\pi} \int_{\mathcal{K}} K e^{2\psi} dudv = 2 \quad \Rightarrow \quad \frac{KV}{2\pi} = 2 \quad \Rightarrow \quad V = \frac{4\pi}{K}, \tag{17}$$

which leads to an algebraic equation for  $K$ :

$$K = \Lambda + \left(\frac{Q}{V}\right)^2 = \Lambda + \left(\frac{QK}{4\pi}\right)^2. \tag{18}$$

The previous equation has two solutions:

$$K_{\pm} = 2\Lambda \left(\frac{Q_{\max}}{Q}\right)^2 \left[ 1 \pm \sqrt{1 - \left(\frac{Q}{Q_{\max}}\right)^2} \right], \quad Q_{\max} = \frac{2\pi}{\sqrt{\Lambda}}. \tag{19}$$

The magnetic charge should not exceed  $Q_{\max}$ . For greater charges curvatures become complex and therefore the solution makes no sense.

The two-dimensional cosmological constant has also two branches

$$\lambda_{\pm} = 2\Lambda - K_{\mp}. \tag{20}$$

Assuming the usual Dirac quantization condition on the magnetic charge in terms of the elemental charge  $e$  of the particles coupled to the electromagnetic field,

$$Qe = 2\pi n, \quad \text{with } n \in \mathbb{Z}, \tag{21}$$

we have a maximum value of the integer  $n$ ,

$$n_{\max} = \left\lfloor \frac{e}{\sqrt{\Lambda}} \right\rfloor \tag{22}$$

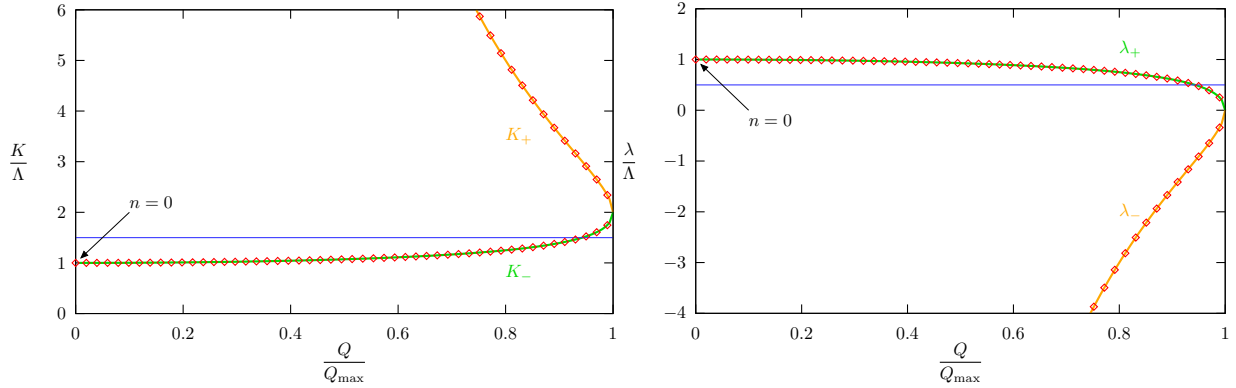


Figure 1: Curvature  $K$  (left) and two-dimensional cosmological constant  $\lambda$  (right) of the two branches of the one-flux four-dimensional Einstein-Maxwell landscape are shown with  $n_{\max} = 50$ , corresponding to  $\Lambda = 3.915 \times 10^{-4}$  (a random value, expressed in units such that  $e = 1$ ). The state  $n = 0$  is present only in the  $K_-$ ,  $\lambda_+$  branch. The branching point is absent because  $Q_{\max}$  is (generically) not an integer. The  $n = 1$  point on the  $K_+$ ,  $\lambda_-$  branch produces finite values  $K_+(1) \approx -\lambda_-(1) \approx 10^4 \Lambda$ . The horizontal line signals the onset of stability, all states above it in the  $\lambda_+$  branch being unstable. Thus, this landscape contains 50 AdS<sub>2</sub> states and 3 dS<sub>2</sub> states.

and all integers  $n$  satisfying  $0 < |n| \leq n_{\max}$ , plus  $n = 0$ , constitute the one-flux four dimensional Einstein-Maxwell landscape<sup>1</sup>.

The case  $n = 0$  deserves further comment. In this case we have  $Q = 0$ , and we have only one branch,  $K = \lambda = \Lambda$ , which cannot be supported because the electromagnetic field vanishes. Thus we should expect this solution to be unstable, as we will see below.

Thus far, we have considered  $\Lambda > 0$ . In the case  $\Lambda < 0$ , it can be seen that the solutions of equation (18) yield  $K_- < 0$  and thus only the  $K_+$  branch remains as a solution, with a cosmological constant  $\lambda_- = 2\Lambda - K_+$  always negative. In addition we have no restriction in the quantum number  $n$ , and therefore this  $\Lambda < 0$  infinite landscape is less interesting than its  $\Lambda > 0$  counterpart, which we will be considering henceforth.

Equation (20) can be interpreted as a distribution of the dS<sub>4</sub> curvature  $\Lambda$  between the (A)dS<sub>2</sub> and S<sup>2</sup> parts. The solutions obtained show that a positive curvature  $\Lambda$  can be distributed between positive  $K$  and positive or negative  $\lambda$  (two possible ways), but a negative curvature  $\Lambda$  should be distributed between a positive  $K$  and a negative  $\lambda$  (a unique way), yielding a physically less interesting landscape.

Figure 1 shows curvatures and cosmological constants for  $n_{\max} = 50$  for both branches. Note that this number controls the number of the states in the landscape, whereas  $\Lambda$  controls the magnitude of the moduli  $K$  and  $\lambda$ .

<sup>1</sup>This is the “pedestrian” landscape mentioned in Footnote 2 of Ref. [42].



## 2.2 Modulus stabilization

The landscape considered thus far has only one modulus, namely the Gaussian curvature of the compact sphere or equivalently its radius. This is a volume modulus, which control the volume (surface area) of the compact part of the spacetime. The next question we should ask is the stability of the solutions encountered. If a value of  $K$  in one of the two branches for fixed quantum number  $n$  is not stable, a small perturbation will drive the system out of the solution. If the subsequent evolution makes the sphere radius to grow unbounded we speak of *decompactification*. An unstable state in the landscape should not be included when counting states in the resulting two-dimensional multiverse.

The one-flux compactified solution found is  $dS_2 \times S^2$  or  $AdS_2 \times S^2$  with a sphere radius which is homogeneous throughout the two-dimensional spacetime. The perturbation will alter this situation, assuming that the compactification radius can be different on different  $t, x$  points, yielding an ansatz

$$ds^2 = e^{2\phi(t,x)-2\xi(t,x)}(-dt^2 + dx^2) + e^{2\psi(u,v)+2\xi(t,x)}(du^2 + dv^2). \quad (23)$$

The perturbation  $\xi(t, x)$  appears also on the non-compact part of the metric, and in this way the local volume element remains invariant. This reflects that the perturbation exchanges locally volume between the compact and non-compact parts of the metric. Functions  $\phi$  and  $\psi$  are solutions of the Liouville equations encountered before.

We will investigate the dynamics of the perturbation field  $\xi(t, x)$  from a two-dimensional perspective. The four-dimensional action of the Einstein-Maxwell system is

$$S^{(4)} = \frac{1}{16\pi} \int L^{(4)} dt dx du dv, \quad L^{(4)} = \sqrt{-g^{(4)}}(R^{(4)} - 2\Lambda - F^2), \quad (24)$$

where we use superscripts to distinguish between four- and two-dimensional quantities. The curvature scalar and the electromagnetic scalar are

$$\begin{aligned} R^{(4)} &= -2 \left[ (\phi_{xx} - \phi_{tt}) e^{-2\phi+2\xi} + (\psi_{uu} + \psi_{vv}) e^{-2\psi-2\xi} + (\xi_{xx} + 3\xi_x^2 - \xi_{tt} - 3\xi_t^2) e^{2\xi-2\phi} \right], \\ F^2 &= 2B_x^2 e^{-4\psi-4\xi}. \end{aligned} \quad (25)$$

Using  $\sqrt{-g^{(4)}} = e^{2\phi+2\psi}$  and integrating by parts the second derivatives of  $\xi$ , the four-dimensional Lagrangian is

$$\begin{aligned} L^{(4)} &= -2 \left[ (\phi_{xx} - \phi_{tt}) e^{2\psi+2\xi} + (\psi_{uu} + \psi_{vv}) e^{2\phi-2\xi} \right. \\ &\quad \left. + (\xi_x^2 - \xi_t^2) e^{2\xi+2\psi} + \Lambda e^{2\phi+2\psi} + B_x^2 e^{2\phi-2\psi-4\xi} \right] \end{aligned} \quad (26)$$

Now, we will substitute the sphere ansatz  $-(\psi_{uu} + \psi_{vv})e^{-2\psi} = K$  and the magnetic monopole configuration  $B_x = \frac{Q}{V}e^{2\psi}$  as backgrounds for the dynamics of the perturbation.

Integrating with respect to  $u, v$  we obtain the two-dimensional action

$$\begin{aligned} S^{(2)} &= \frac{V}{4\pi} \int L^{(2)} dt dx, \\ L^{(2)} &= \sqrt{-g^{(2)}} \left[ \frac{1}{4} e^{2\xi} R^{(2)} - \frac{1}{2} e^{2\xi} (g^{(2)})^{\alpha\beta} \xi_\alpha \xi_\beta - U(\xi) \right], \end{aligned} \quad (27)$$

where the summation in  $\alpha, \beta \in \{t, x\}$  is implied, and

$$\begin{aligned} (g^{(2)})_{\alpha\beta} d\alpha d\beta &= e^{2\phi} \eta^{\alpha\beta} d\alpha d\beta = e^{2\phi} (-dt^2 + dx^2), \\ R^{(2)} &= -2(\phi_{xx} - \phi_{tt}) e^{-2\phi}, \\ U(\xi) &= \frac{1}{2} \left[ \Lambda - K e^{-2\xi} + \left( \frac{QK}{4\pi} \right)^2 e^{-4\xi} \right], \end{aligned} \quad (28)$$

that is, a model of 1+1 spacetime with gravity non-minimally coupled with a scalar (called the *dilaton* or the *radion*) which experiences self-interaction through a potential. Note that the dependence with respect to the dilaton is not relegated to the potential, and so a direct stability analysis using  $U(\xi)$  is not possible.

The next step is to show that the Euler-Lagrange equations of the previous two-dimensional model are equivalent to the Einstein equations of its four-dimensional counterpart, that is, the truncation of the model is consistent. Firstly, we recast the Lagrangian (27) displaying explicitly all fields and removing the second derivatives of  $\phi$  by integrating by parts, which amounts to the substitution

$$\phi_{\alpha\alpha} e^{2\xi} \longrightarrow -2\phi_\alpha \xi_\alpha e^{2\xi}, \quad (29)$$

for  $\alpha \in \{t, x\}$ . The resulting Lagrangian is

$$\begin{aligned} L^{(2)} &= -\frac{1}{2} e^{2\xi} \eta^{\alpha\beta} \phi_{\alpha\beta} - \frac{1}{2} e^{2\xi} \eta^{\alpha\beta} \xi_\alpha \xi_\beta - e^{2\phi} U(\xi) \\ &= e^{2\xi} \eta^{\alpha\beta} \phi_\alpha \xi_\beta - \frac{1}{2} e^{2\xi} \eta^{\alpha\beta} \xi_\alpha \xi_\beta - e^{2\phi} U(\xi). \end{aligned} \quad (30)$$

The equations of motion are

$$\eta^{\alpha\beta} (\phi_{\alpha\beta} - \xi_{\alpha\beta} - \xi_\alpha \xi_\beta) e^{2\xi} = -e^{2\phi} U'(\xi) \quad (31)$$

with respect to  $\xi$ , and

$$\eta^{\alpha\beta} (\xi_{\alpha\beta} + 2\xi_\alpha \xi_\beta) e^{2\xi} = -2e^{2\phi} U(\xi) \quad (32)$$

with respect to  $\phi$ . The absence of perturbation  $\xi = 0$  should be a solution of the equations, so that equation (31) with  $\xi = 0$  reduces to

$$-e^{-2\phi} \eta^{\alpha\beta} \phi_{\alpha\beta} = (-\phi_{xx} + \phi_{tt}) e^{-2\phi} = U'(0) = \lambda, \quad (33)$$

which is the two-dimensional cosmological solution, and equation (32) gives

$$U(0) = 0 \quad \Rightarrow \quad \Lambda - K + \left( \frac{QK}{4\pi} \right)^2 = 0, \quad (34)$$

which is the same equation previously found for  $K$ , see (18). We will now assume that  $\xi$  is a small perturbation, thereby neglecting the backreaction of the perturbation on the geometry of the cosmological solution. This allows us to fix  $\phi$  as another background field by means of equation (33). This eliminates  $\phi$  as a dynamical variable in the Lagrangian (30) and therefore equation (32) will not be used. In other words, we assume that equation (32) is satisfied to zeroth order, which is the content of (34), and we are left with (31) as the evolution equation for the perturbation  $\xi$  in the background  $\phi$ .

Thus, we substitute eq. (33) into eq. (31), resulting in a dynamical equation for  $\xi$  which is

$$-e^{-2\phi}\eta^{\alpha\beta}(\xi_{\alpha\beta} + \xi_{\alpha}\xi_{\beta}) = \lambda - e^{-2\xi}U'(\xi) = -U'_{\text{eff}}(\xi). \quad (35)$$

The linear stability analysis of equation (35) requires its linearization (the effect of neglecting the non-linear derivative term does not spoil linear stability, as discussed in appendix A)

$$e^{-2\phi}(\xi_{tt} - \xi_{xx}) = -U''_{\text{eff}}(0)\xi, \quad (36)$$

which is a 1 + 1 Klein-Gordon equation. We also consider a small spacetime region such that  $\phi$  can be treated approximately as a constant. We thus obtain the linear stability condition of the solution  $\xi = 0$  as being a minimum of the effective potential:

$$U''_{\text{eff}}(0) = 4(2K - 3\Lambda) > 0, \quad (37)$$

which is  $K > \frac{3}{2}\Lambda$ . All points in the  $K_+$  branch satisfy this condition, and therefore all AdS<sub>2</sub> states are stable, but this is not so in the  $K_-$  branch. The condition  $K_- > \frac{3}{2}\Lambda$  is met by all charges satisfying

$$Q > Q_{\min} = \frac{2\sqrt{2}}{3} Q_{\max}. \quad (38)$$

Upon quantization, the previous condition is

$$n \geq n_{\min} = \left\lceil \frac{Q_{\min}e}{2\pi} \right\rceil. \quad (39)$$

Thus, all states in the dS<sub>2</sub> branch characterized by a quantum number  $n < n_{\min}$  are unstable. This includes also the state  $n = 0$ , as mentioned above. We conclude that the flux number labeling true vacuum states should obey a double inequality, obtained by combining (22) and (39):

$$n_{\min} \leq n \leq n_{\max}. \quad (40)$$

Therefore, the number of stable states in this one-flux landscape is

$$\mathcal{N}_1 = \underbrace{n_{\max}}_{\text{AdS}_2} + \underbrace{n_{\max} - n_{\min} + 1}_{\text{dS}_2} = 2 \left\lfloor \frac{e}{\sqrt{\Lambda}} \right\rfloor - \left\lceil \frac{2\sqrt{2}}{3} \frac{e}{\sqrt{\Lambda}} \right\rceil + 1 \approx \frac{e}{\sqrt{\Lambda}} \left( 2 - \frac{2\sqrt{2}}{3} \right). \quad (41)$$

In the example shown in Figure 1 we have  $Q_{\max} = 317.54$  (corresponding to  $\Lambda = 3.915 \times 10^{-4}$ ) which gives  $\mathcal{N}_1 = 53$  (50 AdS<sub>2</sub> states and only 3 dS<sub>2</sub> states).

The physical description of these states is simple: The self-gravitating electromagnetic field of the monopole stabilizes a geometry  $(A)dS_2 \times S^2$  whose natural behaviour is decompactification<sup>2</sup>, that is, the curvature of the sphere part, which tends to vanish, is sustained by the magnetic field. The distribution of curvature contributions between the compact and non-compact parts of the geometry is whatever allowed by magnetic charge quantization in the AdS<sub>2</sub> case, while in the dS<sub>2</sub> case only large charges can sustain positive curvature of de Sitter states.

### 3 Adding many fluxes

Obtaining a non-trivial landscape with many fluxes is not easy. The easiest technique is to extend the electromagnetic field  $F$  to a  $SO(J)$ -invariant  $J$ -component field, in which all charges are different [1, 42]. This approach is not convenient to address the problem of stabilization, because the charges do not come from a transparent compactification scheme, and therefore nothing is known about the stabilizing potential.

In all known compactifications, the charges come from moduli describing the shape of the inner manifold. These moduli are free geometric parameters, but they are promoted to dynamical scalar fields in the perturbation analysis. The charges are considered coupling *constants*, and therefore their dynamics should be governed by a potential with at least one minimum. The stabilization problem consists of finding this potential. Different models provide a wide variety of potentials; if the potential does not possess any minimum, then the dynamics of the moduli will lead them to grow unbounded; this phenomenon is known as *decompactification*.

In an ideal model, we should expect that all moduli come from a compactification manifold which is derived from the equations of motion. Nevertheless, these equations are very difficult to solve in its full generality, and therefore the inner manifold is chosen at the very beginning of the process, and its validity is confirmed afterwards, by proving that the chosen ansatz is actually a solution. Of course, the chosen manifold may not provide a solution, or the solution may lack some desired properties.

In looking for a many-fluxes landscape, we have tried the following candidates as compactification manifold:

- The complex Riemann curves

$$w^2 = P_k(z),$$

where  $w$  and  $z$  are complex coordinates, are the simplest surfaces of known genus  $g > 0$ .  $P_k(z)$  is a  $k$ -degree polynomial with real coefficients,

$$P_k(z) = z^k + a_{k-2}z^{k-2} + \dots + a_1z + a_0,$$

---

<sup>2</sup>Note that equation (36), when the state is unstable, as happens in absence of electromagnetic field, predicts an exponential increase with time of the perturbation  $\xi(t)$ . By inspecting equation (23), we see that it corresponds to decompactification.

which are the  $k-1$  deformation moduli of the surface. The coefficients of  $z^k$  and  $z^{k-1}$  can be removed by rescaling and shifting  $z$  respectively. The genus of the surface is given by  $k = 2\mathbf{g} + 2$  (if  $k$  is even) or  $k = 2\mathbf{g} + 1$  (if  $k$  is odd).

These surfaces are not compact, but they can approximate locally a compact surface of the same genus. Thus, Einstein equations are to be solved only locally near the approximation region. But this ansatz turns out to yield no solutions, not even in this approximate fashion.

- The compact hyperbolic manifolds (CHM) are fundamental domains of nonabelian lattices in the Lobachevskian plane, in which the lattices are generated by discrete subgroups of  $SL_2(\mathbb{R})$ . By choosing identification of the sides of the fundamental cell a compact surface of genus  $\mathbf{g} \geq 2$  is obtained, which has constant negative curvature<sup>3</sup>. These surfaces are indeed solutions of Einstein equations, but only if the cosmological constant  $\Lambda$  is *negative*. This generates a sector of the Einstein-Maxwell landscape with no de Sitter states, and therefore will not be considered here.

The previous examples show that sometimes the appropriate compactification can be elusive, maybe because is far more complex than expected, or because it may not exist. So we are forced to consider another simple extension of the four dimensional Einstein-Maxwell landscape, which is discussed in the following subsections.

### 3.1 Multi-sphere compactification

We consider a  $J$ -sphere metric ansatz given by

$$ds^2 = e^{2\phi(x,t)}(-dt^2 + dx^2) + \sum_{i=1}^J e^{2\psi_i(u,v)}(du_i^2 + dv_i^2). \quad (42)$$

The metric (42) represents a manifold of the form

$$\mathcal{K} = (A)dS_2 \times \overbrace{S^2 \times \cdots \times S^2}^{J \text{ spheres}} = (A)dS_2 \times [S^2]^J \quad (43)$$

which is nothing but a sector of the Einstein-Maxwell theory in  $2J + 2$  dimensions. The  $\phi$  exponent defines the conformal factor of a two-dimensional cosmological spacetime in  $(t, x)$  coordinates. The functions  $\psi_i$  depend only on the corresponding coordinates  $(u_i, v_i)$  (but not on  $(u_j, v_j)$  with  $j \neq i$ ), and they give a conformal representation of the  $i$ -th sphere metric.

The Ricci tensor of the metric (42) is

$$\begin{aligned} R_{xx} &= -R_{tt} = \phi_{tt} - \phi_{xx}, \\ R_{u_i u_i} &= R_{v_i v_i} = -\Delta_i \psi_i, \end{aligned} \quad (44)$$

---

<sup>3</sup>Refs. [43, 44, 45, 46, 47, 48] contain more details on hyperbolic compactifications in cosmology.

all remaining components being zero. The  $i$ -th Laplacian operator is  $\Delta_i = \partial_{u_i}^2 + \partial_{v_i}^2$ .

The metric (42) should be complemented with the electromagnetic field

$$\mathbf{F} = \sum_{i=1}^J B_i(u_i, v_i) du_i \wedge dv_i \quad (45)$$

where the magnetic  $u_i, v_i$ -component  $B_i$  depends only on the corresponding coordinates  $(u_i, v_i)$  (but not on  $(u_j, v_j)$  with  $j \neq i$ ). Thus, the electromagnetic tensor  $F_{\mu\nu}$  is analogous to (10), with  $J \times 2$  blocks along the diagonal. Maxwell equations (11) reduce to

$$\partial_{u_i} \sqrt{-g} F^{v_i u_i} = 0, \quad \partial_{v_i} \sqrt{-g} F^{u_i v_i} = 0. \quad (46)$$

Using the volume element prefactor  $\sqrt{-g} = e^{2\phi+2\sum_{i=1}^J \psi_i}$  and the relation  $F^{u_i v_i} = e^{-4\psi_i} F_{u_i v_i}$ , we find that a solution of the equations is

$$F_{u_i v_i} = B_i = \frac{Q_i}{V_i} e^{2\psi_i}, \quad (47)$$

where  $V_i$  is the volume of the  $i$ -th sphere,

$$V_i = \int_{S^2} e^{2\psi_i} du_i \wedge dv_i, \quad (48)$$

and  $Q_i$  is an integration constant. When integrating the two-form we obtain

$$\int \mathbf{F} = \sum_{i=1}^J \frac{Q_i}{V_i} \int_{S^2} e^{2\psi_i} du_i \wedge dv_i = \sum_{i=1}^J Q_i = Q, \quad (49)$$

so that  $Q$  is the total magnetic charge of the configuration, and each constant  $Q_i$  can be interpreted as the magnetic charge contribution of the corresponding magnetic field component.

The most convenient way of obtaining the field equations is writing the action

$$S = \frac{1}{16\pi} \int \sqrt{-g} (R - 2\Lambda - F^2) dt dx \prod_{i=1}^J du_i dv_i \quad (50)$$

in terms of the fields  $\phi$ ,  $\psi_i$  and  $B_i$  and then derive the equations from it. The curvature scalar of the metric ansatz (42) is

$$R = 2(\phi_{tt} - \phi_{xx})e^{-2\phi} - 2 \sum_{i=1}^J \Delta_i \psi_i e^{-2\psi_i}. \quad (51)$$

The Lagrangian density of the electromagnetic field (45) is

$$F^2 = 2 \sum_{i=1}^J B_i^2 e^{-4\psi_i}. \quad (52)$$

Thus, the action specialized to our ansatz is

$$S = \frac{1}{8\pi} \int e^{2\phi+2\sum_{i=1}^J \psi_i} \left[ (\phi_{tt} - \phi_{xx}) e^{-2\phi} - \sum_{i=1}^J \Delta_i \psi_i e^{-2\psi_i} - \Lambda - \sum_{i=1}^J B_i^2 e^{-4\psi_i} \right] dt dx \prod_{i=1}^J du_i dv_i \quad (53)$$

The variation of the action (53) with respect to the vector potential  $A_\mu$  (which determines the magnetic field  $B_i = \partial_{u_i} A_{v_i} - \partial_{v_i} A_{u_i}$ ) gives the Maxwell equations (46). Varying with respect to  $\phi$  and  $\psi_j$  gives

$$\begin{aligned} \Lambda &= - \sum_{i=1}^J \left\{ \Delta_i \psi_i e^{-2\psi_i} + B_i^2 e^{-4\psi_i} \right\}, \\ (\phi_{tt} - \phi_{xx}) e^{-2\phi} &= \Lambda + \sum_{i=1}^J \left\{ \Delta_i \psi_i e^{-2\psi_i} + B_i^2 e^{-4\psi_i} \right\} - \Delta_j \psi_j e^{-2\psi_j} - 2B_j^2 e^{-4\psi_j}. \end{aligned} \quad (54)$$

Note that the first equation in (54) cancels some terms in the second. Now, we recognize the Gaussian curvatures of conformally flat metrics with signatures  $-+$  and  $++$ ; so we substitute the constant curvature ansatz implied in the geometry of  $\mathcal{K}$  (43) as we did previously (16), introducing the constants

$$\lambda = (\phi_{tt} - \phi_{xx}) e^{-2\phi}, \quad K_i = -\Delta_i \psi_i e^{-2\psi_i}, \quad (55)$$

where  $\lambda$  is the curvature of the non-compact part (the cosmological constant of the two-dimensional spacetime) and  $K_i$  is the curvature of the  $i$ -th sphere in the product  $[\mathbb{S}^2]^J$ . If we finally substitute  $B_i$  by the solution (47), we obtain

$$\Lambda = \sum_{i=1}^J \left\{ K_i - \left( \frac{Q_i}{V_i} \right)^2 \right\}, \quad (56)$$

$$\lambda = K_j - 2 \left( \frac{Q_j}{V_j} \right)^2. \quad (57)$$

We can substitute equation (57) in (56), obtaining

$$\Lambda = \frac{1}{2} \left( J\lambda + \sum_{i=1}^J K_i \right). \quad (58)$$

The relation (17) between volume and curvature is valid, and transforms equation (57) in an algebraic equation for  $K_j$ :

$$2 \left( \frac{Q_j K_j}{4\pi} \right)^2 - K_j + \lambda = 0, \quad (59)$$

which has two solutions

$$K_j^{(\pm)} = \frac{4\pi^2}{Q_j^2} \left[ 1 \pm \sqrt{1 - 2\lambda \frac{Q_j^2}{4\pi^2}} \right]. \quad (60)$$

Substituting (60) in equation (58), we obtain a single equation for  $\lambda$ , whose solution can be substituted back in equation (60), determining the curvatures.

It should be noted that if  $Q_j = 0$ , then equation (59) has a single solution, namely  $K_j = \lambda$ , which is the limit of the  $K_j^{(-)}$  solution when  $Q_j \rightarrow 0$ .

Now, the usual Dirac quantization condition is

$$Q_j e = 2\pi n_j \quad \text{with } n_j \in \mathbb{Z}, \quad (61)$$

which can be justified in the following way. We will use the conformal representation of the sphere metric:

$$(ds^2)_{S_j^2} = \frac{du_j^2 + dv_j^2}{K_j \cosh^2 u_j} \quad (62)$$

such that the  $u_j$  coordinates separate hemispheres ( $u_j > 0$  is the northern hemisphere,  $u_j = 0$  is the equator, etc.) and  $v_j$  are angles mod  $2\pi$ . A quantum wavefunction  $\Psi$  defined on the manifold  $\mathcal{K}$  depends on the coordinates  $t, x, \{u_j, v_j\}_{j=1, \dots, J}$ . The loops  $\gamma_j$  in which  $v_j$  varies along  $[0, 2\pi]$  and the remaining coordinates are fixed can be used to define holonomies  $h_j$  acting on the wavefunction:

$$h_j \Psi = \exp\left(ie \int_{\gamma_j} A\right) \Psi, \quad (63)$$

where the electromagnetic potential is used as the connection to parallel transport the wavefunction values along the loop. It is well known that the potential of a magnetic monopole can be defined in two patches on the sphere which overlap at the equator:

$$A = \sum_{i=1}^J A_i, \quad A_j = \begin{cases} A_j^{(+)} = \frac{Q_j}{K_j V_j} [\tanh u_j - 1] dv_j & \text{if } u_j \geq 0, \\ A_j^{(-)} = \frac{Q_j}{K_j V_j} [\tanh u_j + 1] dv_j & \text{if } u_j \leq 0. \end{cases} \quad (64)$$

Here,  $V_j = \frac{4\pi}{K_j}$ , as usual, and the magnetic field is

$$B_j = dA_j^{(\pm)} = \frac{Q_j}{K_j V_j} \frac{du_j \wedge dv_j}{\cosh^2 u_j} = \frac{Q_j}{V_j} e^{2\psi_j} du_j \wedge dv_j. \quad (65)$$

Thus, the potential is discontinuous at the equator, but the discontinuity is given by a gauge transformation  $\chi_j$ , namely

$$A_j^{(+)} - A_j^{(-)} = -\frac{2Q_j}{K_j V_j} dv_j = d\chi_j. \quad (66)$$

If we move the loop slightly upwards or downwards from the equator, the discontinuity in  $A$  will leave a different phase on  $\Psi$ , thus violating gauge invariance, unless the phase difference is an integer times  $2\pi$ , that is, equation (61).

Therefore, we can substitute (61) in the equation satisfied by  $\lambda$  (58), obtaining

$$\Lambda = \frac{1}{2} \left[ J\lambda + \sum_{j=1}^J \frac{e^2}{n_j^2} \left( 1 \pm \sqrt{1 - 2\frac{\lambda}{e^2} n_j^2} \right) \right]. \quad (67)$$



Note that  $e^2$  is a scale which can be used to measure  $\Lambda$  and  $\lambda$ . In order to simplify the formulae, we will assume henceforth that the substitutions  $\frac{\lambda}{e^2} \rightarrow \lambda$  and  $\frac{\Lambda}{e^2} \rightarrow \Lambda$  have been made. Equation (67) takes the form

$$L_{\{s_j\},\{n_j\}}(\lambda) = \Lambda, \quad \text{with} \quad L_{\{s_j\},\{n_j\}}(\lambda) = \frac{1}{2} \left[ J\lambda + \sum_{j=1}^J \frac{1}{n_j^2} \left( 1 + s_j \sqrt{1 - 2\lambda n_j^2} \right) \right]. \quad (68)$$

The function  $L_{\{s_j\},\{n_j\}}(\lambda)$  depends on the signs  $\{s_j\}$  of the curvatures involved and on the winding numbers  $\{n_j\}$  of the magnetic field. When some  $n_j$  vanishes, the curvature should be taken as  $K_j = K_j^{(-)} = \lambda$ , the  $K_j^{(+)}$  branch is absent. The solutions of equation (68) constitute the states of the multi-sphere Einstein-Maxwell landscape.

The set of integers  $\{n_j\}$  will be called a *node*, while the set of signs  $\{s_j\}$  will be called a *branch* of the  $L_{\{s_j\},\{n_j\}}$  function. Fixing a node with all  $n_j$  nonzero, we have  $2^J$  branches, one for each possible choice of the signs  $\{s_j\}$ . The number of solutions of the equation is different for each  $\Lambda$  value; in figure 2 it is shown an example with  $J = 3$ , where the eight branches of the node  $(n_1, n_2, n_3) = (2, 3, 1)$  are shown. The displayed value of  $\Lambda$  yields eight solutions, but it is obvious from figure 2 that the number of solutions vary when  $\Lambda$  is moved upwards, and becomes zero when the  $\{+, +, +\}$  branch is surpassed. The highest branch will be always the all-+ branch, and will be called the *principal* branch.

Not all solutions of equation (68) give valid states; for example, curvatures (60) can become complex if  $\lambda$  is too large. The smallest value of  $\lambda$  at which some of the pairs of curvatures  $K_j^{(\pm)}$  meet is the *branching point* of the node, and is given by

$$\lambda_b = \frac{1}{2 \max_{1 \leq j \leq J} \{n_j^2\}}. \quad (69)$$

This is the maximum positive value that  $\lambda$  can achieve when all  $n_j \neq 0$ . Curvatures can also become negative; this happens when  $\lambda < 0$  in all branches except the principal one. Those states are not well defined, but we might define them in detail by replacing the corresponding sphere by a CHM. Nevertheless, to keep things simple, this sector of the landscape will be deliberately left out, because all its states are AdS. This leaves the principal branch as the only source of AdS states with positive curvature in all places of the compact part.

The problem of the stability of the states just found is addressed in subsection 3.2, and the problem of counting them is the subject of section 4.

## 3.2 Moduli stabilization

The next step in the analysis is to determine if the states of the multi-sphere Einstein-Maxwell landscape are stable or not. Our approach will follow closely that of subsection 2.2. We begin by introducing perturbations  $\xi_j(t, x)$  which represent deviations of the curvatures found as solutions of the Einstein equations; the perturbed metric ansatz in the Einstein

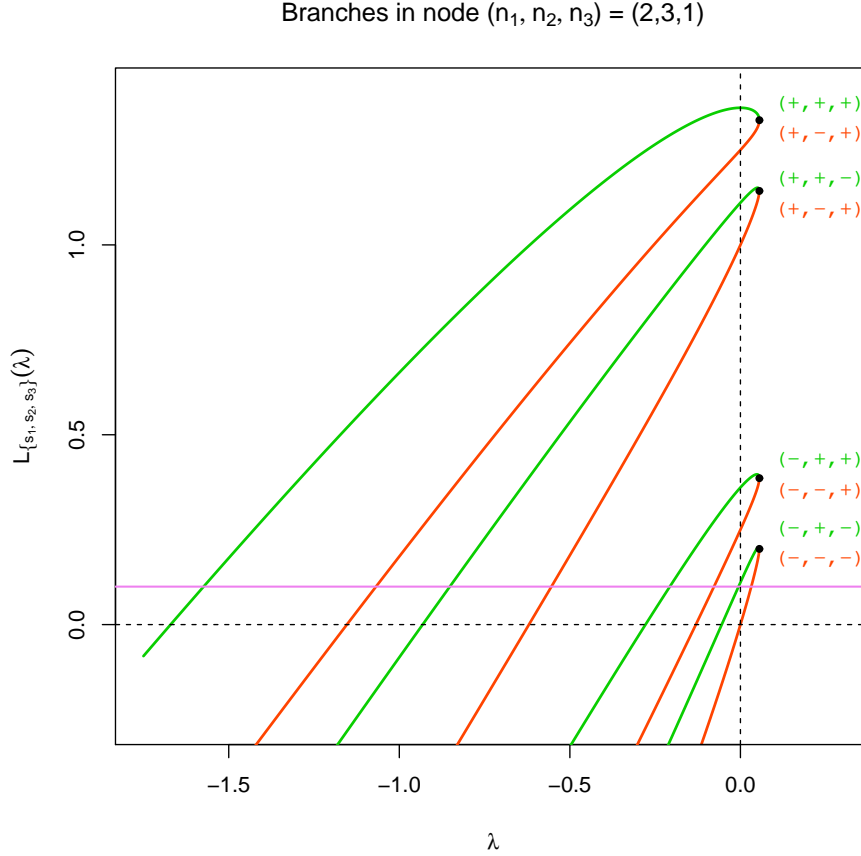


Figure 2: The eight branches of the  $J = 3$  multi-sphere Einstein-Maxwell landscape at the node  $(n_1, n_2, n_3) = (2, 3, 1)$  are shown. Note that each pair of branches meet at a branching point, whose horizontal position is the same in all branches, see text. The solid horizontal line corresponds to a random value of the cosmological constant  $\Lambda$ ; with this choice, there are eight solutions of the equation  $L(\lambda) = \Lambda$ , yielding a single de Sitter state and seven anti-de Sitter states. Note that if  $\Lambda$  were at 0.5 height, there would be only four solutions, and if it were at 1.5 height, there would be no solutions at all. All statistic plots in this paper were done using R [49].

frame is

$$ds^2 = e^{2\phi(t,x)-2\sum_{j=1}^J \xi_j(t,x)} (-dt^2 + dx^2) + \sum_{j=1}^J e^{2\psi_j(u_j,v_j)+2\xi_j(t,x)} (du_j^2 + dv_j^2). \quad (70)$$

As before,  $\phi(t, x)$  represents a 1 + 1 cosmological solution, and  $\psi_j(u_j, v_j)$  corresponds to the metric of the internal spheres in conformal coordinates. The perturbations  $\xi_j(t, x)$  describe changes in the radii of the internal spheres, and thus they will be referred to as the *multi-radion* fields.

We will proceed by writing the action (50) specialized for the metric (70). The Ricci scalar is

$$R = 2 e^{-2\phi+2\sum_{j=1}^J \psi_j} \left\{ \phi_{tt} - \phi_{xx} + \sum_{j=1}^J \left[ (\xi_j)_{tt} - (\xi_j)_{xx} + 3(\xi_j)_t^2 - 3(\xi_j)_x^2 \right. \right. \\ \left. \left. + 2(\xi_j)_t \left( \sum_{k \neq j} \xi_k \right)_t - 2(\xi_j)_x \left( \sum_{k \neq j} \xi_k \right)_x - e^{2\phi-2\psi_j-2\xi_j-2\sum_{k=1}^J \xi_k} \Delta_j \psi_j \right] \right\} \quad (71)$$

Note that the previous expression involves second derivatives of the multi-radion fields. We can replace those terms by first derivatives by integrating by parts in the action. This amounts to the following replacement rule:

$$(\xi_j)_{tt} e^{2\sum_{k=1}^J \xi_k} \longrightarrow -2(\xi_j)_t \left( \sum_{k=1}^J \xi_k \right)_t e^{2\sum_{k=1}^J \xi_k}, \quad (72)$$

and another analogous equation with the  $x$  derivatives.

The next step is to note that the expression (47) for the magnetic field remains unchanged, because the perturbations appear in Maxwell equations (46) only as factors depending on variables  $(t, x)$ , and thus they can be factored out of the equations. Thus, the contribution of the magnetic field to the action is not exactly (52) but

$$F^2 = 2 \sum_{j=1}^J B_j^2 e^{-4\psi_j-4\xi_j}, \quad (73)$$

with the same magnetic field  $B_j = \frac{Q_j}{V_j} e^{2\psi_j}$ .

Finally, we will insert in the action the unperturbed sphere metric ansatz  $-e^{2\psi_j} \Delta_j \psi_j = K_j$ .

Gathering all these ingredients, we obtain the following Lagrangian for the perturbed metric:

$$L = \sqrt{-g} (R - 2\Lambda - F^2) \\ = 2 e^{2\phi+2\sum_{k=1}^J \psi_k} \left\{ (\phi_{tt} - \phi_{xx}) e^{-2\phi+2\sum_{k=1}^J \xi_k} - \Lambda \right. \\ \left. + \sum_{j=1}^J \left[ \left( (\xi_j)_t^2 - (\xi_j)_x^2 \right) e^{-2\phi+2\sum_{k=1}^J \xi_k} + K_j e^{-2\xi_j} - \left( \frac{Q_j}{V_j} \right)^2 e^{-4\xi_j} \right] \right\}. \quad (74)$$

Now, we can perform the integration in the internal variables  $\{u_j, v_j\}$  and thus obtain a dimensionally reduced model for the cosmological part together with the multi-radion fields:

$$S = \frac{1}{16\pi} \int L dt dx \prod_{j=1}^J du_j dv_j = \frac{1}{4\pi} \left( \prod_{j=1}^J V_j \right) \int L^{(2)} dt dx, \quad (75)$$

with a 1 + 1 Lagrangian

$$L^{(2)} = \sqrt{-g^{(2)}} \left\{ \frac{1}{4} e^{2\sum_{k=1}^J \xi_k} R^{(2)} - \frac{1}{2} e^{2\sum_{k=1}^J \xi_k} \sum_{j=1}^J (g^{(2)})^{\alpha\beta} (\xi_j)_\alpha (\xi_j)_\beta - \sum_{j=1}^J U_j(\xi_j) \right\} \quad (76)$$

where the summation in  $\alpha, \beta \in \{t, x\}$  is implied, and we have used (see (28))

$$\begin{aligned} (g^{(2)})_{\alpha\beta} d\alpha d\beta &= e^{2\phi} \eta^{\alpha\beta} d\alpha d\beta = e^{2\phi} (-dt^2 + dx^2), \\ R^{(2)} &= -2(\phi_{xx} - \phi_{tt}) e^{-2\phi}, \\ U_j(\xi_j) &= \frac{1}{2} \left[ \frac{\Lambda}{J} - K_j e^{-2\xi_j} + \left( \frac{Q_j K_j}{4\pi} \right)^2 e^{-4\xi_j} \right]. \end{aligned} \quad (77)$$

It is apparent from (76) that all radions are coupled by the dilatonic factors. When exhibiting all fields explicitly we obtain

$$\begin{aligned} L^{(2)} &= -\frac{1}{2} e^{2\sum_k \xi_k} \eta^{\alpha\beta} \phi_{\alpha\beta} - \frac{1}{2} e^{2\sum_k \xi_k} \sum_{j=1}^J \eta^{\alpha\beta} (\xi_j)_\alpha (\xi_j)_\beta - e^{2\phi} \sum_{j=1}^J U_j(\xi_j), \\ &= e^{2\sum_k \xi_k} \eta^{\alpha\beta} \phi_\alpha \sum_{j=1}^J (\xi_j)_\beta - \frac{1}{2} e^{2\sum_k \xi_k} \sum_{j=1}^J \eta^{\alpha\beta} (\xi_j)_\alpha (\xi_j)_\beta - e^{2\phi} \sum_{j=1}^J U_j(\xi_j), \end{aligned} \quad (78)$$

which is the generalization of the Lagrangian previously found for  $J = 1$ , see eq. (30). Note that a substitution rule analogous to (29)

$$\phi_{\alpha\alpha} e^{2\sum_k \xi_k} \longrightarrow -2\phi_\alpha \sum_{j=1}^J (\xi_j)_\alpha e^{2\sum_k \xi_k}, \quad (79)$$

has been used in passing from the first line to the second in (78). The equations of motion are as follows;  $\partial_\alpha \frac{\partial L^{(2)}}{\partial \phi_\alpha} = \frac{\partial L^{(2)}}{\partial \phi}$  is

$$e^{2\sum_k \xi_k} \eta^{\alpha\beta} \left[ 2 \left( \sum_k (\xi_k)_\alpha \right) \left( \sum_k (\xi_k)_\beta \right) + \sum_k (\xi_k)_{\alpha\beta} \right] = -2e^{2\phi} \sum_k U_k(\xi_k), \quad (80)$$

and  $\partial_\alpha \frac{\partial L^{(2)}}{\partial (\xi_j)_\alpha} = \frac{\partial L^{(2)}}{\partial \xi_j}$  are

$$e^{2\sum_k \xi_k} \eta^{\alpha\beta} \left[ \phi_{\alpha\beta} - (\xi_j)_{\alpha\beta} - 2(\xi_j)_\alpha \left( \sum_k (\xi_k)_\beta \right) + \sum_k (\xi_k)_\alpha (\xi_k)_\beta \right] = -e^{2\phi} U'_j(\xi_j). \quad (81)$$

The absence of perturbations should be a solution of the previous equations. We can verify this requirement by substituting  $\xi_j = 0$  in (81):

$$-\eta^{\alpha\beta}\phi_{\alpha\beta}e^{-2\phi} = U'_j(0) = \lambda, \quad (82)$$

which is the cosmological solution previously obtained (16),(55). Using eq. (77), eq. (82) is reduced to

$$U'_j(0) = K_j - 2\left(\frac{Q_j K_j}{4\pi}\right)^2 = \lambda, \quad (83)$$

that is, exactly equation (59) determining the curvatures. By substituting  $\xi_j = 0$  in (80) we obtain

$$\sum_j U_j(0) = 0 \quad \Rightarrow \quad \frac{1}{2} \sum_j \left[ \frac{\Lambda}{J} - \frac{K_j}{2} - \frac{\lambda}{2} \right] = 0, \quad (84)$$

which is exactly equation (58). Thus, both equations (83),(84) are the correct, unperturbed ones.

At this point, we proceed as in subsection 2.2 by fixing the cosmological background  $\phi$  by means of (82). This fixing is equivalent to neglecting the backreaction of the perturbations  $\xi_j$  on the cosmology  $\phi$ . This being done,  $\phi$  is not a degree of freedom anymore, and the variation of the Lagrangian  $L^{(2)}$  in (78) with respect to  $\phi$  is meaningless. This background fixing step can also be viewed as solving equation (80) to zeroth order. In this approximation, the multi-radion field moves in a fixed cosmological background and its evolution is determined by equation (81).

We now turn to the analysis of equation (81). It is a strongly coupled, nonlinear system of equations with only one known solution,  $\xi_j = 0$ , which gives rise to the landscape under study. There is no hope of finding a nontrivial solution to this system; nevertheless, we are only interested in a description of the stability of the trivial solution.

To this end, we substitute (82) back to equation (81), obtaining

$$-e^{-2\phi}\eta^{\alpha\beta}\left[(\xi_j)_{\alpha\beta} + 2(\xi_j)_\alpha\left(\sum_k(\xi_k)_\beta\right) - \sum_k(\xi_k)_\alpha(\xi_k)_\beta\right] = \lambda - e^{-2\sum_k\xi_k}U'_j(\xi_j). \quad (85)$$

The derivative couplings appear in a quadratic form. The linear stability analysis allows us to approximate the system of equations by Taylor-expanding to first order the right-hand side of equation (85) and neglecting the quadratic derivative couplings, thus considering the much simpler linear system (written in matrix form)

$$-e^{-2\phi}\eta^{\alpha\beta}\xi_{\alpha\beta} = -H\xi. \quad (86)$$

We have used the symbol  $\xi$  to denote the  $J$ -component column vector of the perturbations  $\xi_j$ , and the frequency matrix  $H$  is given by

$$H_{jk} = \left. \frac{\partial}{\partial\xi_k} e^{-2\sum_\ell\xi_\ell}U'_j(\xi_j) \right|_{\xi=0} = 2[(K_j - 2\lambda)\delta_{jk} - \lambda], \quad (87)$$

that is,

$$H = 2 \begin{pmatrix} K_1 - 3\lambda & -\lambda & \cdots & -\lambda \\ -\lambda & K_2 - 3\lambda & \cdots & -\lambda \\ \vdots & \vdots & \ddots & \vdots \\ -\lambda & -\lambda & \cdots & K_J - 3\lambda \end{pmatrix}. \quad (88)$$

The linear stability condition is therefore that all eigenvalues of the matrix  $H$  should be positive. We will call  $\kappa$  the minimum eigenvalue of  $H$ , so that the stability criterion is simply

$$\kappa > 0. \quad (89)$$

In order to complete the linear stability analysis we should justify the neglecting of the derivative couplings. These non-linear terms have a generically negative sign<sup>4</sup>, as opposed to a positive sign characteristic of a dissipative force, and thus they could be interpreted as an “anti-dissipative” force. It is legitimate to ask if these non-linear terms can spoil the linear stability of the solution.

It turns out that these nonlinear terms do not spoil the linear stability criterion (89) as long as the amplitude of the perturbation is sufficiently small. The magnitude of the threshold and the corresponding heuristic argument leading to these conclusions, not being central to this discussion, have been placed in appendix A.

The exact computation of the spectrum of  $H$  is not possible in the general case. Therefore, we cannot derive a formula  $\kappa(\lambda)$  to quickly establish the stability of a state. As a result, the computation of  $\kappa$  should be done numerically on each individual state. Nevertheless, we can obtain some general stability results by computing the determinant of  $H$ , a task which can be done as follows.

Firstly we note that if all  $K_j$  are equal, the determinant of  $H$  would be (we drop from now on the unimportant factor 2 of  $H$ ) the characteristic polynomial of the matrix

$$B = \begin{pmatrix} 3\lambda & \lambda & \cdots & \lambda \\ \lambda & 3\lambda & \cdots & \lambda \\ \vdots & \vdots & \ddots & \vdots \\ \lambda & \lambda & \cdots & 3\lambda \end{pmatrix}. \quad (90)$$

This matrix has an eigenvalue  $2\lambda$  with degeneracy  $(J-1)$  and a simple eigenvalue  $(J+2)\lambda$ . Its characteristic polynomial is

$$\det(K\mathbb{1} - B) = [K - (J+2)\lambda] \prod_{j=1}^{J-1} (K - 2\lambda). \quad (91)$$

Specializing the variable  $K$  at a single curvature value  $K_j$  would give the determinant of  $H$  if all curvatures were equal to  $K_j$ . This is not the value of the determinant we are seeking;

---

<sup>4</sup>Note that the derivative couplings appear in a quadratic form having all negative eigenvalues except for one, see the paragraph following equation (175) in appendix A.

but we can form a permutation-invariant superposition of all those expressions:

$$\det H = \frac{1}{J} \sum_{i=1}^J [K_i - (J+2)\lambda] \prod_{\substack{j=1 \\ j \neq i}}^J (K_j - 2\lambda). \quad (92)$$

The factor  $1/J$  comes from a normalization condition. This turns out to be the correct expression for the determinant of  $H$ , and it is straightforwardly transformed in the characteristic polynomial of  $H$ .

$$\det(H - \mu \mathbb{1}) = \frac{1}{J} \sum_{i=1}^J [K_i - \mu - (J+2)\lambda] \prod_{\substack{j=1 \\ j \neq i}}^J (K_j - \mu - 2\lambda). \quad (93)$$

Nevertheless, the computation of its roots is not possible in general.

Based on expression (93), it follows that whenever  $\lambda < 0$  the determinant  $\det H$  is positive, and furthermore  $\det(H - \mu \mathbb{1})$  cannot vanish at a negative value of  $\mu$ , and thus the stability eigenvalue should be positive. As a result, *all AdS states of the model are stable*.

Another case worth investigating is those states which have at least a vanishing quantum number  $n_j = 0$ . The corresponding  $K_j^{(+)}$  curvature is not defined in this case, because equation (59) is linear and it has only the solution  $K_j^{(-)} = \lambda$ . Thus, we can substitute  $K_j = \lambda + \delta_j$  ( $\delta_j > 0$ ) in  $\det H$ . Assuming we can vary independently  $\lambda$  and  $\delta_j$ , we can expand  $\det H$  for small  $\lambda$  values:

$$\det H \xrightarrow{\lambda \rightarrow 0} \prod_{i=1}^J \delta_i - 2\lambda \sum_{i=1}^J \prod_{\substack{j=1 \\ j \neq i}}^J \delta_j + \mathcal{O}(\lambda^2). \quad (94)$$

The previous expression shows again that a negative value value of  $\lambda$  cannot make this determinant to change sign. A positive value indeed can change the sign in the determinant, and this indicates that de Sitter states are likely to be unstable. Of course no general statement of this sort can be formulated, because this depends on the magnitude of  $\lambda$  as well as on all  $\delta_j$ : for sufficiently small  $\lambda > 0$  and fixed  $\delta_j$ , the determinant can be positive. But if a *single*  $\delta_k = 0$ , then the determinant reduces to

$$\det H \xrightarrow{\lambda \rightarrow 0} -2\lambda \prod_{\substack{j=1 \\ j \neq k}}^J \delta_j + \mathcal{O}(\lambda^2), \quad (95)$$

which is certainly negative for  $\lambda > 0$ ! Thus, we conclude that an odd number of eigenvalues of  $H$  have changed their signs and the state is unstable. We can suspect that in this case a single eigenvalue has reversed sign, because if we would take two vanishing  $\delta_k$  the sign of the determinant would again be positive. We can see that if all  $\delta_j = 0$ ,  $H$  has a completely negative spectrum. Thus we can expect that the vanishing of each  $\delta_j$  changes sign of an eigenvalue, and thus *all states with some  $n_j = 0$  are unstable*.

The previous reasoning is heuristic, because we cannot assume that  $\lambda$  and  $\delta_j$  vary independently. They depend on the discrete numbers  $\{n_1, \dots, n_J\}$  and thus the stability criterion should be validated numerically. Nevertheless, heuristics works in this case. As it is shown in the following subsection, all states with a single  $n_j = 0$  are unstable, at least in all searches we have carried out.

We will close this subsection by giving a perturbative argument showing that all low- $\lambda$  states lying in all non-principal branches are unstable. This way, the principal branch remains as the only source of AdS and stable dS states. We begin by splitting the  $H$  matrix (88) as follows:

$$H = 2 \operatorname{diag}\{K_1 - 2\lambda, \dots, K_J - 2\lambda\} - 2\lambda U, \quad (96)$$

where  $U$  is a  $J \times J$  matrix filled with ones. If  $\lambda$  is small, we can consider the diagonal matrix as a “dominant” term and the off-diagonal terms as a perturbation. The perturbation is permutation-invariant, and thus all eigenvalues of the diagonal matrix are shifted the same amount. The perturbative stability eigenvalue is

$$\kappa = 2 \left[ \min_j K_j - 3\lambda \right]. \quad (97)$$

If the minimum curvature is taken from the (+) branch, then  $K_j^{(+)} \xrightarrow{\lambda \rightarrow 0} \frac{2}{n_j^2}$  and the state has a chance of being stable. But if some curvature is taken from a (-) branch, then we have  $K_j^{(-)} \xrightarrow{\lambda \rightarrow 0} \lambda$  and the corresponding eigenvalue is negative. But then  $\kappa$  should be negative also, showing that no matter how small  $\lambda$  might be, if the state comes from a non-principal branch, it will be unstable.

The previous argument does not rule out the existence of higher  $\lambda$  stable dS states in non-principal branches, but our numerical searches have not found them.

### 3.3 State searching in concrete examples

Once the analysis of the model is reasonably complete, we should ask for concrete examples where we can exhibit some states and their associated magnitudes such as reduced cosmological constant  $\lambda$ , curvatures  $K_i$  and the stability eigenvalue  $\kappa$ .

We repeat here the relevant equations for the reader’s convenience. Given a  $J$ -tuple of integers  $\{n_1, \dots, n_J\}$  we compute the solutions of equation (68), which is

$$L_{\{s_j\}, \{n_j\}}(\lambda) = \Lambda, \quad \text{with} \quad L_{\{s_j\}, \{n_j\}}(\lambda) = \frac{1}{2} \left[ J\lambda + \sum_{j=1}^J \frac{1}{n_j^2} \left( 1 + s_j \sqrt{1 - 2\lambda n_j^2} \right) \right]. \quad (98)$$

All solutions for each branch  $\{s_1, \dots, s_J\}$ , where the  $s_j$  are signs  $\pm 1$ , should be computed. The corresponding solutions must be real, and all its curvatures must be real and positive:

$$K_j^{(s_j)} = \frac{1}{n_j^2} \left( 1 + s_j \sqrt{1 - 2\lambda n_j^2} \right). \quad (99)$$



If a single curvature turns out to be real and negative or complex, then the state should be discarded. If all curvatures are positive, we form the frequency matrix  $H$  (dropping the unimportant factor 2 which appears in (88)) and compute its minimum eigenvalue  $\kappa$ , called the *stability eigenvalue* of the state:

$$H = \begin{pmatrix} K_1 - 3\lambda & -\lambda & \cdots & -\lambda \\ -\lambda & K_2 - 3\lambda & \cdots & -\lambda \\ \vdots & \vdots & \ddots & \vdots \\ -\lambda & -\lambda & \cdots & K_J - 3\lambda \end{pmatrix}, \quad \kappa = \min_{\mu \in \text{spec}(H)} \mu. \quad (100)$$

The stability condition is simply  $\kappa > 0$ .

Thus, the searching method has the following steps:

1. Choose  $J$  and  $\Lambda$ , the parameters of the model.
2. Choose a set of integers  $\{n_1, \dots, n_J\}$ .
3. Solve equation (98) for  $\lambda$ .
4. Compute the curvatures (99) associated with the solutions found and accept the state if all curvatures are real and positive.
5. Compute the stability eigenvalue and flag the state as stable or unstable.
6. Go to step 2 until some bounding search criterion is met.

The choosing of the integers can be done in various ways. In the simplest models with  $J = 2^5$  we can scan a large square in the  $(n_1, n_2)$  plane in a brute-force search. In this way we cannot miss any state. The symmetries  $n_1 \leftrightarrow n_2$  and  $n_j \rightarrow -n_j$  allow us to restrict to  $n_2 \geq n_1 \geq 0$ . This brute-force method cannot be used for higher values of  $J$ . In those cases, we should generate states randomly in an efficient manner; but prior to the discussion on how this is done, we present some results in the  $J = 2$  case.

We have chosen two values of the 4D cosmological constant  $\Lambda$ , 0.01 and 0.005, in order to exhibit how the lowering of  $\Lambda$  causes the proliferation of states. In figure 3 we plot a point in each place of the  $(n_1, n_2)$  plane where a state has been found; of course, we have four branches for searching, so some states overlap here. States with negative and positive 2D cosmological constant have been separated, so that we can see AdS states at left panels and dS states at right panels. Stable states have been drawn using circles, and diamonds for unstable states. Note that all AdS states are stable, while most dS states are unstable. The colors are related with the magnitude of the cosmological constant as shown in the legend of each graphic.

Features of these models which can be seen in figure 3 include:

---

<sup>5</sup>The two-sphere Einstein-Maxwell landscape is a sector of the six-dimensional Einstein-Maxwell not considered in Refs. [34, 36].

- All AdS states are stable.
- There is no AdS states with  $n_1 = 0$  or  $n_2 = 0$  because in those cases there is no curvature associated with this branch.
- All dS states with  $n_1 = 0$  or  $n_2 = 0$  are unstable, as expected by the heuristic argument exhibited at the end of the previous subsection.
- There is a curve which limits the existence both of dS and AdS states. The form of this curve is easily computed by substituting  $\lambda = 0$  in equation (98) with all positive  $s_j$ :

$$\sum_{j=1}^J \frac{1}{n_j^2} = \Lambda. \quad (101)$$

Minkowski states, which ideally may be present, lie on this hypersurface which will be called *branching hypersurface* (curve in the  $J = 2$  case). In practice, Minkowski states require fine-tuning of  $\Lambda$  and thus they are generically absent.

- All dS states are located *above* AdS ones, and they are located near the branching curve. The discrete states are located on a multi-branch surface whose branches meet at the branching curve, hence its name. Thus, states of  $\lambda$  near zero from either side are located near this curve, which would contain, if present, the  $\lambda = 0$  states.
- All stable dS states are located near the branching curve, and only there, but closeness is not enough for a state to be stable, as will be seen below.

A feature of these models which cannot be seen in figure 3 is that all AdS states come from the  $\{+, +\}$  branch (which will be called the *principal branch*). This is so because the solutions in the remaining branches have the  $K_j^{(-)}$  curvatures negative, as can be seen in formula (99). Thus, only the principal branch is a source of AdS states.

In contrast, dS states can come from each of the four branches, but each branch brings in states with very different properties. For example, all dS states near the branching curve come from the principal branch. In particular, all stable dS states come from this branch. The bunch of dS states lying in the reddish square in the right panels of figure 3 come from the  $\{-, -\}$  branch, and they are “most” unstable in the sense that they have the greater (in absolute value) negative stability eigenvalue. All these features can be seen in the left panels in figure 4. These left panels show cosmological constant versus curvature, and they exhibit clearly the different nature of the states coming from different branches:

- The states coming from the principal branch (bullets) form the core of the figure, and at the bottom of this figure are located the stable states, all of them coming from the principal branch. Note that stability does not mean lower cosmological constant! In the right panels of figure 4 we can see that stable states are mixed with unstable ones in the cosmological constant value distribution. Nevertheless, all lowest-lying states are stable.

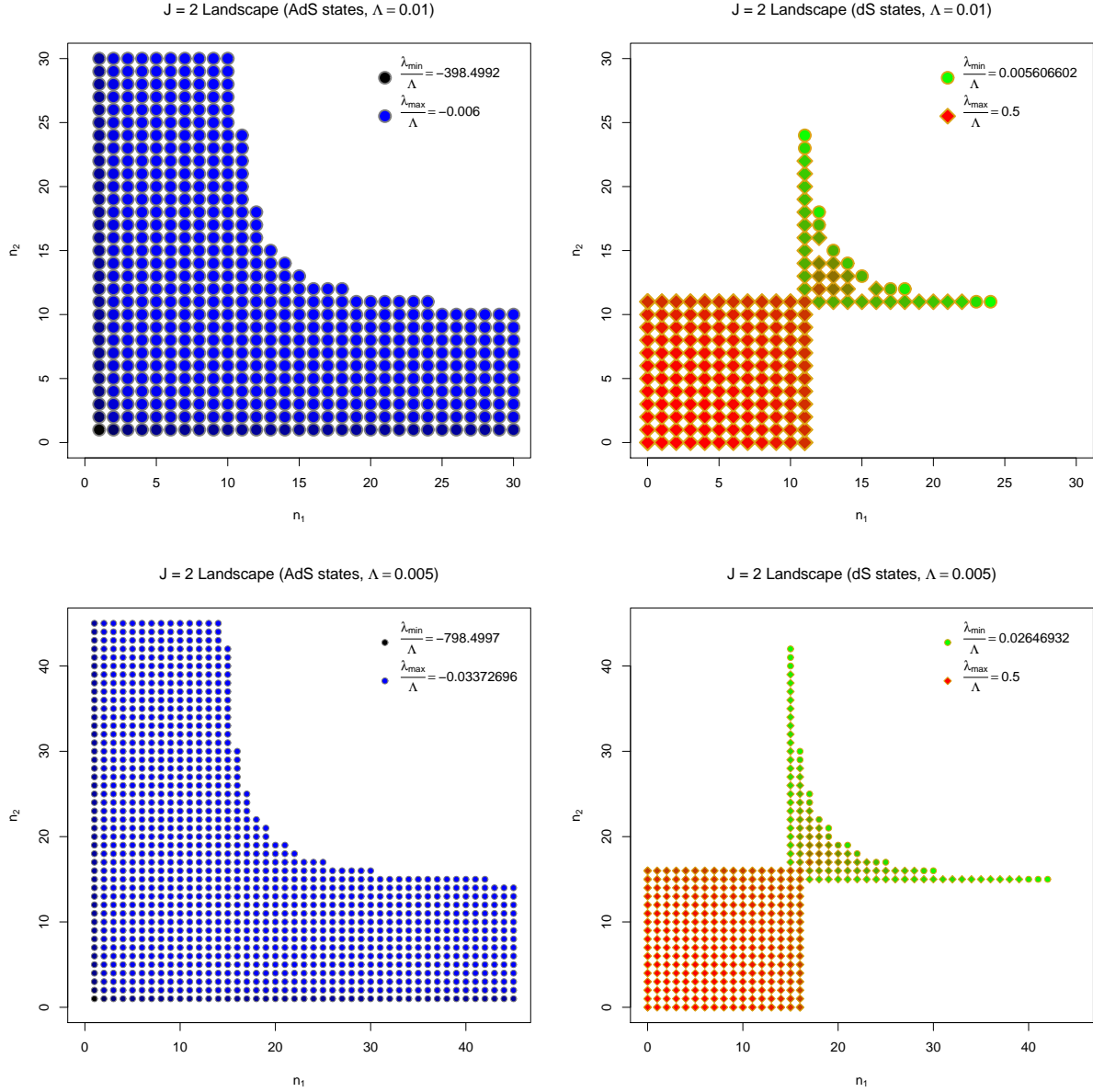


Figure 3: Landscape examples with  $\Lambda = 0.01$  (top panels) and  $\Lambda = 0.005$  (bottom panels). AdS (left) and dS (right) states are shown, using a circle for a stable state and a diamond for a unstable one. A state is drawn if a solution has been found for  $\lambda$  with real and positive curvatures. The magnitude of  $\lambda$  is reflected in the color of each symbol. Finally, all dS states lie above AdS ones, and meet at the branching curve, beyond which the landscape has no states.

- The states coming from the  $\{+, -\}$  and  $\{-, +\}$  branches are at both sides of the triangle-shaped graphic shown at the left panels of figure 4. All of them are unstable, but the values of the cosmological constant in this subset range from lowest to highest.
- The states coming from the  $\{-, -\}$  branch are located at the cusp of the triangle (figure 4, left panels) and all of them have the highest values of the cosmological constant and also the highest (in absolute value) negative stability exponents (see figure 5). In particular, the  $n_1 = 0, n_2 = 0$  state, which is the cusp of the triangle, belongs to the  $\{-, -\}$  branch.

In the right panels of figure 4 we can see the cosmological constant distribution of dS states. The contribution of the branches can be seen as different peaks; while the principal branch contributes with the stable states and other unstable distributed in the lowest range, the  $\{+, -\}$  and  $\{-, +\}$  show two peaks in the low and middle range, and the bulk of the  $\{-, -\}$  states are relegated to the high range.

Finally, in figure 5 is shown the behaviour of the cosmological constant versus the stability eigenvalue. Its almost linear relation can be seen to be dispersed in branches, which are the same structures showing up in left panels of figure 4. Here, we can see that the states with lower cosmological constant have a “less negative” stability eigenvalue than the states with higher  $\lambda$ , which include the  $\{-, -\}$  states, as said above.

Thus, the different branches provide very different states. Among them, the most interesting seem to be those coming from the principal branch, because they include AdS as well as stable and unstable dS states, which are the ingredients we need to construct a toy model of a multiverse.

For  $J > 2$ , we can exploit the fact that stable dS states are near the branching hypersurface (it is a curve only for  $J = 2$ ) and design a sampling method which looks for states in  $(n_1, \dots, n_J)$  space whose Voronoi cell (which is the cube with its center at the point in question) intersects the branching hypersurface. Those states are called *secant* states [50, 51], and all states near the branching surface belong to this category (but the reciprocal is false, that is, a secant state may not be near the branching surface if  $J$  is large enough!). Thus, we can sample the principal branch by sampling the secant states. In this way, we always find a state with a fair chance of being a true state of the model in the principal branch, that is, we have an efficient sampling method, much better than brute-force node enumeration or completely random node sampling.

The sampling of secant states is simple: we choose a uniformly random direction in  $J$ -space and find the point of intersection between the ray having the chosen direction starting from the origin and the branching hypersurface. This intersection point belongs to the Voronoi cell of a single secant state, which we find by rounding the coordinates of the intersection point. Once we have the state, we solve the equation for  $\lambda$  in the principal branch and follow the steps detailed above.

In the following section we use this sampling method to obtain a sample of the cosmological constant distribution which can be compared with an approximate formula to be obtained below.

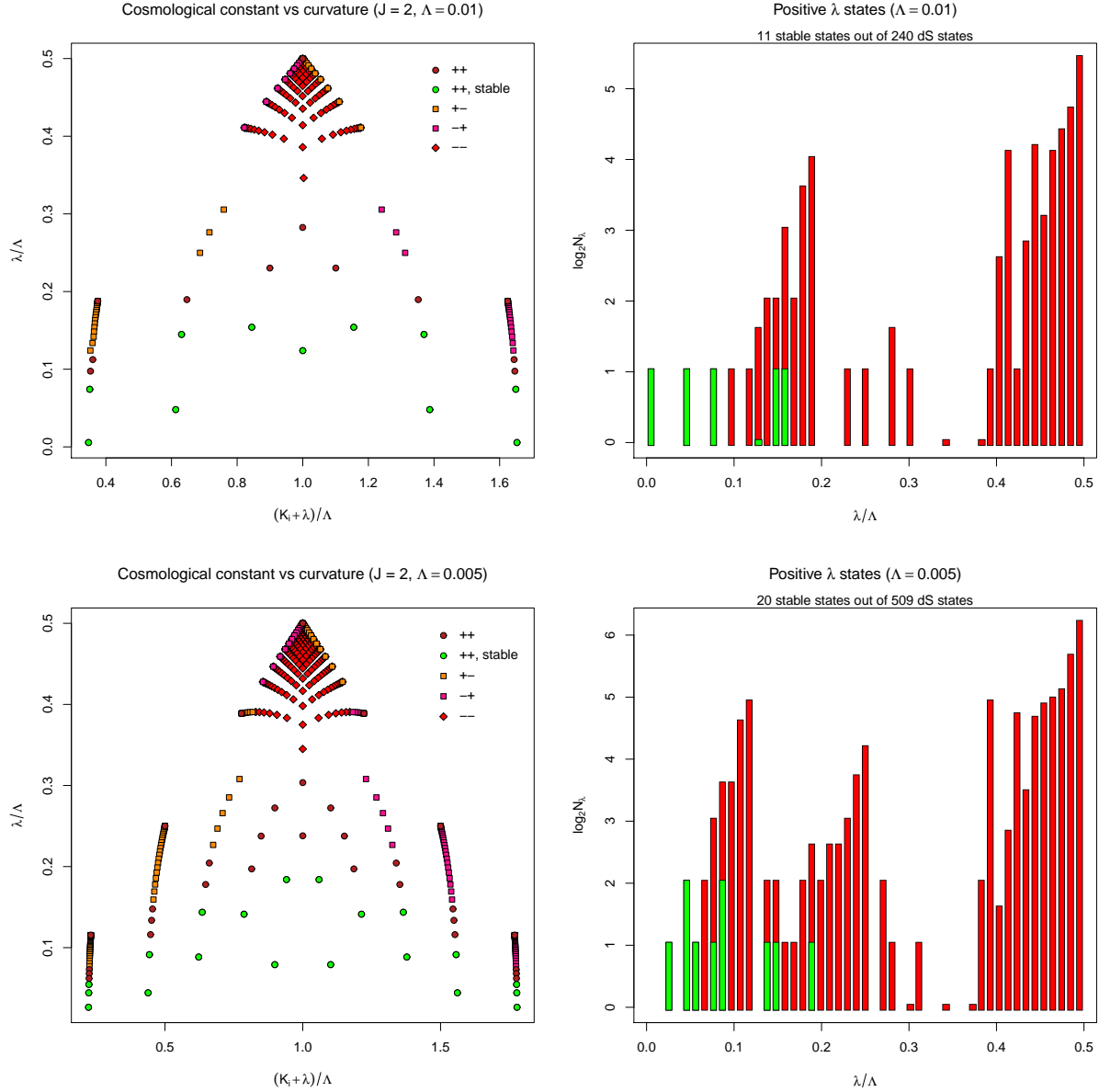


Figure 4: Landscape examples with  $\Lambda = 0.01$  (top panels) and  $\Lambda = 0.005$  (bottom panels). Left panels show the variation of the cosmological constant  $\lambda$  with curvature. These triangle-shaped graphics show structures which the states seem to follow, and clearly separates the different branches by the  $\lambda$  values they provide. Right panels show the  $\lambda$  distributions of dS states, whose peaks come from the different branches. The only branch that has not a peak associated to it is the principal branch, which provides all stable dS states.

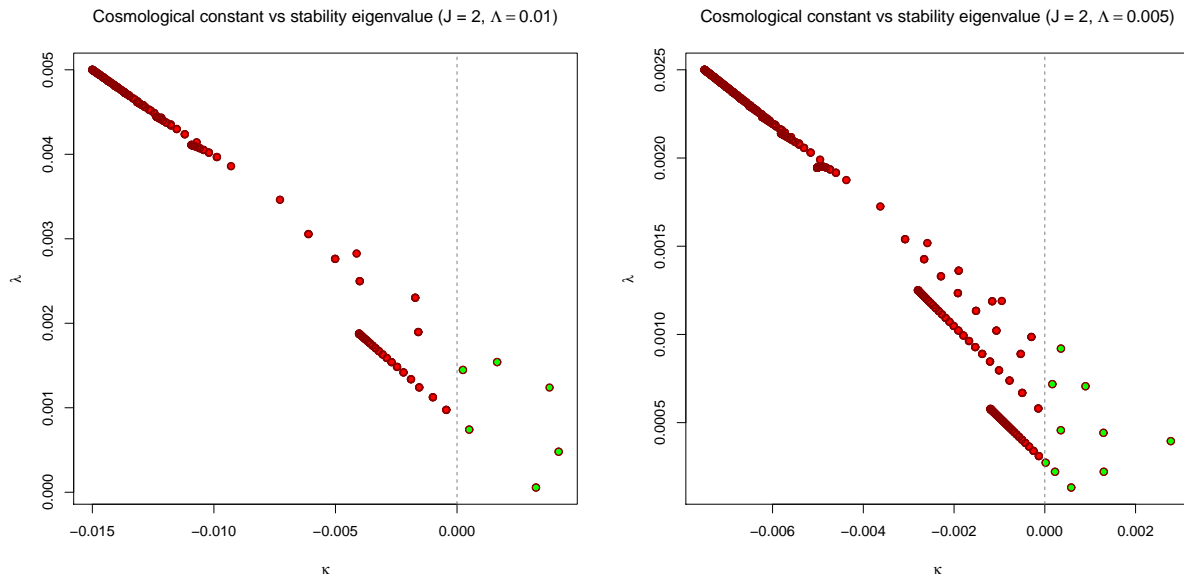


Figure 5: Landscape examples with  $\Lambda = 0.01$  (left panel) and  $\Lambda = 0.005$  (right panel). Dependence of the cosmological constant versus the stability eigenvalue is shown, with an almost linear behaviour. Stable states are located to the right of the vertical dashed line, which is thus the onset of stability.

## 4 State counting

As we have seen in the previous section, the states of the multi-sphere Einstein-Maxwell landscape can come from different branches, and the richest of those branches is the principal one. In this section we turn to the problem of counting states on this branch. Our main aim is to compute the distribution of cosmological constant values in this branch.

As discussed above, only the principal branch can have both AdS and dS states, both stable and unstable, and moreover the large- $J$  sampling method is especially adapted to the principal branch. Therefore, we can obtain samples to compare with the approximate formula to be obtained in subsection 4.2 below.

### 4.1 Counting states in the principal branch

Given a node  $n = (n_1, \dots, n_J)$  in  $J$ -space, there exists a state in the principal branch of the multi-sphere Einstein-Maxwell landscape with cosmological constant  $\Lambda$  if the equation

$$L_n(\lambda) = \Lambda \tag{102}$$

has a solution in  $\lambda$ . The principal branch  $L_n$  function is given in (98) with all positive signs  $s_j = +$ . In the principal branch there are no states with some  $n_j = 0$ , and thus the function  $L_n(\lambda)$  has a maximum at  $\lambda = 0$  and it is monotonically decreasing from  $\lambda = 0$

to  $\lambda = \lambda_b$ , where  $\lambda_b$ , see equation (69), is the branching point of the node  $n$ . A dS state exists therefore if  $\Lambda$  is between the two extremal values of the  $L_n(\lambda)$  function:

$$L_n(\lambda_b) \leq \Lambda \leq L_n(0). \quad (103)$$

Equation (103) is the existence condition for a dS state at node  $n$  in the principal branch. The corresponding equalities define two surfaces in node space: The *branching surface*

$$L_n(0) = \sum_{j=1}^J \frac{1}{n_j^2} = \Lambda, \quad (104)$$

whose integer points, if any, have vanishing  $\lambda$ , and the *limiting surface*

$$L_n(\lambda_b) = \frac{J}{4n_{\max}^2} + \frac{1}{2} \sum_{j=1}^J \frac{1}{n_j^2} \left( 1 + \sqrt{1 - \frac{n_j^2}{n_{\max}^2}} \right) = \Lambda, \quad (105)$$

which signals the end of the principal branch. In terms of a characteristic function, the existence condition is

$$\chi_{[L_n(\lambda_b), L_n(0)]}(\Lambda) = \begin{cases} 1 & \text{if a state exists at } n, \\ 0 & \text{if a state does not exist at } n. \end{cases} \quad (106)$$

The previous existence condition should be supplemented with the stability condition (89), that is,  $\kappa(n) > 0$ , where  $\kappa(n)$  is the minimum eigenvalue of the stability matrix  $H$  at node  $n$  if a state exists there. This stability condition can also be ascribed to a surface (the *stability surface*) signaling the stability threshold. The stability surface should be comprised between the branching and limiting surfaces; unfortunately, the analytic expression of it cannot be found for general  $J > 1$ . As a consequence, we will represent this condition by adding the factor  $\theta(\kappa(n))$  to the existence condition. Therefore, the exact number of stable states with given  $\Lambda$  in the principal branch of the multi-sphere EM landscape is

$$\mathcal{N}_J(\Lambda) = \sum_{\substack{n \in \mathbb{Z}^J \\ n_j \neq 0}} \chi_{[L_n(\lambda_b), L_n(0)]}(\Lambda) \theta(\kappa(n)). \quad (107)$$

The exact evaluation of the previous expression is possible only for  $J = 1$  as is showed in subsection 2.2, equation (41). We repeat it here for the reader's convenience, omitting from it AdS states and setting  $e = 1$ :

$$\mathcal{N}_1(\Lambda) = \left\lfloor \frac{1}{\sqrt{\Lambda}} \right\rfloor - \left\lfloor \frac{2\sqrt{2}}{3\sqrt{\Lambda}} \right\rfloor + 1 \approx \frac{1}{\sqrt{\Lambda}} \left( 1 - \frac{2\sqrt{2}}{3} \right). \quad (108)$$

We will shortly turn into the approximate evaluation of (107). But prior to that, we need to grasp some general ideas on the structure of the stable state set which we are willing to count.

We will emphasize two main aspects: asymptotic hyperplanes and state chains.

**Asymptotic hyperplanes** Both equations (104) and (105) corresponding to the branching and limiting surfaces, and likewise the stability surface, have asymptotic hyperplanes located at

$$|n_j| = \frac{1}{\sqrt{\Lambda}} \quad (\text{for fixed } j), \quad |n_{k \neq j}| \rightarrow \infty, \quad (109)$$

and thus all states are restricted to the region

$$|n_j| > \frac{1}{\sqrt{\Lambda}} = \nu_0 \quad (1 \leq j \leq J). \quad (110)$$

Therefore, all dS states should have a charge greater than  $\nu_0$  as a necessary condition. Note that no integer  $n_j$  can be equal to  $\nu_0$  while preserving the existence condition unless all the remaining integers  $n_{i \neq j}$  are infinite, hence the name ‘‘asymptotic’’. It is easy to see that the corresponding states would have  $\lambda = 0$  and all curvatures vanishing except for one, and thus they would not represent compactified states. Moreover, the associated stability matrix has  $J - 1$  zero eigenvalues (see eq. (100)), and thus these states are only marginally stable. These properties suggest that they should be excluded from the landscape.

**State chains** There is also a natural upper bound on the charge, which can be obtained by considering the following straight line in flux space:

$$n_1 = \dots = n_{J-1} = \sqrt{\frac{J-1}{\Lambda}}, \quad n_J \in \mathbb{R} \quad (\text{free parameter}). \quad (111)$$

The previous line is asymptotic to the branching surface, in the sense that it satisfies equation (104) when  $n_J \rightarrow \infty$ . This line do not contain nodes because the quotient  $\sqrt{\frac{J-1}{\Lambda}}$  is generically not an integer. But we can slightly modify the previous line:

$$n_1 = \dots = n_{J-1} = \left\lceil \sqrt{\frac{J-1}{\Lambda}} \right\rceil = \nu_1, \quad n_J \in \mathbb{R} \quad (\text{free parameter}). \quad (112)$$

This modified line can contain valid states if  $n_J$  lies between  $\lceil \nu_0 \rceil$  and  $\nu_2$ , where  $\nu_2$  is the intersection height with the branching surface:

$$\nu_2 = \frac{\nu_1}{\sqrt{\Lambda \nu_1^2 - (J-1)}}. \quad (113)$$

All states on the line above  $\nu_2$  are beyond the branching surface. Therefore, we have the bound  $\nu_0 < n_j < \nu_2$  ( $1 \leq j \leq J$ ). All states which might happen to lie on this line are said to form a *state chain*.

It should be noted that when  $\sqrt{\frac{J-1}{\Lambda}}$  coincides with the integer  $\nu_1$ , then  $\nu_2$  diverges, which at first sight would be interpreted as an infinite dS state chain of ever decreasing



$\lambda$ . But those nodes in the chains have no states, as can be seen by explicitly writing equation (102) for the nodes in the line (112), and look for solutions with small  $\lambda$  and large  $n_J$ :

$$2\Lambda = J\lambda + (J-1)\frac{1 + \sqrt{1 - 2\lambda\nu_1^2}}{\nu_1^2} + \frac{1 + \sqrt{1 - 2\lambda n_J^2}}{n_J^2}, \quad (114)$$

We can consider  $\lambda \ll \frac{1}{\nu_1^2}$ , but  $\lambda \ll \frac{1}{2n_J^2}$  is not true, because  $n_J$  is large. Therefore, equation (114) can be rewritten as

$$2\Lambda - \frac{2(J-1)}{\nu_1^2} - \lambda = \frac{1 + \sqrt{1 - 2\lambda n_J^2}}{n_J^2}. \quad (115)$$

The right hand side of (115) is positive, thus a solution to equation (115) can exist only if  $\Lambda - \frac{J-1}{\nu_1^2}$  is strictly positive, which leads to

$$\nu_1 = \left\lceil \sqrt{\frac{J-1}{\Lambda}} \right\rceil > \sqrt{\frac{J-1}{\Lambda}}, \quad (116)$$

that is, if  $\sqrt{\frac{J-1}{\Lambda}}$  is an integer then there is no solution to equation (115). As a consequence,  $\nu_2$  can be made as large as we want by fine-tuning  $\Lambda$  but it is never infinite. This argument shows that all state chains are finite.

This discussion on the state chains can be generalized to other asymptotic affine manifolds that the branching surface can have. For instance, asymptotic hyperplanes (109), as we have seen above, are likewise devoid of states, but there are close hyperplanes (having nodes) each one containing a replica of a  $(J-1)$ -dimensional landscape.

We will now consider the evaluation of the number of stable states  $\mathcal{N}_J(\Lambda)$ . Firstly, we get rid of the sign degeneracy  $2^J$ , which is always trivially present. Secondly, we invoke the permutation symmetry, which allows us to arrange the integers  $n_j$  in decreasing order. The corresponding permutation degeneracy is  $J!$  except on those nodes having repeated components. This difference will be ignored for simplicity; we will see below that it will be of little importance in the small- $\lambda$  region. Thirdly, we consider a node  $n = \{n_1, \dots, n_J\}$  with  $n_1 > n_2 > \dots > n_J$  and the corresponding equation for the existence of a state (102):

$$L_n(\lambda) = \frac{1}{2} \left[ J\lambda + \sum_{j=1}^J K_j(\lambda) \right] = \Lambda. \quad (117)$$

The  $L_n(\lambda)$  curve has a branching point  $\lambda_b$  given by (69), that is,  $\lambda_b = \frac{1}{2n_1^2}$ . Any approximation method we might wish to apply on the  $L_n(\lambda)$  curve should respect this branching point in order to accurately represent the existence condition. In particular, we cannot

assume  $\lambda \ll \lambda_b$ . But we do have  $n_1 > n_J = \min_j \{n_j\}$ , and in the case  $n_J \ll n_1$ , we can assume  $\lambda \ll \frac{1}{2n_J^2}$  and write

$$K_J(\lambda) \approx \frac{2}{n_J^2} - \lambda, \quad (118)$$

which leaves equation (117) as

$$\frac{1}{2} \left[ (J-1)\lambda + \sum_{j=1}^{J-1} K_j(\lambda) \right] = \Lambda - \frac{1}{n_J^2}. \quad (119)$$

Equation (119) represents the solutions of a landscape in which the  $J^{\text{th}}$  curvature has been removed, and the cosmological constant  $\Lambda$  has been replaced with  $\Lambda - \frac{1}{n_J^2}$ . We can now let  $n_J$  run from  $\lfloor \frac{1}{\sqrt{\Lambda}} \rfloor + 1$  through the diagonal node having  $n_J = \lfloor \sqrt{\frac{J}{\Lambda}} \rfloor$ , thus obtaining the recurrence law

$$\mathcal{N}_J(\Lambda) \approx J! \sum_{m=\lfloor \frac{1}{\sqrt{\Lambda}} \rfloor + 1}^{\lfloor \sqrt{\frac{J}{\Lambda}} \rfloor} \mathcal{N}_{J-1} \left( \Lambda - \frac{1}{m^2} \right). \quad (120)$$

The previous formula is valid under the following conditions:

- The fraction of states with repeated components is small.
- The cosmological constant  $\lambda$  of the states included is small, so that equation (118) can be valid.

The states near the asymptotic hyperplanes will satisfy the previous conditions more accurately, so that the first terms in the sum (120) will be more precise than the terms near the diagonal. The latter states will fail to satisfy the strong inequality  $n_J \ll n_1$ . This means that the low-lying (that is, small- $\lambda$ ) states will be taken into account, but the formula can miss or overcount some high-lying (high- $\lambda$ ) states.

Equation (108) triggers the recurrence relation, the first consequence being

$$\mathcal{N}_2(\Lambda) \approx 2 \sum_{m=\lfloor \frac{1}{\sqrt{\Lambda}} \rfloor + 1}^{\lfloor \sqrt{\frac{2}{\Lambda}} \rfloor} \left\{ \left\lfloor \frac{1}{\sqrt{\Lambda - \frac{1}{m^2}}} \right\rfloor - \left\lfloor \frac{2\sqrt{2}}{3\sqrt{\Lambda - \frac{1}{m^2}}} \right\rfloor + 1 \right\}. \quad (121)$$

The previous equation can be approximated by a smoother version by removing the floor-ceiling functions inside the sum:

$$\mathcal{N}_2(\Lambda) \approx 2 \left( 1 - \frac{2\sqrt{2}}{3} \right) \sum_{m=\lfloor \frac{1}{\sqrt{\Lambda}} \rfloor + 1}^{\lfloor \sqrt{\frac{2}{\Lambda}} \rfloor} \frac{1}{\sqrt{\Lambda - \frac{1}{m^2}}}. \quad (122)$$

The previous formula can be refined by cutting off the chains whose lower ends pass the diagonal and counting the states on the diagonal accurately. This “diagonal corrected” formula is to be used in figures 6 and 7 below.

Further simplification can be achieved by isolating the first term (which carries the discontinuities) and estimating the remaining sum by means of an integral:

$$\mathcal{N}_2(\Lambda) \approx 2 \left( 1 - \frac{2\sqrt{2}}{3} \right) \left\{ \frac{\lfloor \frac{1}{\sqrt{\Lambda}} \rfloor + 1}{\sqrt{\Lambda (\lfloor \frac{1}{\sqrt{\Lambda}} \rfloor + 1)^2 - 1}} + \int_{\frac{1}{\sqrt{\Lambda}+1}}^{\sqrt{\frac{2}{\Lambda}}} \frac{dx}{\sqrt{\Lambda - \frac{1}{x^2}}} \right\}. \quad (123)$$

Formulae (122) and (123) show clearly the effect of state chains as discontinuities at integer values of  $\frac{1}{\sqrt{\Lambda}}$ . When  $\frac{1}{\sqrt{\Lambda}}$  approaches an integer from below, a very long state chain develops which increases dramatically the number of states. When  $\Lambda$  is reduced, the number of “bulk” states, that is, those not in the chains, increases as reflected by the well-behaved integral contribution, which for  $\Lambda \ll 1$  is

$$\int_{\frac{1}{\sqrt{\Lambda}+1}}^{\sqrt{\frac{2}{\Lambda}}} \frac{dx}{\sqrt{\Lambda - \frac{1}{x^2}}} \xrightarrow{\Lambda \ll 1} \frac{1}{\Lambda} - \frac{\sqrt{2}}{\Lambda^{\frac{3}{4}}}. \quad (124)$$

Figure 6 provides a good example of the performing of equations (121), (122) and (123). These formulae are to be compared with brute-force determination of the number of stable states in the corresponding models. The discreteness of the lattice induces strong fluctuations in the actual number of states, which is well represented by formula (123), provided we interpret it as an average behaviour.

While figure 6 emphasizes the strongly discontinuous nature of the state number, we can also show the steady increase in the state number by avoiding the discontinuities. This can be done, for example, by sampling landscape models with half-integer values of  $\frac{1}{\sqrt{\Lambda}}$ . These samples never encounter large state chains and thus a regular, well-behaved curve emerges, very well described by the formulae just obtained. This smooth component of the state number is illustrated in figure 7.

We will close this subsection by summarizing the properties of formula (123) as follows:

- It accurately captures the spikes in the state number when  $\frac{1}{\sqrt{\Lambda}}$  approaches integer values from below. These spikes come from the presence of very long state chains in this regime.
- It correctly represents the main behaviour of the state number in a generic sense, that is, when  $\frac{1}{\sqrt{\Lambda}}$  is not near integer values.
- We can interpret formula (123) as an average behaviour which turn the fine details of the lattice into a smooth profile while taking into account the main discontinuities.
- Finally, the approximation formulae seem to be missing some states. The reason for this is the approximation we are using to count stable states: Equation (120)

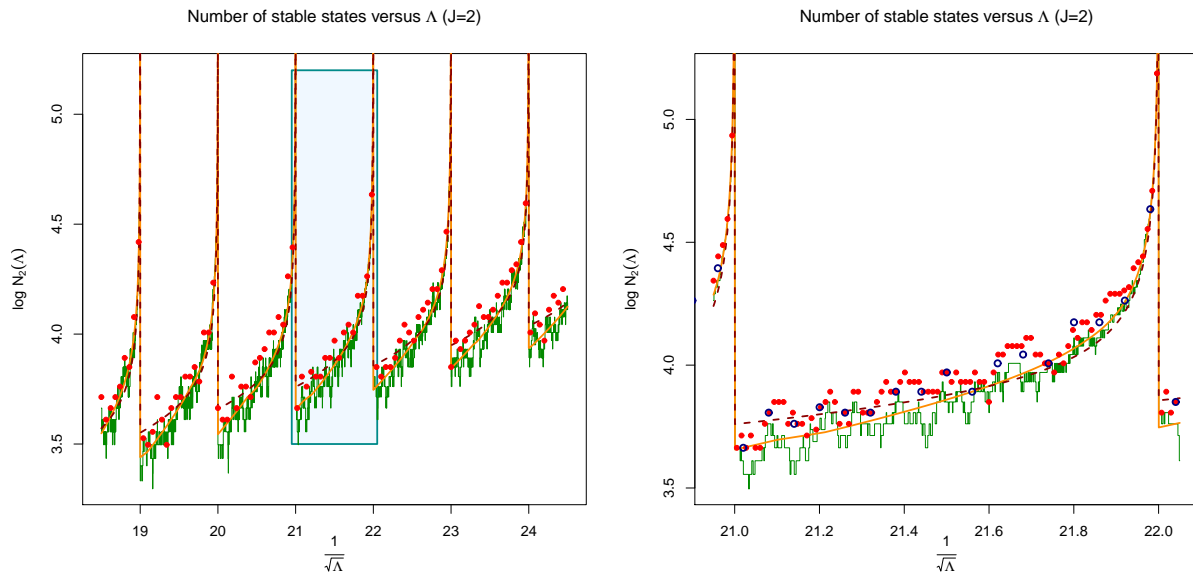


Figure 6: Number of stable dS states as a function of  $\Lambda$  for the two-sphere Einstein-Maxwell landscape. Left panel shows the strongly discontinuous variation of the state number when  $\frac{1}{\sqrt{\Lambda}}$  crosses several integer values. Bullets are brute-force computed state numbers, thin green line is the outcome of formula (121), thick solid line is formula (122) (with diagonal corrections) and thick dashed line is formula (123). Right panel shows an amplification of the small rectangle shown in left panel. Data are to be interpreted as before, with the addition of hollow bullets, which mark the data displayed in left panel. Simplified formulae seem to have an averaging effect on the lattice details, which are reflected in the fast-varying nature of the discrete formula and brute-force data.

Number of stable states versus  $\Lambda$  (J=2)

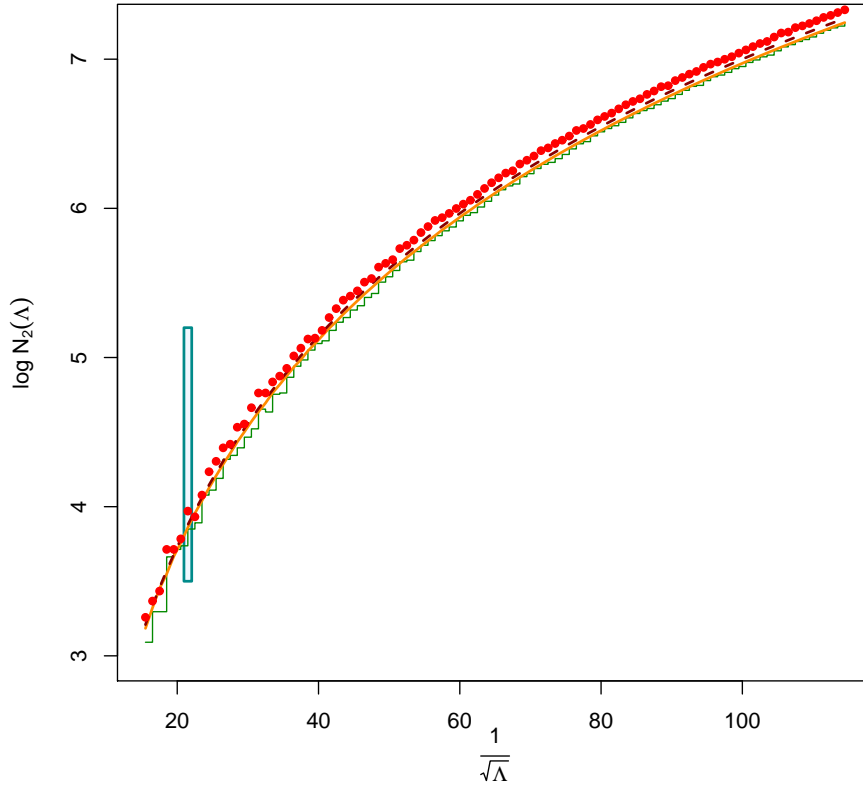


Figure 7: Number of stable dS states as a function of  $\Lambda$  for the two-sphere Einstein-Maxwell landscape. Only half-integer values of  $\frac{1}{\sqrt{\Lambda}}$  have been considered in this plot, in order to avoid the spikes shown in figure 6. Bullets are brute-force computed state numbers, thin green line is the outcome of formula (121), thick solid line is formula (122) (with diagonal corrections) and thick dashed line is formula (123). A smooth behaviour is observed, showing a very good agreement between approximate formulae and numerical searches. The narrow vertical rectangle is at the same position as the rectangle shown in figure 6 (left panel).

implies using the  $J - 1$  stability criterion to count stable states in the  $J$  model, which introduces the error. In the following subsection we will see that the missing states are located near the discontinuities of the density of states, and thus they correspond to relatively high values of  $\lambda$ . This is precisely the condition which makes (119) to break down, so this behaviour was to be expected.

## 4.2 Small cosmological constant distribution

In this subsection, we will call  $\lambda(n)$  the 1+1 cosmological constant of a stable dS state at node  $n$  (assuming the state exists), and we will denote by  $\rho$  a fixed value to be compared with  $\lambda(n)$ . With this in mind, we define the distribution function of  $\rho$  in a given multi-sphere EM landscape as the number of stable dS states whose  $\lambda(n)$  value does not exceed  $\rho$ :

$$\Omega_J(\rho, \Lambda) = \sum_{\substack{n \in \mathbb{Z}^J \\ n_j \neq 0}} \chi_{[L_n(\lambda_b), L_n(0)]}(\Lambda) \theta(\kappa(n)) \theta(\rho - \lambda(n)). \quad (125)$$

The derivative of  $\Omega_J(\rho, \Lambda)$  with respect to  $\rho$  is the density of states of the model

$$\omega_J(\rho, \Lambda) = \frac{\partial \Omega_J(\rho, \Lambda)}{\partial \rho}. \quad (126)$$

As a result of the discreteness of the landscape,  $\lambda$  values are drawn from a discrete set, and thus  $\Omega_J(\rho, \Lambda)$  is a stepwise-varying non-decreasing function of  $\rho$ , while  $\omega_J(\rho, \Lambda)$  has Dirac deltas at the values of  $\rho$  coincident with actual  $\lambda(n)$  of existing states at  $n$ . The amplitudes of the Dirac peaks are given by the degeneracies of the corresponding states. In this subsection we will obtain some analytic approximations of the density of states in the regime of small  $\lambda$ , and we will use the expressions thus obtained to study the  $\lambda$  spectrum.

We will denote by  $\lambda_{\max}$  the maximum  $\lambda$  value a state can have. Clearly, if  $\rho \geq \lambda_{\max}$  then

$$\Omega_J(\rho, \Lambda) = \mathcal{N}_J(\Lambda). \quad (127)$$

Analogously, we denote by  $\lambda_{\min}$  the minimum  $\lambda$  value a state can have. It is also clear that, if  $\rho \leq \lambda_{\min}$ , then

$$\Omega_J(\rho, \Lambda) = 0. \quad (128)$$

Thus, the interval  $[\lambda_{\min}, \lambda_{\max}]$  is the support of the density  $\omega_J$ .

The upper bound  $\lambda_{\max}$  can be computed as follows. Let us consider the gradient of the function  $\lambda(n)$  computed as if the components of  $n$  were continuous variables. We can derive equation (117) implicitly:

$$J \partial_{n_j} \lambda + \sum_{i=1}^J \left\{ \delta_{ij} \partial_{n_j} K_i + \partial_{n_j} \lambda \partial_\lambda K_i \right\} = 0. \quad (129)$$

It follows

$$\partial_{n_j} \lambda = - \frac{\partial_{n_j} K_j}{J + \sum_{i=1}^J \partial_\lambda K_i} = \frac{2}{n_j} \frac{K_j + \frac{\lambda}{\sqrt{1-2\lambda n_j^2}}}{J - \sum_{i=1}^J \frac{1}{\sqrt{1-2\lambda n_i^2}}}. \quad (130)$$

The denominator of (130) is clearly negative, and thus the gradient is always pointing from the branching surface to the limiting surface. Right at the branching surface  $\lambda = 0$  and the gradient is always infinite. Right at the limiting surface all components of the gradient vanish except that of maximum  $n_j$ . Thus, the gradient is always pointing towards the diagonal, except right at the diagonal, where it points towards the origin. From this gradient configuration we conclude that the maximum value of  $\lambda$  is achieved at the cusp of the limiting surface. But this point is not in the stability window, and thus the maximum  $\lambda$  should be achieved at the onset of stability along the diagonal. But right on the diagonal the stability matrix  $H$  is permutation-invariant and we can compute exactly its stability eigenvalue, which is

$$\kappa_{\text{diag}} = K - (J + 2)\lambda, \quad (131)$$

where  $K$  is the common value of all curvatures on the diagonal of flux space. But then, equation (117) reads

$$\Lambda = \frac{J}{2}[\lambda + K], \quad (132)$$

which allows us to eliminate  $K$  and gives the exact diagonal stability condition:

$$\lambda < \frac{2\Lambda}{J(J + 3)} = \lambda_{\text{max}}. \quad (133)$$

Thus, we have exactly computed the maximum  $\lambda$  value.

Things are far more difficult when we address  $\lambda_{\text{min}}$ . We know that the minimum will be close to the branching surface, but its exact position is unpredictable in general. The  $J = 1$  case is easier, because the landscape is a single state chain. In this case, equation (132) is exact, so we can obtain the dS spectrum as

$$\lambda(n) = 2 \left( \frac{1}{|n|} - \sqrt{\frac{1}{n^2} - \Lambda} \right) \sqrt{\frac{1}{n^2} - \Lambda}. \quad (134)$$

The end state of this chain is at node  $n_{\text{max}} = \lfloor \frac{1}{\sqrt{\Lambda}} \rfloor$ , and this implies

$$\lambda_{\text{min}} = 2 \left( \frac{1}{|\lfloor \frac{1}{\sqrt{\Lambda}} \rfloor|} - \sqrt{\frac{1}{\lfloor \frac{1}{\sqrt{\Lambda}} \rfloor^2} - \Lambda} \right) \sqrt{\frac{1}{\lfloor \frac{1}{\sqrt{\Lambda}} \rfloor^2} - \Lambda}. \quad (135)$$

In this case, it is possible to give an exact answer to the minimum  $\lambda$  value. When  $\frac{1}{\sqrt{\Lambda}}$  is an integer, then  $\lambda_{\text{min}} = 0$ , but, as we know, this is not the generic situation.

Generalizing the result (135) is difficult. We can argue as in the previous subsection and approximate the  $J = 2$  case by the  $J = 1$  case just considered. Then we can assume that the longest state chains will host the minimum  $\lambda$  states at its end nodes. These end nodes have an approximate  $J = 1$  spectrum which can be computed by replacing  $\Lambda$  in (132) (with  $J = 1$ ) by  $\Lambda - (\lfloor \frac{1}{\sqrt{\Lambda}} \rfloor + 1)^{-2}$ . Now the same substitution can be performed in formula (135), giving a fairly cumbersome expression of nested fractions, square roots

and floor functions, and hence it will be omitted. This formula will approximately give the minimum  $\lambda$  provided the corresponding state is located at the end of the longest chains. The minimum- $\lambda$  state can also be located among bulk states, but this is non-generic, as we will see shortly, because long state chains are generically low-lying states. So such a formula can be trusted, but it is neither exact, nor a bound, but rather it is an approximate expression for the particular (if generic) case when the min- $\lambda$  state is located at the end of the longest state chain.

Similar arguments can give analogous (but much more complex) expressions for higher  $J$ , with the same caveats as before.

Nevertheless,  $\lambda_{\min}$  is not quite relevant for our purposes, because a precise computation of it requires taking into account even the finest details of the lattice, and thus no continuous approximation can yield this value. Instead, we will be interested in an approximation of the density of states, whose expression will allow us to estimate  $\lambda_{\min}$  in more familiar terms.

Let us consider first the case  $J = 1$ . By inverting the relation  $\lambda(n) = \rho$ , we obtain

$$n_\rho = \frac{2\sqrt{\Lambda - \rho}}{2\Lambda - \rho}, \quad (136)$$

so that the condition  $\lambda(n) \leq \rho$  can be rephrased as  $n \geq n_\rho$ . Thus, the distribution function  $\Omega_1(\rho, \Lambda)$  is simply the number of integers between  $n_\rho$  and  $n_{\max}$ , that is,

$$\Omega_1(\rho, \Lambda) = \left\lceil \frac{1}{\sqrt{\Lambda}} \right\rceil - \left\lceil \frac{2\sqrt{\Lambda - \rho}}{2\Lambda - \rho} \right\rceil, \quad (137)$$

supplemented with conditions (128) and (127). This exact result can be approximated by a continuous function by simply omitting the ceiling functions. Doing this and taking the  $\rho$ -derivative afterwards, we obtain

$$\omega_1(\rho, \Lambda) = \frac{\rho \chi_{[0, \frac{\Lambda}{2}]}(\rho)}{(2\Lambda - \rho)^2 \sqrt{\Lambda - \rho}}. \quad (138)$$

Equation (138) is the  $J = 1$  density of stable dS states. It has the following properties:

$$\begin{aligned} \mathcal{N}_1(\Lambda) &\approx \int_{\mathbb{R}} \omega_1(\rho, \Lambda) d\rho = \left(1 - \frac{2\sqrt{2}}{3}\right) \frac{1}{\sqrt{\Lambda}}, \\ \langle \lambda \rangle_{\omega_1} &= \frac{1}{\mathcal{N}_1(\Lambda)} \int_{\mathbb{R}} \rho \omega_1(\rho, \Lambda) d\rho = \frac{12 + 12 \tan^{-1} \frac{1}{\sqrt{2}} - 3\pi - 7\sqrt{2}}{3 - 2\sqrt{2}} \Lambda, \end{aligned} \quad (139)$$

That is, it is consistent with equation (108), and the mean value of the density is around  $0.7167\frac{\Lambda}{2}$ . This curve has a jump discontinuity at  $\rho = \frac{\Lambda}{2}$ , which is the upper limit of its support, and the position of its maximum, which is  $\frac{2\sqrt{2}}{9\Lambda^{\frac{3}{2}}}$ . Figure 8 illustrates this density compared with the actual spectrum of a  $J = 1$  model.



Density of states and  $\lambda$  spectrum ( $J = 1, \Lambda = 10^{-8}$ )

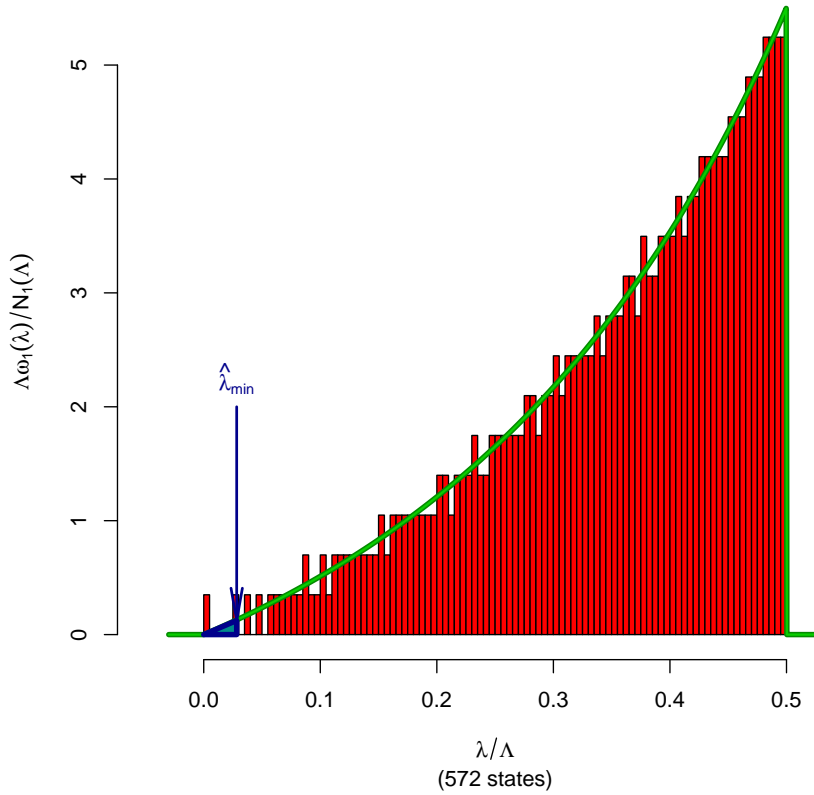


Figure 8: Density of states of the  $J = 1$  landscape (thick line) compared with the actual  $\lambda$ -spectrum for  $\Lambda = 10^{-8}$ . This model has 572 stable states, and the density shown is normalized to unity. The agreement between discrete data and continuous density is complete, in the sense that the histogram, which approximates a continuous curve when the spacing between neighboring states is much smaller than the bin width, accurately fits the approximation  $\omega_1(\lambda, \Lambda)$ . The construction of the estimate  $\hat{\lambda}_{\min}$  is also shown: the small triangle located at the origin has area  $1/572$  in this model, and its vertical side marks the position of the minimum- $\lambda$  estimate. This value of  $\Lambda$  allows for a  $\lambda = 0$  state, which is isolated by the bins used in the histogram.

In figure 8 is also displayed a naive estimate of  $\lambda_{\min}$ , defined as the abscissa  $\widehat{\lambda}_{\min}$  which encloses area 1 under the density's graph:

$$\int_0^{\widehat{\lambda}_{\min}} \omega_1(\rho, \Lambda) d\rho = 1. \quad (140)$$

Assuming that  $\widehat{\lambda}_{\min}$  is small enough, we can approximate  $\omega_1(\rho, \Lambda) = \frac{\rho}{4\Lambda^{\frac{5}{2}}} + \mathcal{O}(\rho^2)$  and obtain

$$\widehat{\lambda}_{\min} = 2\sqrt{2}\Lambda^{\frac{5}{4}}. \quad (141)$$

Figure 9 shows this estimate versus the exact minimum. Of course, this estimate does not provide the true minimum: it has neither zeros nor peaks, but it grows at the same average rate.

We will now consider the  $J = 2$  case. The recurrence relation (121) extends to distributions and densities as well, and thus we have the approximation

$$\omega_2(\rho, \Lambda) = 2 \sum_{m=\lfloor \frac{1}{\sqrt{\Lambda}} \rfloor + 1}^{\lfloor \sqrt{\frac{2}{\Lambda}} \rfloor} \omega_1\left(\rho, \Lambda - \frac{1}{m^2}\right). \quad (142)$$

We interpret this equation as a decomposition of the  $J = 2$  landscape in a superposition of several  $J = 1$  landscapes, which are state chains. Of course, the previous equation will be only valid for small  $\rho$ . The maximum value of  $m$  in the sum (142), which is  $\lfloor \sqrt{\frac{2}{\Lambda}} \rfloor$ , gives a maximum effective cosmological constant  $\Lambda_{\text{eff,max}} = \Lambda - \lfloor \sqrt{\frac{2}{\Lambda}} \rfloor^{-2}$ , and the maximum  $\lambda$  of the corresponding state chain is

$$\lambda_{\max} = \frac{\Lambda_{\text{eff,max}}}{2} \approx \frac{\Lambda}{4}, \quad (143)$$

in contrast with (133), which gives  $\lambda_{\max} = \frac{\Lambda}{5}$ . Thus, we see that this approximation gives a wrong maximum  $\lambda$  value. The origin of this discrepancy is the stability condition, because the superposition of state chains extends the validity of the  $J = 1$  stability criterion to  $J = 2$ , and this is true only for small  $\lambda$ .

An example of this density of states compared with actual  $\lambda$ -spectrum data is given in figure 10. We can see that the histogram shows a peak near the origin, and the density of states extends its support to  $\frac{\Lambda}{4}$  instead of the correct  $\frac{\Lambda}{5}$  value. In the logarithmic version of the histogram, we can see the first peaks resolved enough, and the correctness of the state chain approximation in the low- $\lambda$  region. Only a few peaks get resolved; the remaining peaks merge in a bulk distribution whose approximation computed from (142) is incorrect in the high- $\lambda$  region. We will not need this bulk distribution here.

The mean value of the  $\omega_2$  distribution can be directly computed from equations (142) and (139). We denote the summation interval as  $I(\Lambda)$ :

$$I(\Lambda) = \left[ \left\lfloor \frac{1}{\sqrt{\Lambda}} \right\rfloor + 1, \left\lfloor \sqrt{\frac{2}{\Lambda}} \right\rfloor \right], \quad (144)$$

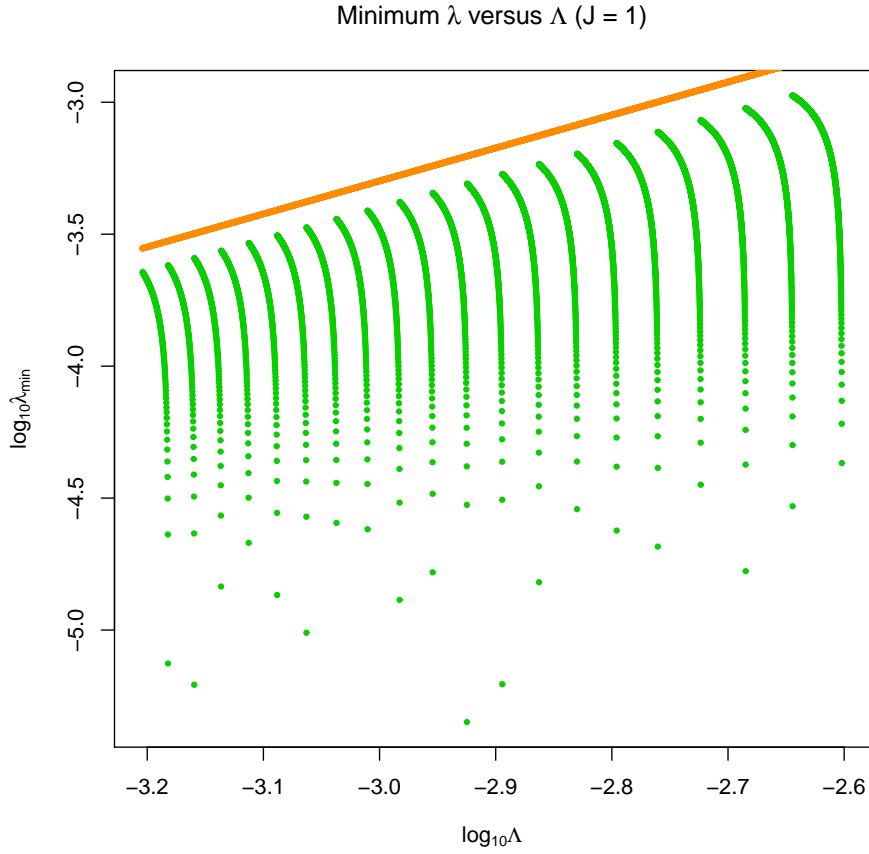


Figure 9: Comparison between the exactly computed minimum- $\lambda$  (equation (135)) and its estimate  $\hat{\lambda}_{\min}$  (equation (141)). The latter seems to be an upper bound of the former, closely following the decreasing of the worst-case minimum as  $\Lambda$  decreases. The spikes shown by  $\log \lambda_{\min}$  are the values for which  $\frac{1}{\sqrt{\Lambda}}$  is an integer. This continuous-density-based estimate is not accurate because the value of  $\lambda_{\min}$  is dictated by the finest details of the lattice and not by the continuous density  $\omega_1(\lambda, \Lambda)$ .

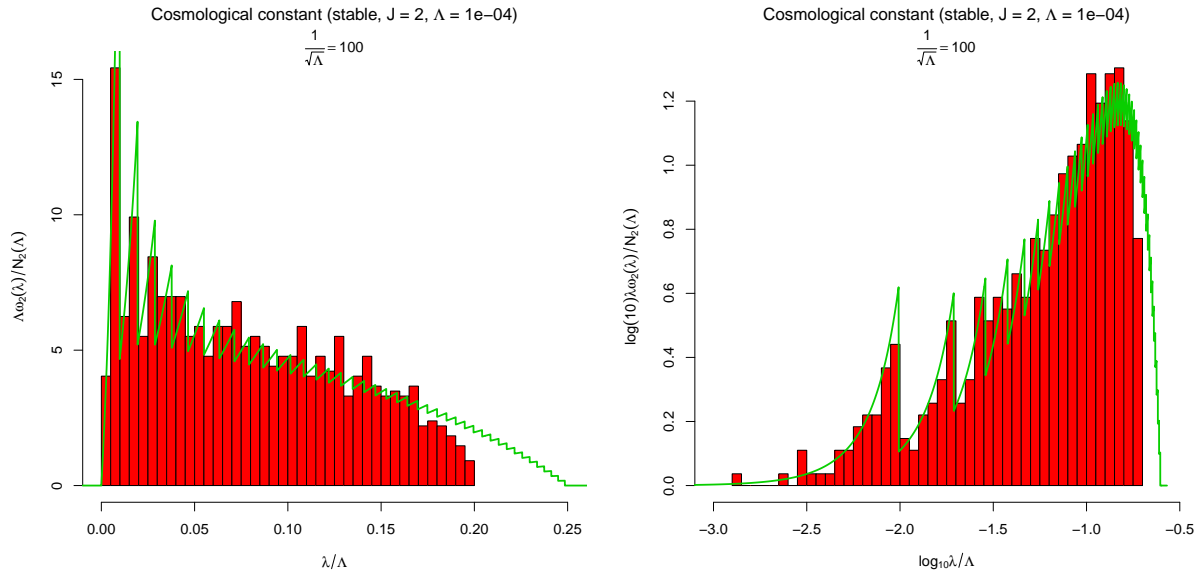


Figure 10: Comparison between a brute-force-computed  $\lambda$ -spectrum (histograms) and the approximated density of states (thick line) in a  $J = 2$  model of the Einstein-Maxwell landscape ( $\Lambda = 10^{-4}$ ). Left panel: The ordinary histogram shows a narrow peak near the origin (most of them come from long state chains) and a tail of bulk states. The jagged density of states accurately accounts for the first few peaks, but it fails to describe the high- $\lambda$  values. Right panel: The logarithmic histogram shows the resolved structure of the first peaks, well described by the density of states. This histogram also accumulates the bulk states in a single, broad peak. The corresponding bulk part of the density of states is shifted to the right.

and then we have

$$\begin{aligned}
\langle \lambda \rangle_{\omega_2} &= \frac{1}{\mathcal{N}_2(\Lambda)} \int_{\mathbb{R}} \rho \omega_2(\rho, \Lambda) d\rho \\
&= \frac{2}{\mathcal{N}_2(\Lambda)} \sum_{m \in I(\Lambda)} \mathcal{N}_1\left(\Lambda - \frac{1}{m^2}\right) \langle \lambda \rangle_{\omega_1\left(\Lambda \rightarrow \Lambda - \frac{1}{m^2}\right)} \\
&= \xi \frac{\sum_{m \in I(\Lambda)} \sqrt{\Lambda - \frac{1}{m^2}}}{\sum_{m \in I(\Lambda)} \frac{1}{\sqrt{\Lambda - \frac{1}{m^2}}}}.
\end{aligned} \tag{145}$$

In (145), the constant  $\xi$  is the prefactor of  $\Lambda$  in the formula for  $\langle \lambda \rangle_{\omega_1}$  appearing in equation (139). An illustration of the general behavior of the mean cosmological constant is given in figure 11. The average  $\lambda$  diminishes towards zero when  $\frac{1}{\sqrt{\Lambda}}$  approaches integer values from below, as a consequence of the development of large state chains. Formula (144) is not diagonal-corrected (see above), which gives small unevenly-spaced jumps. It is compared with brute-force-computed averages, which fluctuate because of lattice details. The global decreasing of the mean value as  $\Lambda$  decreases when  $\frac{1}{\sqrt{\Lambda}}$  is half-integer is shown also in figure 11 (right panel).

Figure 11 also shows the minimum  $\lambda$ , computed using formula (141) with the longest chain of  $J = 2$  models, compared with brute-force-computed minimum values. The fluctuation here is caused by the unpredictable nature of the minimum, which can be located at any point near the branching curve. When  $\frac{1}{\sqrt{\Lambda}}$  approaches an integer, the very long state chains are mainly formed out of low-lying states, and thus the approximate and exact minima approach zero. We can see a weak correlation between mean and minimum values: this happens because both values are strongly influenced by the presence of large state chains, but the minimum value depends on lattice details in an even stronger way.

Large state chains give rise also to a gap between the two lowest-lying peaks. This gap develops as  $\frac{1}{\sqrt{\Lambda}}$  approaches an integer from below, giving the  $\lambda$ -spectrum a very different aspect, as shown in figure 12. As the longest state chain grows, the peak near the origin becomes taller and well separated from the second peak. This separation is greater than the first peak's width, so that it is effectively isolated from the second peak.

We can compute an estimate of the gap using the minimum  $\lambda$  estimate given in equation (141). This estimate will be reliable because the approximations leading to it are valid in the two first peaks of the distribution. We can define the gap  $\Gamma$  as the distance between the maximum  $\lambda$  of the first peak and the minimum  $\lambda$  of the second. Both of them are known (see equations (141) and (133)), so we have the following formula for the gap as a function of  $\Lambda$ :

$$\Gamma(\Lambda) = \widehat{\lambda}_{\min}^{(2\text{nd})} - \lambda_{\max}^{1\text{st}} = 2\sqrt{2} \left[ \Lambda - \left( \left\lfloor \frac{1}{\sqrt{\Lambda}} \right\rfloor + 2 \right)^{-2} \right]^{\frac{5}{4}} - \frac{1}{2} \left[ \Lambda - \left( \left\lfloor \frac{1}{\sqrt{\Lambda}} \right\rfloor + 1 \right)^{-2} \right]. \tag{146}$$

This gap is shown in figure 13, where it is shown with respect to the width of the first peak. This width is computed using the standard deviation  $\sigma_1(\Lambda)$  of the  $\omega_1(\rho, \Lambda)$  distribution,

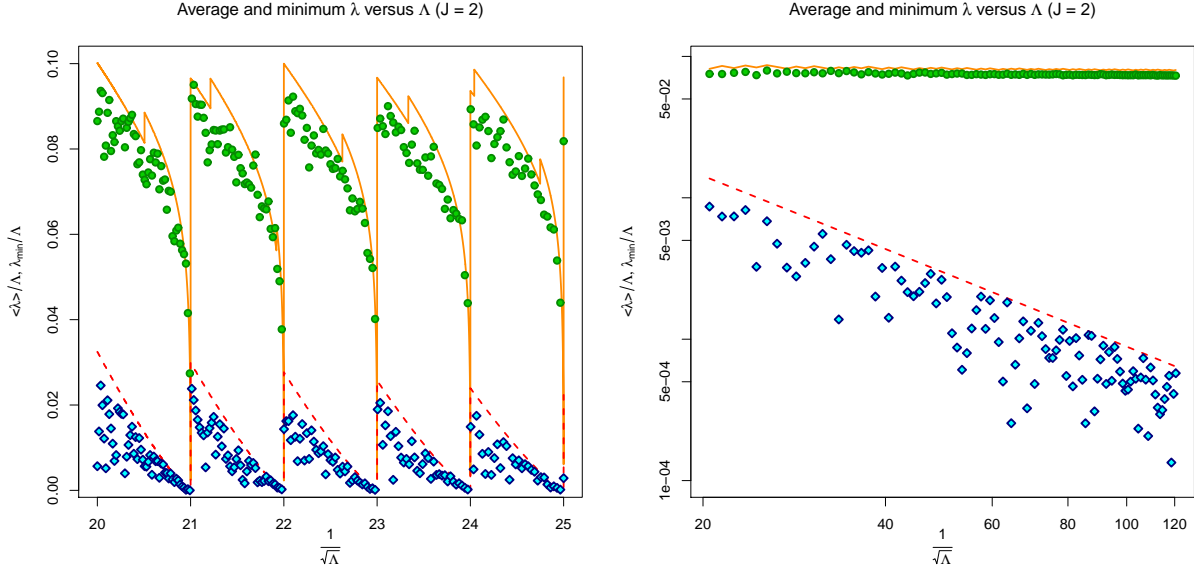


Figure 11: Comparison between brute-force data (bullets, diamonds) and approximate formulae (solid, dashed lines) for  $\langle \lambda \rangle_{\omega_2}$  (bullets, solid lines) and  $\lambda_{\min}$  (diamonds, dashed lines). Left panel focuses on a small interval enclosing six integer values of  $\frac{1}{\sqrt{\Lambda}}$ . Valleys of both magnitudes at those integer values are caused by long state chains. The wild fluctuation of samples is a consequence of the lattice details. The small unevenly-spaced peaks of the solid line are there because formula (145) lacks a diagonal correction as in figure 6. Right panel shows a much larger interval, but samples have been taken only at half-integer values of  $\frac{1}{\sqrt{\Lambda}}$ . The apparently constant profile of  $\langle \lambda \rangle_{\omega_2}$  is caused by the scale: it is actually decreasing at a rate ten times smaller than  $\lambda_{\min}$ . Note how formula (141) for  $\lambda_{\min}$  (dashed line) works as an almost saturated upper bound for  $\lambda_{\min}$ .

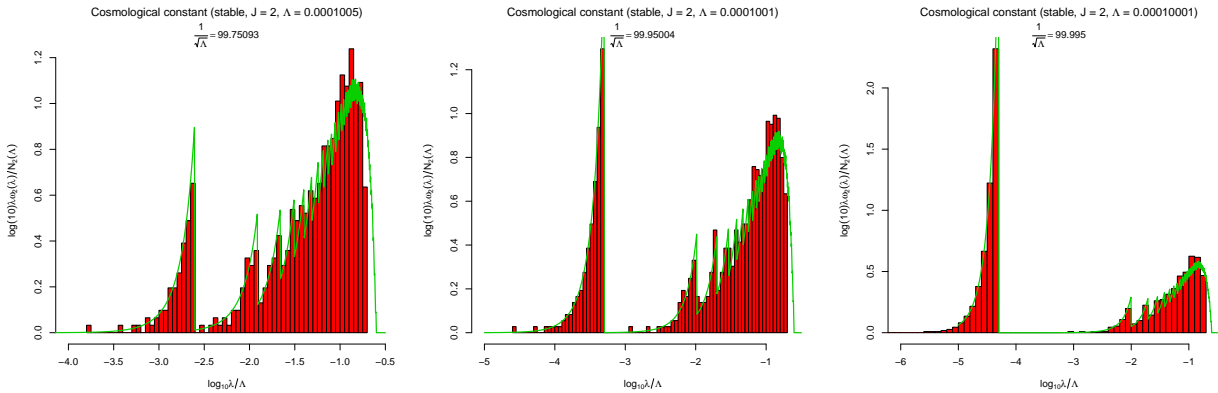


Figure 12: Logarithmic histograms and density of states (solid line) for three near values of  $\Lambda$  characterizing three different examples of the  $J = 2$  Einstein-Maxwell landscape. When  $\frac{1}{\sqrt{\Lambda}}$  approaches an integer from below (100 in this case), the first peak shifts to the left and becomes isolated, thus creating a gap in the  $\lambda$ -spectrum.

which is

$$\begin{aligned}
\sigma_1(\Lambda)^2 &= \langle (\lambda - \langle \lambda \rangle_{\omega_1})^2 \rangle_{\omega_1} \\
&= \frac{1}{\mathcal{N}_1(\Lambda)} \int_{\mathbb{R}} (\rho - \langle \lambda \rangle_{\omega_1})^2 \omega_1(\rho, \Lambda) d\rho \\
&\approx (0.11\Lambda)^2.
\end{aligned} \tag{147}$$

The first peak of  $\omega_2$  is a  $\omega_1$  distribution with  $\Lambda$  replaced by  $\Lambda - (\lfloor \frac{1}{\sqrt{\Lambda}} \rfloor + 1)^{-2}$ , and thus its width is given by

$$\sigma_{1^{\text{st}}}(\Lambda) \approx 0.11 \left( \Lambda - \left( \left\lfloor \frac{1}{\sqrt{\Lambda}} \right\rfloor + 1 \right)^{-2} \right). \tag{148}$$

or some multiple of it. Immediately we can see that this width will approach zero as  $\frac{1}{\sqrt{\Lambda}}$  approaches an integer, and therefore the relative gap will become enormous. There is some values of  $\Lambda$  for which the gap becomes negative, that is, the two first peaks of  $\omega_2$  overlap. This can happen if  $\frac{1}{\sqrt{\Lambda}} > 37$ , as can be seen in figure 13. This gap will never disappear for large values of  $\frac{1}{\sqrt{\Lambda}}$  because the width of the first peak will always vanish at integers, but the intervals of positive gaps are smaller when  $\Lambda$  decreases. That is, the gap is positive for  $\frac{1}{\sqrt{\Lambda}} \leq 36$ , and for greater values the gap changes sign between two consecutive integer values of  $\frac{1}{\sqrt{\Lambda}}$ , with the zero being closer and closer to  $\lceil \frac{1}{\sqrt{\Lambda}} \rceil$  as  $\Lambda$  decreases.

## 5 Anthropic states in the multi-sphere Einstein-Maxwell landscape

Stable dS states in the multi-sphere Einstein-Maxwell landscape can be interpreted as inflating 1+1 cosmologies. Such states are devoid of matter, of course, and thus no real observers can live in such universes. Nevertheless, as a toy model of a multiverse, a natural question one may ask is if anthropic states are present in this model, that is, if states with very low, realistic effective cosmological constant exist, and if they are generic, or some fine-tuning is needed to obtain them. We have seen above that special values of  $\Lambda$  can yield particularly small values of  $\lambda$ , but a huge amount of fine-tuning is needed to obtain a realistic value. Surprisingly enough, anthropic states *do* exist indeed, and this section is devoted to describe how to find and count them. We also draw some conclusions regarding the multiverse prediction of the cosmological constant with these anthropic states in mind.

### 5.1 Step-by-step construction of anthropic states

We start by considering equation (101) for the branching surface, which is the  $\lambda = 0$  locus. We can try to solve this equation by successive approximations, looking for the best choice of an integer at each step in a greedy fashion:

$$\sum_{j=1}^J \frac{1}{n_j^2} = \Lambda \equiv \Lambda_1 \quad \longrightarrow \quad \sum_{j=2}^J \frac{1}{n_j^2} = \Lambda_1 - \frac{1}{n_1^2} \equiv \Lambda_2 > 0 \quad \Rightarrow \quad n_1 = \left\lceil \frac{1}{\sqrt{\Lambda_1}} \right\rceil. \tag{149}$$

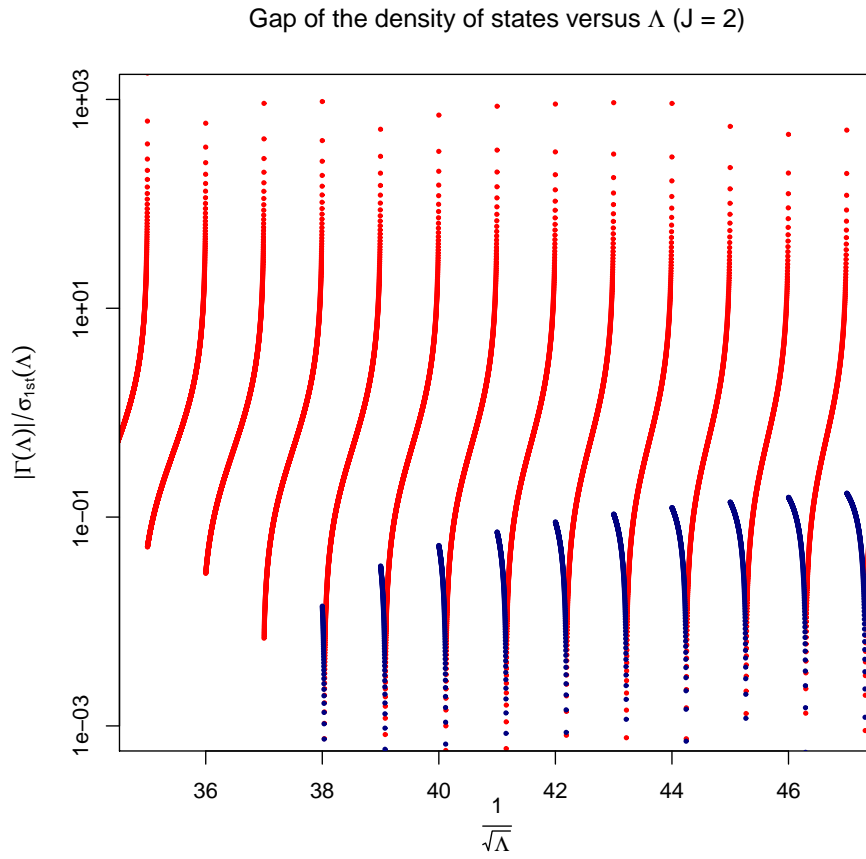


Figure 13: Gap of the  $J = 2$  density of states as a function of  $\Lambda$  (equation (146)). It is shown the quotient between the (absolute value of the) gap and the first peak width. Gaps can be negative for sufficiently low  $\Lambda$ , and the negative-gap intervals become greater when  $\Lambda$  becomes smaller. Decreasing curves represent negative values of the gap, while increasing ones represent positive values.



We have called  $\Lambda \equiv \Lambda_1$  for the start of a recurrence relation replicating the previous step:

$$\Lambda_{j+1} = \Lambda_j - \frac{1}{n_j^2}, \quad n_j = \left\lceil \frac{1}{\sqrt{\Lambda_j}} \right\rceil. \quad (150)$$

The recurrence relation (150) gives the best integer choice at each step for getting the smallest possible difference between the two sides of the formula

$$\sum_{i=j}^J \frac{1}{n_i^2} = \Lambda_j. \quad (151)$$

The last step of the approximation is

$$\Lambda_J - \frac{1}{n_J^2} = \Lambda - \sum_{j=1}^J \frac{1}{n_j^2} \equiv \Lambda_{J+1} < 0, \quad (152)$$

that is, the last remainder should be negative, so that the existence condition (103) can be satisfied. This gives the last integer as

$$n_J = \left\lfloor \frac{1}{\sqrt{\Lambda_J}} \right\rfloor, \quad (153)$$

where the floor function is taken instead of the ceiling to guarantee that the last remainder is negative. Thus, we can run the recurrence relation (150) starting from any positive value of  $\Lambda_1$  until some desired number of steps  $J$  is reached, and then finish it with the last step (153).

Before the final step closes the algorithm, we can rewrite the recurrence relation as a fixed-point iteration:

$$\Lambda_{j+1} = f(\Lambda_j), \quad \text{with} \quad f(x) = x - \frac{1}{\left\lceil \frac{1}{\sqrt{x}} \right\rceil^2}. \quad (154)$$

The iteration function just defined  $f(\Lambda)$  has jump discontinuities when  $\frac{1}{\sqrt{\Lambda}}$  is an integer, and it is simply  $\Lambda - 1$  if  $\Lambda > 1$ . Its continuous envelope, which is easily obtained replacing  $\left\lceil \frac{1}{\sqrt{x}} \right\rceil$  with  $\frac{1}{\sqrt{x}} + 1$ , gives the magnitude of the jumps, and it has a particularly attractive behaviour when  $x \rightarrow 0$ :

$$f(x) = x - \frac{1}{\left\lceil \frac{1}{\sqrt{x}} \right\rceil^2} \leq x - \frac{1}{\left(\frac{1}{\sqrt{x}} + 1\right)^2} \xrightarrow{x \rightarrow 0} 2x^{\frac{3}{2}}. \quad (155)$$

The iteration function, its envelope and its first-order term are plotted in figure 14. The figure also shows the first-quadrant diagonal, thereby proving that the only fixed point of the recurrence is at  $x = 0$ .

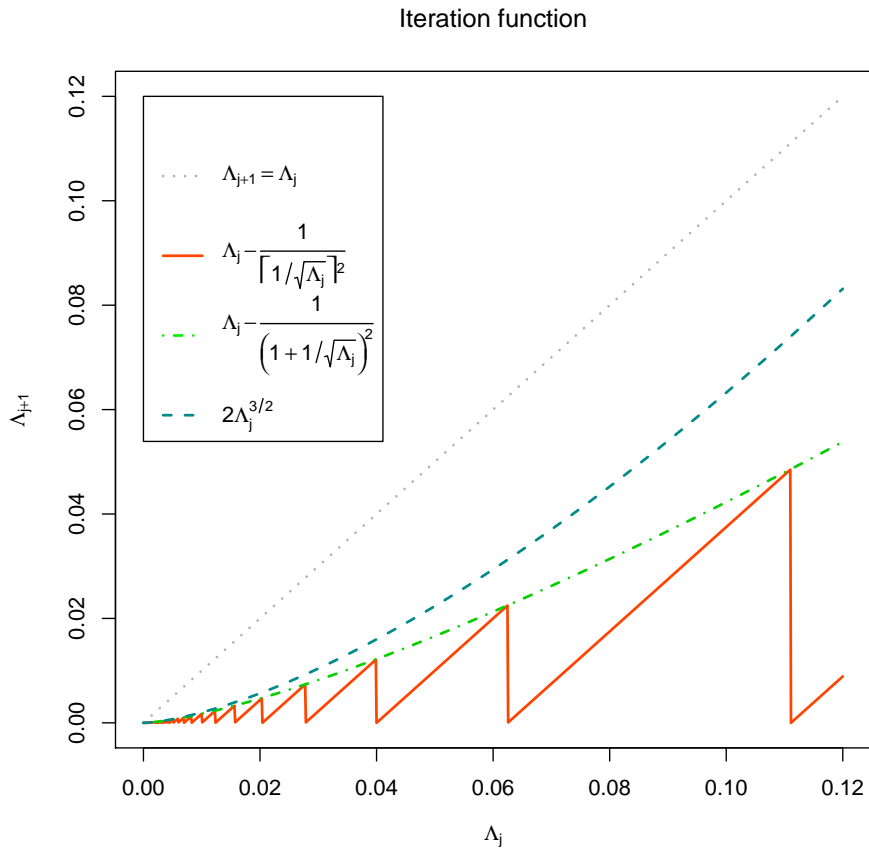


Figure 14: Iteration function of recurrence relation (154). It is shown along with its envelope and its first-order Taylor approximation, which is used as upper bound in equation (156). The first quadrant diagonal is also drawn, showing that the only fixed point of the iteration is at  $\Lambda = 0$ .

The super-linear behaviour of  $f(x)$  near  $x \rightarrow 0$  has the nice consequence of giving the recurrence relation a very fast convergence rate. This can be seen by replacing  $f(x)$  by its first-order approximation, which is an upper bound:

$$\Lambda_{j+1} = f(\Lambda_j) < 2\Lambda_j^{\frac{3}{2}}. \quad (156)$$

The resulting approximate recurrence relation is exactly solvable, and its solution starting from  $\Lambda_1$  is

$$\Lambda_j = 2^{\sum_{k=0}^{j-2} (\frac{3}{2})^k} \Lambda_1^{(\frac{3}{2})^{j-1}} \quad (j \geq 2). \quad (157)$$

Thus, as long as  $\Lambda_1 < 1$ , the previous upper bound decreases at a double-exponential rate, thus providing very small values of the negative remainder  $\Lambda_{J+1}$  when the last step is taken for moderate values of  $J$ .

We have thus a recipe for obtaining a node  $\{n_1, \dots, n_J\}$  with the property of being an approximate solution of the branching surface equation with a very small negative remainder. Nevertheless, it should be shown that both inequalities of the existence condition (103) are satisfied, because only one of them is guaranteed by the last step (153). The solution of the existence equation (102) should be smaller than the branching point  $\lambda_b$ , which in this case is

$$\lambda_b = \frac{1}{2n_J^2} \approx \frac{\Lambda_J}{2}. \quad (158)$$

Equation (153) guarantees that  $L_n(0) > \Lambda$ , thus it remains to show that  $L_n(\lambda_b) < \Lambda$ . The  $L_n$  function evaluated at  $\lambda_b$  is

$$L_n(\lambda_b) = \frac{1}{2} \left( J\lambda_b + \sum_{j=1}^J \frac{1 + \sqrt{1 - 2\lambda_b n_j^2}}{n_j^2} \right) = \frac{J}{4n_J^2} + \frac{1}{2} \sum_{j=1}^J \frac{1 + \sqrt{1 - \frac{n_j^2}{n_J^2}}}{n_j^2}. \quad (159)$$

The convergence rate of the approximate recurrence relation (156) is so fast that the integers  $n_j$  grow in such a way that  $n_J$  is overwhelmingly larger than the rest, and thus all square roots in equation (159) can be approximated by first-order Taylor expansions, except for the last, which is zero:

$$L_n(\lambda_b) \approx \frac{J}{4n_J^2} + \frac{1}{2} \sum_{j=1}^{J-1} \left[ \frac{2}{n_j^2} - \frac{1}{2n_J^2} \right] + \frac{1}{2n_J^2} = \sum_{j=1}^J \frac{1}{n_j^2} - \frac{1}{4n_J^2}. \quad (160)$$

The difference with  $\Lambda$  is

$$L_n(\lambda_b) - \Lambda = \sum_{j=1}^J \frac{1}{n_j^2} - \Lambda - \frac{1}{4n_J^2} \approx |\Lambda_{J+1}| - \frac{\Lambda_J}{4} < 0, \quad (161)$$

where the last inequality follows from the recurrence relation at its final step, because  $|\Lambda_{J+1}|$  is much smaller than  $\Lambda_J$ . This proves that a state exists at the node provided by the recurrence relation.

We now estimate the corresponding solution  $\lambda$  of the existence equation  $L_n(\lambda) = \Lambda$ , and prove its stability. We can obtain a solution by using again that the integers  $\{n_1, \dots, n_J\}$  grow very fast, so that we can replace all curvatures by its first-order expansions in  $\lambda$  (we know that  $\lambda < \lambda_b$ ) except for the last, which remains untouched, thus respecting the location of the branching point:

$$\Lambda = L_n(\lambda) = \frac{1}{2} \left( J\lambda + \sum_{j=1}^J K_j \right) \approx \frac{1}{2} \left[ J\lambda + \sum_{j=1}^J \left( \frac{2}{n_j^2} - \lambda \right) + K_J \right] = \sum_{j=1}^{J-1} \frac{1}{n_j^2} + \frac{1}{2} (\lambda + K_J). \quad (162)$$

We can rewrite the previous equation as

$$\Lambda_J = \Lambda - \sum_{j=1}^{J-1} \frac{1}{n_j^2} = \frac{1}{2} (\lambda + K_J), \quad (163)$$

which is exactly the existence equation for a EM landscape with a single curvature  $K_J$  and an effective four-dimensional cosmological constant  $\Lambda_J$ . This  $J = 1$  EM landscape has been obtained by fixing the integers  $\{n_1, \dots, n_{J-1}\}$  by means of the recurrence relation (150). The last integer  $n_J$ , if chosen as in (153), gives the last node verifying the existence equation. We know that no greater value of  $n_J$  will satisfy the existence equation, but smaller values can also give valid solutions. Thus, varying  $n_J$  downwards from (153) provides us with a state chain embedded in the  $J$ -sphere EM landscape: This state chain is simply the single-sphere EM landscape described by equation (163).

The analysis of the  $J = 1$  EM landscape performed in subsections 2.1, 2.2 and 4.2 is now entirely applicable to (163). In particular, the exact minimum two-dimensional cosmological constant of this chain is given by equation (135) (with  $\Lambda$  replaced by  $\Lambda_J$ ) or by its continuum approximation given in equation (141) (with the same replacement):

$$\widehat{\lambda}_{\min} \approx 2\sqrt{2}(\Lambda_J)^{\frac{5}{4}}. \quad (164)$$

We know that  $\Lambda_J$  is very small, and we now see that  $\widehat{\lambda}_{\min}$  is even smaller.

The stability condition for the  $J = 1$  landscape (133) reads  $\lambda < \frac{\Lambda_J}{2}$ . We can see that  $\widehat{\lambda}_{\min} = 4\sqrt{2}\Lambda_J^{\frac{1}{4}} \frac{\Lambda_J}{2} \lll \frac{\Lambda_J}{2}$ , and thus this minimum- $\lambda$  state is always stable. Moreover, we can let  $n_J$  decrease until it reaches the stability limit. This generates all dS stable states in the chain, whose number is given by (108), which is

$$\mathcal{N}_1(\Lambda_J; n_1, \dots, n_{J-1}) \approx \left( 1 - \frac{2\sqrt{2}}{3} \right) \frac{1}{\sqrt{\Lambda_J}} \approx 0.05719 \cdot n_J. \quad (165)$$

This is an enormous number, as we now see. We will choose a reference value  $\lambda_A$ , and we wish  $\widehat{\lambda}_{\min}$  to reach it. We can compute the value of  $J$  we need for this to happen by inserting the worst-case approximate formula (157) in equation (164) for the minimum  $\lambda$  value:

$$\lambda_A = 2\sqrt{2}(\Lambda_J)^{\frac{5}{4}} = 2^{\frac{3}{2} + \frac{5}{4}} \left[ \frac{\left(\frac{3}{2}\right)^{J-1-1}}{\frac{3}{2}-1} \right] \Lambda^{\frac{5}{4} \left(\frac{3}{2}\right)^{J-1}}. \quad (166)$$

Solving for  $J$ , we obtain

$$J = 1 + \log_{\frac{3}{2}} \left( \frac{4}{5} \frac{\log(2\lambda_A)}{\log(4\Lambda)} \right). \quad (167)$$

We can also demand a much more restrictive condition, that the whole chain is inside the anthropic range. The peak of the density is located at  $\frac{\Lambda_J}{2}$ , and thus the relation  $\lambda_A = \frac{\Lambda_J}{2}$  together with (157) leads to a value of  $J$  given by

$$J = 1 + \log_{\frac{3}{2}} \left( \frac{\log(\lambda_A/2)}{\log(4\Lambda)} \right). \quad (168)$$

Using the emblematic number  $\lambda_A = 10^{-120}$  and  $\Lambda = 0.1$ , we obtain a non-integer  $J = 14.5$  with the first formula and 15.08 with the second; using  $J = 15$  we find  $2.43 \cdot 10^{58}$  states in the chain with a minimum of order  $10^{-146}$ . In this case, the stability limit is around  $10^{-117}$ , well inside the anthropic range. As another example, starting from  $\Lambda = 0.0008$ , we obtain  $J = 10$  almost exactly with the first formula and  $10^{47}$  states. The second formula provides  $J = 10.55$ , and with  $J = 11$  we obtain  $10^{72}$  states.

Therefore, we can see that moderate values of  $J$  and  $\Lambda$  can yield an enormous number of anthropic states in the multi-sphere EM landscape.

We may ask if the states just found are generic inside the  $J$ -dimensional landscape, because the recurrence relation (150), (153) leading to them gives very precise values for the integers  $\{n_1, \dots, n_J\}$ , and therefore they seem to be located at a very special place in flux space. We will now see that, despite being very numerous, these anthropic states are not generic.

We have just obtained a very long state chain by fixing  $n_1, \dots, n_{J-1}$  and letting  $n_J$  to vary from (153) downwards. This state chain is a one-dimensional landscape embedded in  $J$ -dimensional flux space. We can let  $n_{J-1}$  vary downwards as well, thus generating a two-dimensional landscape embedded in  $J$ -dimensional flux space. The effective high-dimensional cosmological constant of this landscape is  $\Lambda_{J-1}$ , and it is very small, which allows us to use formula (123) with the approximation (124) to give the number of states of this two-dimensional landscape as

$$\mathcal{N}_2(\Lambda_{J-1}; n_1, \dots, n_{J-2}) \approx 2 \left( 1 - \frac{2\sqrt{2}}{3} \right) (n_J + n_{J-1}^2), \quad (169)$$

where we have used that  $n_{J-1} \approx \frac{1}{\sqrt{\Lambda_{J-1}}}$ . The first contribution in formula (169),  $n_J$ , comes from the longest state chain, while the second,  $n_{J-1}^2$ , comes from the bulk. The simplified recurrence (156) shows that  $n_J \approx \frac{1}{\sqrt{2}} n_{J-1}^{3/2}$ , that is, the number of states in the chain scales as  $n_{J-1}^{3/2}$  while the number of states in the bulk scales as  $n_{J-1}^2$ . Thus, the fraction of states in this two-dimensional landscape belonging to the chain scales as  $n_{J-1}^{-1/2}$ , and therefore they are non-generic.

For example, choosing  $\Lambda = 0.0008$  and  $J = 10$  we obtain  $n_J \approx 10^{48}$ , but  $n_{J-1}^2 \approx 10^{64}$ . Thus, states in the chain are in a proportion  $1 : 10^{16}$ .

We may as well let the remainder of the integers  $n_1, \dots, n_{J-2}$  vary downwards from (150), thus generating the entire  $J$ -dimensional landscape. In this complete landscape the proportion will be much smaller than  $n_{J-1}^{-1/2}$ , and thus we see that anthropic states are very rare, despite being very numerous. We cannot exclude the possibility that other corners of flux space may contain low- $\lambda$  states, either as isolated, randomly close nodes, or as very long chains obtained in a different way, but they will be non-generic also.

Summarizing, we have seen that for any value of  $\Lambda$  (say, between  $10^{-4}$  and  $10^{-1}$ ) moderate values of  $J$  (between 10 and 15 respectively) lead to the existence of a huge chain of anthropic states, that is, states having a two-dimensional cosmological constant of order  $10^{-120}$ . Those states represent a tiny fraction of the total number of states, and thus they are non-generic. But they are very numerous, and they can be found with no fine tuning at all, which is a very remarkable feature of the multi-sphere EM landscape.

## 5.2 Implications for the multiverse prediction of the cosmological constant

The very long chains of anthropic states found in the previous subsection are another form of the discretuum introduced by Bousso and Polchinski [1] as part of the solution of the cosmological constant problem. Moderate values of  $J$  can yield a 1+1 effective cosmological constant of the order of the observed value in our universe. The only parameter of the model,  $\Lambda$ , can be chosen as any positive real number to achieve that. Thus, the multi-sphere EM landscape do not need fine-tuning  $\Lambda$  to contain anthropic states in the discretuum.

There are another possibilities to produce a discretuum. A very small charge produces a finely spaced tower of states as in the Brown-Teitelboim mechanism [52, 53], or a number of different, incommensurable elemental charges can yield a BP-like discretuum. In the first case, a single, very small parameter is needed, while in the multi-sphere EM model the parameter is not restricted at all. In the second case, as commented above, a number of parameters are given from the start, thus bypassing the need for a stabilization mechanism. This mechanism works only for large  $J$ , which are easily obtained in some Calabi-Yau compactification scenarios, but large values of  $J$  give rise to the  $\alpha^*$ -problem discussed in section 1. Thus, no fine-tuning is needed in such cases, but the counting of states becomes tricky, because most of them might be unstable if its stability were correctly addressed, as is demonstrated in the multi-sphere Einstein-Maxwell model. Thus, we conclude that, as a discretuum-generating method, state chains circumvent some previously encountered problems.

Anthropic state chains have further implications in the prediction of the cosmological constant distribution in realistic landscapes. As stated in section 1, a multiverse prediction of the cosmological constant requires a prior probability distribution counting the states present in the model, a cosmological measure to weigh relative probabilities, and an anthropic factor taking into account the existence of observers [4]. Authors in [4] state that the prediction is very sensitive to changes in the prior distribution, so we may wonder how state chains can change the prediction.

The current multiverse prediction of the cosmological constant assumes that the prior distribution has a scale of variation of order the Planck scale, which is enormous when compared with the anthropic range. Thus it is safe to consider that the prior distribution is almost constant in the anthropic range, and the cosmological constant prediction is dominated by the anthropic factor.

The anthropic range, also called “Weinberg window”, is an interval of values of the cosmological constant which allow the formation of structures, such as galaxies, which may contain observers like us. The order of magnitude of such an interval is large when compared with the observed value of the cosmological constant [25]. Thus, if the prior probability has a very narrow peak inside the anthropic range of width comparable to the observed value  $\lambda_{\text{obs}}$ , then the anthropic factor, varying on a much larger scale, can be considered as almost constant. Therefore, the prediction of the cosmological constant would be dominated by the prior distribution. This is precisely the case with anthropic chains in the multi-sphere EM model.

Obviously, an anthropic factor is entirely out of question in the context of a 1+1 cosmology. Thus, the prior distribution will dominate the prediction if anthropic state chains can be shown to exist in a multi-sphere EM model with a 3+1 cosmology. The construction of such a model is left as future work.

## 6 Comparison between the Bousso-Polchinski and multi-sphere Einstein-Maxwell landscapes

Obviously, the multi-sphere Einstein-Maxwell landscape cannot be considered as a model of the string theory landscape, because it belongs to a completely different family of theories. Nevertheless, the features we have described in the previous sections are not excluded from the string theory landscape, and they are qualitatively different in other simplified models, such as the Bousso-Polchinski (BP) landscape [1]. We will now provide a brief summary of the main features of the BP landscape, and then we will stress the differences with the multi-sphere EM landscape.

### 6.1 The Bousso-Polchinski landscape

The BP landscape is a simplified model which provides an elegant method for solving the cosmological constant problem<sup>6</sup>. The starting point is M-theory, which is formulated in 10+1 dimensions, compactified down to 3+1. One of the main ingredients of this theory is a seven-form, which is used to introduce the Brown-Teitelboim cosmological constant neutralization mechanism [52, 53], which is a generalization of the Schwinger pair creation process responsible for the spontaneous lowering of a strong electric field.

In the presence of a compactification manifold having three-cycles, the seven-form is expanded in a basis of harmonic three-forms, whose coefficients are four-forms. After

---

<sup>6</sup>Good reviews of the cosmological constant problem can be found in references [10, 11]

dimensional reduction, the four-dimensional duals of the four-forms are zero-forms, that is, scalars, which are quantized by virtue of generalized Dirac quantization conditions. The total value of the flux of a four-form in the  $j^{\text{th}}$  three-cycle is an integer multiple of a fundamental charge  $q_j$  which is proportional to the volume of the three-cycle. These charges are moduli of the theory, whose stabilization is given *a priori* in the BP model.

A vacuum state of this model is given by specifying the integers representing the value of the four-form flux stored in each three-cycle. Transitions between the states are mediated by instantons, which can be viewed as M5-brane bubbles with two “legs” enclosing a three-dimensional interior of a different vacuum energy density, while having three remaining “legs” wrapping the flux in a three-cycle.

Thus, the vacuum states of the model are arranged in the nodes of a lattice in flux space. A given state is specified by  $J$  integers  $n_1, \dots, n_J$ , whose effective cosmological constant  $\lambda$  is given by

$$\lambda = \Lambda + \frac{1}{2} \sum_{j=1}^J q_j^2 n_j^2. \quad (170)$$

In equation (170),  $J$  represents the number of three-cycles inside the compactification manifold;  $\Lambda$  is the bare cosmological constant of the theory, which should be negative, so that  $\lambda$  can reach a small value; and  $q_j$  are the moduli, that is, the elementary charges of the fluxes.

There is a Minkowski surface in flux space separating AdS and dS states, which is obtained by setting  $\lambda = 0$  in (170). A node of the lattice can be located very close to this surface, and the number of such nodes can be huge by choosing a large enough  $J$ . The existence of these nodes, randomly close to the  $\lambda = 0$  surface, is essentially the BP mechanism solving the cosmological constant problem.

In a BP landscape with a large amount of fluxes, the vast majority of the nodes are located far away from the origin. Some criterion is needed to limit the value of the integers  $n_j$  and render the landscape finite. Usually, this is accomplished by introducing a cut-off  $\Lambda_{\text{cutoff}}$  in flux space which characterizes the maximum value of  $\lambda$  to be possibly reached. The computation of the probability of a given state among all available states based on abundance of states gives very small values for a large  $J$ , and a large  $J$  is needed to reach a value of  $\lambda$  as low as the observed value  $10^{-120}$  [22, 23]. So this model has the necessary states, but a very low probability for them to be occupied, which leads to anthropic arguments.

The anthropic window is an interval of cosmological constant values which allow the formation of observed structures (like galaxies, stars and planets) [25]. Even inside this anthropic window, the number of states is so huge that the probability of a state having  $\lambda = 10^{-120}$  is tiny. Dynamical relaxation inside the BP landscape reduces the states to a shell wider than the anthropic window [54], and thus do not solve this problem. This requires less convincing anthropic arguments to explain the observed value of the cosmological constant.

We can rephrase this problem by saying that the distribution of  $\lambda$  values near  $\lambda = 0$  is flat [55, 50], and thus specially small values do not get rewarded. The observed value of



$\lambda$  lies in a very thin shell, very small when compared with the anthropic or dynamically relaxed shells. Thus, the flatness of the distribution gives rise to such small probabilities.

In addition, there is another complication with large values of  $J$ . When the dimension of flux space is large, the vast majority of states in *any* spherical shell are confined to coordinate hyperplanes with a dimension of near  $J\alpha^*$  with  $\alpha^* < 1$  [32]. The bulk of the spherical shell<sup>7</sup> is almost devoid of states, and the number of non-vanishing fluxes is generically less than  $J$ . Nevertheless, stability arguments often force the integers  $n_j$  to be nonzero, even large ones; this would dramatically lower the number of states in the BP landscape, resulting in an empty anthropic shell. This  $\alpha^*$ -problem of the BP landscape is not restricted to sets with spherical symmetry; secant states are not spherically distributed, and share the same problem.

## 6.2 Comparison between BP and ms-EM landscapes

The previously described features of the BP landscape contrast with their counterparts in the multi-sphere Einstein-Maxwell landscape. First of all, this landscape is derived from a  $2J + 2$ -dimensional theory, after its dimensional reduction to 1+1 dimensions. Therefore, the resulting cosmologies are not comparable. Nevertheless, we will focus in the distribution of states and qualitative features of the landscape.

The “bare” cosmological constant  $\Lambda$  is negative in the BP case, allowing cancellation in the effective cosmological constant  $\lambda$ ; if  $\Lambda$  were positive, no AdS nor low-lying dS states would longer exist. In the EM case,  $\Lambda$  should be positive; otherwise, dS states would not exist at all. Thus, both landscapes have twin versions with reversed  $\Lambda$  which are not physically interesting.

The BP model assumes that its moduli are frozen by some external, unspecified mechanism. Therefore, the elementary charges are parameters of the model, as well as  $\Lambda$ . On the other hand, the moduli of the EM theory, which are the radii of the internal spheres, are fixed (at least at a linear level) by an effective potential built from the magnetic field, the curvatures and the vacuum energy density. Thus, this theory needs only one parameter,  $\Lambda$ . It is generally believed that the same stabilization mechanism should work in the BP model, but as far as we know it has not been implemented yet.

The simplicity of the formula for  $\lambda$  in the BP model, (170), is to be compared with the equation determining  $\lambda$  in the EM model, (68), (98) or (102). In this equation,  $\lambda$  cannot be isolated in general, and there are several branches for each node. Nevertheless, only the principal branch has solutions with positive curvatures, and these are the only ones with a chance of being stable. Moreover, this equation can have zero, one or two solutions, depending on  $\Lambda$ , giving zero, one or two states per node in flux space. In contrast, (170) always has one solution, and no more, per node. Thus, the correspondence between nodes and states is one-to-one in the BP model, but this is not the case in the EM model.

The finiteness of the BP landscape is a consequence of a cutoff introduced in flux space.

---

<sup>7</sup>That is, the region of the spherical shell surrounding the diagonals of flux space, where states are located far away from the coordinate hyperplanes.

As commented above, were this cutoff absent, the theory would have an infinite family of states with infinitely high- $\Lambda$ , which would raise the problem of choosing initial conditions. The EM model has a finite amount of stable dS states because of the presence of a branching point in the equation determining  $\lambda$ . The number of unstable dS states is much greater, but these states are excluded from the landscape. Thus, the stability analysis gets rid of the majority of dS states, and so we expect this situation to be analogous in the BP model completed with a stability analysis. This ingredient can thus significantly change a lot the general properties of the BP model, because it would exclude a huge amount of states from the landscape. This might be a feature, though, because it might raise the probability for the system to be in an anthropic state, which is currently very small because of the enormous amount of dS states present. But it is impossible to establish this claim or the opposite without a well-defined model to work with.

AdS states are finite in number in the BP model, because they are located inside a sphere in flux space. In the EM model with  $J > 1$  there is an infinite number of them and they are always stable. Therefore, the probabilistic arguments based on the number of states cannot be applied here, because the probability of dS states would always be zero. This argument might be interpreted as indicating that the method of computing probabilities using simply amounts of states could be completely wrong in both models. As a consequence, the probability measure used in these landscapes should be revised from scratch.

Both models have a  $\lambda = 0$  surface separating dS from AdS states, which in the BP model is

$$2|\Lambda| = \sum_{j=1}^J q_j^2 n_j^2, \quad (171)$$

that is, a sphere in flux space (parametrized in  $q_j n_j$  coordinates), while in the EM model it is

$$\Lambda = \sum_{j=1}^J \frac{1}{n_j^2}, \quad (172)$$

which is a sphere after performing a coordinate inversion. These surfaces provide the BP mechanism for solving the cosmological constant problem: if the landscape contains a state randomly close to this surface then this state can have a realistic value of  $\lambda$ . Both models have this property. Nevertheless, the surface (172) is not compact, and it allows for long state chains whose cosmological constant can approach very small values. This phenomenon is absent in the BP model, and constitutes a basic difference because it increases the amount of states in the anthropic shell. As stated above, we don't know the correct way of computing probabilities, but state chains provide a new source of low-lying states which is absent in the BP model.

State chains are also responsible for a crucial modification in the distribution of  $\lambda$  values, which is flat near  $\lambda = 0$  in the BP case, as stated above. In the EM case, the  $\omega(\lambda)$  density vanishes at  $\lambda = 0$ , but it has a huge peak of small values, corresponding precisely to those lying in the state chains. Thus, this distribution is not flat, which means that the

randomly-close-state mechanism is less important in the EM model than in the BP case, because only states near the diagonal in flux space contribute to it, while all states near the sphere contribute in the BP case, accounting for the difference. State chains provide a dominant peak of small  $\lambda$  values, which is another different mechanism for solving the cosmological constant problem. This mechanism can provide a peak very near  $\lambda = 0$  for very specific values of  $\Lambda$  when  $J$  is small (namely, when  $\frac{1}{\sqrt{\Lambda}}$  is very close to an integer from below), or for generic  $\Lambda$  values when  $J$  is moderate  $J \approx 10, 15$ , leading even to anthropic states. Thus, both mechanisms are different, and both have states with very small values of the cosmological constant, but they differ deeply in the form of the  $\omega(\lambda)$  distribution.

Finally, the  $\alpha^*$ -problem is absent in the EM model, because the  $\lambda = 0$  surface never approaches the coordinate hyperplanes where one or more  $n_j = 0$ . Thus, if the stability results found in the EM model translate to the BP model completed with a stability analysis, then we are forced to conclude that the vast majority of dS states, which are near the hyperplanes, would be unstable, and thus there would be excluded from the BP landscape. This would change all reasoning based on number of states, if it were to be of any use.

Table 1 summarizes all the issues we have addressed while comparing the BP and EM landscapes.

## 7 Possible implications for the string theory landscape

The comparison carried out in the previous section leads to some features that a complete treatment of the BP landscape interpreted as a toy model of the true string theory landscape would bear when compared to what is currently believed. This section is devoted to envision what the BP landscape would look like if some of the main features of the EM landscape were found to hold.

Two key points should be stressed:

- Theories with four-form fluxes have duals which are gauge-gravity theories. The main difference between them is that gauge-gravity theories have a built-in cut-off mechanism which limits the maximum values of the integers characterizing the landscape. Thus, those landscapes have natural finiteness conditions, such as the branching point in the multi-sphere Einstein-Maxwell landscape. This would avoid the necessity of a cut-off scale put by hand in the model. Nevertheless, the KKTL model has some natural cut-off mechanisms built-in [31], [56].
- Stability conditions are important not only because they complete the model, but also because they exclude a huge amount of states from the model. If the same exclusion were to take place in the BP landscape, the vast majority of its nodes would not be true states of the landscape, and the predictions of existence of anthropic states would dramatically change. Thus, stability conditions have a two-fold purpose: on

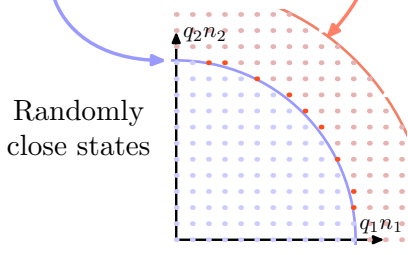
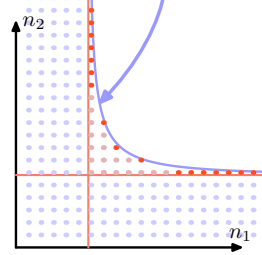
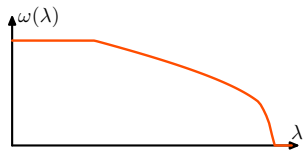
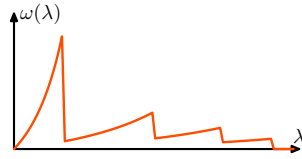
|                                | Bousso-Polchinski  | Multi-sphere Einstein-Maxwell  |
|--------------------------------|--|--|
| Parameters                     | $\Lambda, \{q_j\}_{j=1\dots J}$  | $\Lambda$  |
| Sign of $\Lambda$              | $\Lambda < 0$  | $\Lambda > 0$  |
| Stability                      | Assumed<br>( $q_j$ given <i>a priori</i> )   | Linear stability<br>understood ( $\kappa > 0$ )  |
| $\lambda$ formula              | $\lambda = \Lambda + \frac{1}{2} \sum_{j=1}^J q_j^2 n_j^2$   | $\Lambda = L_n(\lambda)$ (principal branch)  |
| Finiteness                     | $\lambda < \Lambda_{\text{cutoff}}$  | $\lambda < \lambda_b$ (dS)<br>Infinite (AdS) }   |
| $\lambda = 0$ surface          | $2 \Lambda  = \sum_{j=1}^J q_j^2 n_j^2$  | $\Lambda = \sum_{j=1}^J \frac{1}{n_j^2}$   |
| Cosmological constant problem  | Randomly close states<br> | Randomly close states and Long state chains<br> |
| $\omega(\lambda)$ distribution | Flat at 0<br>             | Dominant and many spikes<br>                    |
| $\alpha^*$ problem             | Vast majority of states have $(1 - \alpha^*)J$ vanishing fluxes (and they are probably unstable)             | There are no stable states with vanishing fluxes   |

Table 1: Summary of the differences between the Bousso-Polchinski and multi-sphere Einstein-Maxwell landscapes. The first two graphics emphasize the different distribution of states in flux space, which is the origin of the state chains. These state chains are responsible of the dominant spike in the  $\lambda$ -density, as shown in the two last graphics.

the one hand they fix the values of the elementary charges to be used in the model, on the other hand they limit which nodes have physically relevant states. A priori frozen moduli fulfill the first purpose, but do not help in deciding which nodes have states. This causes a huge proliferation of states, which may be spurious ones. The EM model shows that the vast majority of dS states are unstable. Thus, we can expect the same to be true in a completed BP landscape.

Other features of the EM landscape may not have a direct translation to a completed BP model, such as state chains. They are a consequence of the asymptotes found in the null- $\lambda$  surface, which is non-compact. This is an indication that the details of the null- $\lambda$  surface provide different sources of low-lying states which change the density of states  $\omega(\lambda)$ . This distribution is needed when one has to compute probabilities in a given landscape model; but a completely clear, unambiguous, quantum prescription for computing probabilities with a general model is still lacking, and therefore the implications of the details of  $\omega(\lambda)$  in the computation of probabilities cannot go beyond the naive arguments based on state abundances. At this simple level, details of the null- $\lambda$  surface translate in peaks in the  $\omega(\lambda)$  density, thus producing very different probabilities for the states in the anthropic shell. The BP model has a spherical null- $\lambda$  surface, and thus  $\omega(\lambda)$  has no peaks; if the null- $\lambda$  surface of more realistic flux compactifications of M-theory had other nontrivial shapes, this would be reflected in the  $\omega(\lambda)$  distribution and in the final computation of the probabilities. So this is the last point that the EM landscape brings in: the details of the null- $\lambda$  surface are very important for probability computations.

## 8 Conclusions

We have addressed a simple sector of the Einstein-Maxwell theory as an exactly solvable model of a landscape. The theory, formulated in  $2J + 2$  spacetime dimensions, has a single parameter in the Lagrangian, namely, the “bare” cosmological constant  $\Lambda > 0$ . The compactification has the form  $(A)dS_2 \times (S^2)^J$ , which is referred to as *multi-sphere Einstein-Maxwell* compactification. Equations of motion for the corresponding metric ansatz are algebraic equations for the values of the curvatures of the inner spheres and the effective cosmological constant  $\lambda$  of the cosmological part. In the presence of a magnetic monopole, the magnetic flux in each sphere, which is quantized by a Dirac condition, stabilizes the configuration which spontaneously would decompactify. The cosmological constant  $\Lambda$  helps to evade the Maldacena-Nuñez no-go theorem in this case [57, 27]. The different combinations of the flux quanta stored in the spheres give rise to a complicated landscape, in which each configuration of integers (called a *node*) can host a true stable state of the model, two stable states, an unstable state and a stable one, or no state, giving rise to two branches of (AdS and dS) states. It is found that for  $J > 1$  an infinite family of stable AdS states exist, but stable dS states exist only near the *branching surface*, which is the locus at which both branches meet, that is, the null- $\lambda$  surface. The structure of the null- $\lambda$  surface gives rise to the state chains, which provide a different source of low-lying states besides the randomly close states which help to solve the cosmological constant problem in

the Bousso-Polchinski landscape. State chains also help in counting states approximately, and they translate in peaks in the density of states  $\omega(\lambda)$ , providing anthropic states for moderately large values of  $J$ .

All the previous features of the model are qualitatively different from its counterparts in the Bousso-Polchinski landscape. We think that in a completed BP model, all these differences would render a very different picture with respect to the number of states, probabilities and anthropic reasoning. Thus, despite not being a realistic landscape model, the multi-sphere Einstein-Maxwell model has very appealing features that might propagate in more realistic models of the true string theory landscape.

The account of the multi-sphere Einstein-Maxwell model given in this paper has three main limitations: firstly, it is difficult to extrapolate the stability conditions found from 1+1 spacetime dimensions to a more realistic 3+1 cosmology. Secondly, we have considered a restricted class of linear perturbations; the inclusion of fully general linear perturbations could render unstable some states which are stable. The combination of the two ingredients, that is, 3+1 cosmology and a full set of linear perturbations, can lead to a qualitatively very different sector of the Einstein-Maxwell landscape. Finally, a fundamental missing piece is the cosmological measure. This problem and the construction of the corresponding model will be addressed in future papers.

## Acknowledgments

We would like to thank Concha Orna for carefully reading this manuscript, and the Pedro Pascual Benasque Center of Science. We also thank Frederik Denef, Roberto Emparan, Jaume Garriga, Bert Janssen, Donald Marolf and Jorge Zanelli for useful discussions and encouragement. This work has been supported by CICYT (grant FPA-2009-09638) and DGIID-DGA (grant 2011-E24/2). We thank also the support by grant A9335/10 (Física de alta energía: Partículas, cuerdas y cosmología).

## A Effect of derivative couplings in the multi-radion evolution equations

In this appendix we give a heuristic argument leading to the conclusion that the linear stability analysis of the multi-radion field evolution equations, equation (85), which is achieved by neglecting the derivative couplings, can be promoted to a non-linear stability analysis in which the linear stability is preserved as long as perturbation amplitudes are sufficiently small.

To begin with, we consider again equation (85):

$$-e^{-2\phi}\eta^{\alpha\beta}\left[(\xi_j)_{\alpha\beta} + 2(\xi_j)_\alpha\left(\sum_k(\xi_k)_\beta\right) - \sum_k(\xi_k)_\alpha(\xi_k)_\beta\right] = \lambda - e^{-2\sum_k\xi_k}U'_j(\xi_j). \quad (173)$$

The derivative couplings appear in a quadratic form. We will use the symbol  $\boldsymbol{\xi}$  to denote the  $J$ -component column vector of the perturbations  $\xi_j$ , and then we will write the derivative couplings in matrix form as

$$-e^{-2\phi}\eta^{\alpha\beta}\left[(\xi_j)_{\alpha\beta} + \langle \boldsymbol{\xi}_\alpha, M_j \boldsymbol{\xi}_\beta \rangle\right] = \lambda - e^{-2\sum_k \xi_k} U'_j(\xi_j), \quad (174)$$

where the constant  $J \times J$  matrix  $M_j$  has the number  $-1$  along the diagonal except for  $1$  along the  $j^{\text{th}}$  row and  $j^{\text{th}}$  column and zeroes elsewhere:

$$M_j = \begin{pmatrix} -1 & \cdots & 0 & 1 & 0 & \cdots & 0 \\ \vdots & \ddots & & \vdots & \vdots & & \vdots \\ 0 & \cdots & -1 & 1 & 0 & \cdots & 0 \\ 1 & \cdots & 1 & 1 & 1 & \cdots & 1 \\ 0 & \cdots & 0 & 1 & -1 & \cdots & 0 \\ \vdots & & & \vdots & \vdots & \ddots & \vdots \\ 0 & \cdots & 0 & 1 & 0 & \cdots & -1 \end{pmatrix} \text{ (} j^{\text{th}} \text{ row)}. \quad (175)$$

The matrix  $M_j$  has a spectrum with two simple eigenvalues  $\pm\sqrt{J}$  and a  $(J-2)$ -degenerate  $-1$  eigenvalue. It is therefore an ‘‘almost negative-definite’’ quadratic form, which represents a non-linear force.

We are interested in the effect of the derivative couplings; therefore, we approximate the system of equations by Taylor-expanding to first order the right-hand side of equation (174), thus considering the much simpler system (written in matrix form)

$$-e^{-2\phi}\eta^{\alpha\beta}\left[(\xi_j)_{\alpha\beta} + \langle \boldsymbol{\xi}_\alpha, M_j \boldsymbol{\xi}_\beta \rangle\right] = -\sum_k H_{jk}\xi_k, \quad (176)$$

where the frequency matrix  $H$  is given by equation (88) in section 3.2.

As said above, a complete analysis of the system (176) is not possible, but we can form a single equation out of it by projecting the system of equations along a constant direction  $\mathbf{w} = (w_j)$ :

$$-e^{-2\phi}\eta^{\alpha\beta}\left[\langle \mathbf{w}, \boldsymbol{\xi} \rangle_{\alpha\beta} + \langle \boldsymbol{\xi}_\alpha, M_{\mathbf{w}} \boldsymbol{\xi}_\beta \rangle\right] = -\langle \mathbf{w}, H \boldsymbol{\xi} \rangle. \quad (177)$$

The matrix  $M_{\mathbf{w}}$  is

$$M_{\mathbf{w}} = \langle \mathbf{w}, \mathbf{M} \rangle = \sum_j w_j M_j. \quad (178)$$

Any solution of the system (176) is a solution of equation (177), but the reciprocal is false. Nevertheless, we can look for normal modes of the form  $\boldsymbol{\xi}(t, x) = \chi(t, x)\mathbf{v}$  for constant  $\mathbf{v}$  and a single scalar function  $\chi(t, x)$ :

$$-e^{-2\phi}\eta^{\alpha\beta}\left[\langle \mathbf{w}, \mathbf{v} \rangle_{\alpha\beta} + \langle \mathbf{v}, M_{\mathbf{w}} \mathbf{v} \rangle_{\alpha\beta}\right] = -\langle \mathbf{w}, H \mathbf{v} \rangle \chi. \quad (179)$$

Taking  $\chi = \chi(t)$  and  $\mathbf{w} = \mathbf{v}$  for simplicity, we obtain

$$e^{-2\phi} \left[ \ddot{\chi} + \frac{\langle \mathbf{v}, M_{\mathbf{v}} \mathbf{v} \rangle}{\langle \mathbf{v}, \mathbf{v} \rangle} \dot{\chi}^2 \right] = -\frac{\langle \mathbf{v}, H \mathbf{v} \rangle}{\langle \mathbf{v}, \mathbf{v} \rangle} \chi. \quad (180)$$

If the non-linear term were absent, we would have a simple oscillator equation with a frequency given by the Rayleigh quotient of the matrix  $H$ . The solution of this equation would be a solution of the linear system if  $\mathbf{v}$  were chosen as an eigenmode of  $H$ . In this sense, the projected equation (180) is an *average* equation, and its solution (a *weak* solution henceforth) can indicate the behavior of the true solutions we are inspecting. Of course, this is a heuristic argument, but we can argue that true solutions provide weak solutions; thus, an unstable true solution should be reflected by an unstable weak solution. This argument has the obstacle of the existence of the normal modes we are using as ansatz; thus, as long as the normal modes constitute a reasonable description of the system (179), the projected equation will reflect accurately the character of its non-linear counterpart.

Nevertheless, we can use the projected equation (180) to see if the presence of the non-linear term can render unstable a linearly stable solution.

We will rewrite equation (180) as

$$\ddot{\chi} + m\dot{\chi}^2 = -h\chi, \quad \text{with } m = \frac{\langle \mathbf{v}, M_{\mathbf{v}} \mathbf{v} \rangle}{\langle \mathbf{v}, \mathbf{v} \rangle}, \quad \text{and } h = e^{2\phi} \frac{\langle \mathbf{v}, H \mathbf{v} \rangle}{\langle \mathbf{v}, \mathbf{v} \rangle}. \quad (181)$$

The parameter  $m$  depends on the projection direction  $\mathbf{v}$  but not on time. In contrast,  $h$  depends also on time by the presence of the  $e^{2\phi}$  factor. We will now discuss the expected domain of both parameters in the following.

- The parameter  $m$  is the Rayleigh quotient of the matrix  $M_{\mathbf{v}}$  on the projection direction  $\mathbf{v}$ . The eigenvalues of  $M_{\mathbf{v}}$  are  $\pm\sqrt{J}\sqrt{\sum_j v_j^2}$ , both of them nondegenerate, and  $-\sum_j v_j$  with  $J-2$  degeneracy. Thus, depending on the projection direction  $\mathbf{v}$ ,  $m$  can have both signs. If  $\mathbf{v}$  is taken to have unit norm, then  $m$  will be some value in the interval  $[-\sqrt{J}, \sqrt{J}]$ .
- The 1+1 cosmological solution  $\phi(t)$  has a characteristic evolution time  $t_\phi = \frac{1}{\sqrt{|\lambda|}}$ . On the other hand, the longest characteristic evolution time of the oscillator term is  $t_H = \frac{1}{\sqrt{\kappa}}$ , where  $\kappa$  is the minimum eigenvalue of the frequency matrix  $H$ . Of course, we are considering a linearly stable equation, so that  $\kappa > 0$ . We can consider  $\phi$  as slowly-varying if its characteristic time is much greater than the oscillator characteristic time:

$$t_\phi \gg t_H \quad \Rightarrow \quad \lambda \ll \kappa \quad (182)$$

Thus, for times  $t \approx t_H$ , we may consider  $\phi$  as constant, and thus  $h$  will be a positive number.

Equation (181) is integrable. We can show the form of its trajectories by writing  $\dot{\chi} = \gamma$ :

$$\left. \begin{array}{l} \dot{\chi} = \gamma \\ \dot{\gamma} = -m\gamma^2 - h\chi \end{array} \right\} \Rightarrow \frac{d\gamma}{d\chi} = -m\gamma - h\frac{\chi}{\gamma}. \quad (183)$$



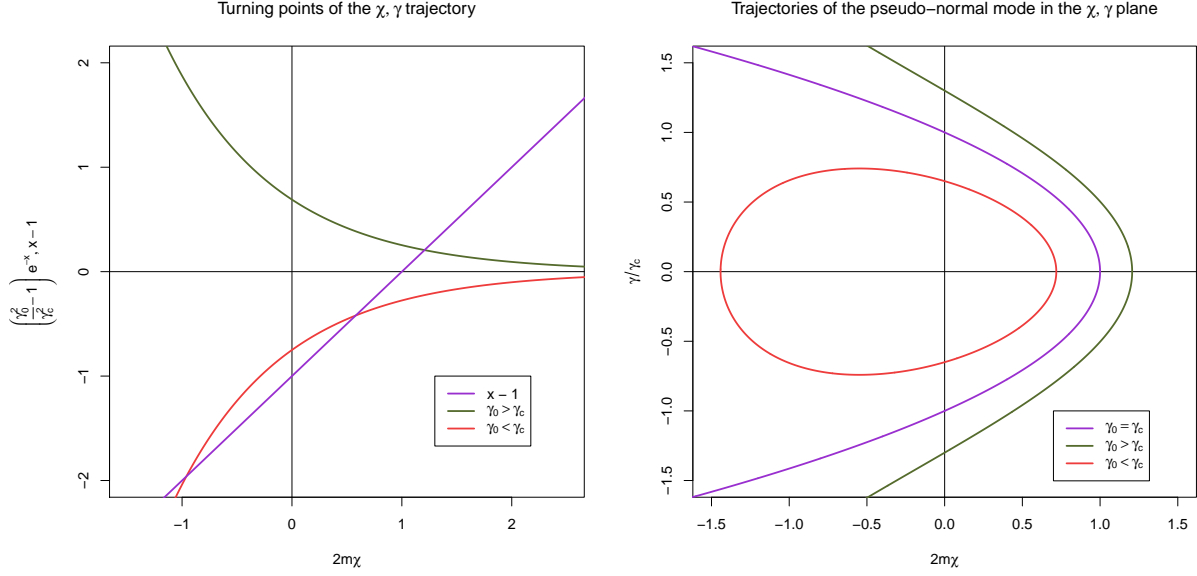


Figure 15: Turning points (left) and actual trajectories (right) of the normal modes of the projected multi-radion evolution equation.

The last equation has the exact solution

$$\gamma(\chi)^2 = \left( \gamma_0^2 - \frac{h}{2m^2} \right) e^{-2m\chi} + \frac{h}{m} \left( \frac{1}{2m} - \chi \right). \quad (184)$$

In the previous equation,  $\gamma_0 = \gamma(0)$ . Specializing  $m = 0$  (which removes the nonlinear term) we obtain the oscillator trajectory  $\gamma^2 + h\chi^2 = \gamma_0^2$ . The points where  $\gamma = 0$  are called *turning points* of the trajectory, and they mark its domain because of the square in (184). The trajectory has one or two turning points given by the equation

$$\left( \gamma_0^2 - \frac{h}{2m^2} \right) e^{-2m\chi} = \frac{h}{m} \left( \chi - \frac{1}{2m} \right) \quad (185)$$

If  $m$  is a fixed positive value, then the previous equation has a single solution if  $\gamma_0^2 - \frac{h}{2m^2} > 0$  but it has two solutions if  $\gamma_0^2 - \frac{h}{2m^2} < 0$ . A single turning point describes an open trajectory, while two turning points describe a closed one, see figure 15. Thus, the oscillator trajectory remains closed when we turn on the non-linearity if

$$\gamma_0^2 < \frac{h}{2m^2} \quad (186)$$

Therefore, a linearly stable trajectory remains non-linearly stable if the amplitude  $\gamma_0$  does not exceed the critical value  $\gamma_c^2 = \frac{h}{2m^2}$ . Beyond this value, the trajectory is open and therefore the linearly stable solution becomes non-linearly unstable.

The lowest value of the critical amplitude is reached when  $m$  is largest; for a unit-norm projection direction, the largest value of  $m$  is  $\sqrt{J}$ , as discussed above. Thus, the lowest

value of the critical amplitude is

$$\gamma_{c,\min}^2 = \frac{e^{2\phi} \kappa}{2J}. \quad (187)$$

As long as amplitudes are smaller than this value, the non-linear derivative couplings cannot spoil linear stability. Nevertheless, when  $\kappa$  is small, perturbations have a chance of trigger a non-linear instability and destabilize a linearly stable state.

Summarizing, the non-linear terms in the multi-radion evolution equations respect the linear stability criterion except in the regime of large amplitudes, which is most easily accessible when the minimum eigenvalue of the frequency matrix becomes small, that is, in the onset of instability.

## References

- [1] R. Bousso and J. Polchinski: *Quantization of four-form fluxes and dynamical neutralization of the cosmological constant*. JHEP **06**: 006 (2000), [arXiv:hep-th/0004134](#)
- [2] L. Susskind: *The Anthropic Landscape of String Theory*. [arXiv:hep-th/0302219](#)
- [3] T. Banks, M. Dine and E. Gorbatov: *Is There A String Theory Landscape?* JHEP **0408:058,2004**. [arXiv:hep-th/0309170](#)
- [4] J. Garriga, D. Schwartz-Perlov, A. Vilenkin and S. Winitzki: *Probabilities in the inflationary multiverse*. JCAP **0601** (2006) 017 [arXiv:hep-th/0509184](#)
- [5] A. H. Guth: *The Inflationary Universe: A Possible Solution to the Horizon and Flatness Problems*. Phys. Rev. D **23**: 347-356 (1981).
- [6] A. D. Linde: *A New Inflationary Universe Scenario: A Possible Solution of the Horizon, Flatness, Homogeneity, Isotropy and Primordial Monopole Problems*. Phys. Lett. B **108**: 389-393 (1982).
- [7] A. D. Linde: *Chaotic Inflation*. Phys. Lett. B **129**: 177-181 (1983).
- [8] A. D. Linde: *Eternal Chaotic Inflation*. Mod. Phys. Lett. A **1**: 81 (1986).
- [9] A. H. Guth: *Inflation and Eternal Inflation*. Phys. Rept. **333**: 555-574 (2000). [arXiv:astro-ph/0002156](#)
- [10] S. Weinberg: *The cosmological constant problem*. Rev. Mod. Phys. **61**, 1-23 (1989).
- [11] R. Bousso: *TASI Lectures on the Cosmological Constant*. Gen. Rel. Grav. **40**: 607 (2008). [arXiv:0708.4231 \[hep-th\]](#)
- [12] D. J. Shaw and J. D. Barrow: *A Testable Solution of the Cosmological Constant and Coincidence Problems*. Phys.Rev.D**83:043518,2011**. [arXiv:1010.4262 \[gr-qc\]](#)

- [13] R. Bousso, B. Freivogel, S. Leichenauer and V. Rosenhaus: *A geometric solution to the coincidence problem, and the size of the landscape as the origin of hierarchy*. Phys.Rev.Lett.106:101301,2011. arXiv:1011.0714 [hep-th]
- [14] S. Ashok and M. R. Douglas: *Counting flux vacua*. JHEP **0401**: 060 (2004). arXiv:hep-th/0307049
- [15] M. R. Douglas: *Basic results in vacuum statistics*. Comptes Rendus Physique **5**: 965-977 (2004). arXiv:hep-th/0409207
- [16] M. R. Douglas: *The Statistics of string / M theory vacua*. JHEP **0305**: 046 (2003). arXiv:hep-th/0303194
- [17] R. Bousso: *Precision cosmology and the landscape*. arXiv:hep-th/0610211
- [18] A. Vilenkin: *A Measure of the multiverse*. J. Phys. A A **40** (2007) 6777 arXiv:hep-th/0609193
- [19] J. M. Maldacena: *The Large N limit of superconformal field theories and supergravity*. Adv. Theor. Math. Phys. **2** (1998) 231. arXiv:hep-th/9711200
- [20] J. Garriga and A. Vilenkin: *Holographic multiverse and conformal invariance*. JCAP **0911** (2009) 020 arXiv:0905.1509 [hep-th]
- [21] J. Maldacena: *Einstein Gravity from Conformal Gravity*. arXiv:1105.5632 [hep-th].
- [22] Supernova Cosmology Project (S. Perlmutter et al.): *Measurements of  $\Omega$  and  $\Lambda$  from 42 high redshift supernovae*. Astrophys. J. **517**: 565-586 (1999). arXiv:astro-ph/9812133
- [23] Supernova Search Team (Adam G. Riess et al.): *Observational evidence from supernovae for an accelerating universe and a cosmological constant*. Astron. J. **116**: 1009-1038 (1998). arXiv:astro-ph/9805201
- [24] J. D. Barrow and F. J. Tipler: *The Anthropic Cosmological Principle*. Oxford University Press (1986), sec. 6.9, 6.10.
- [25] S. Weinberg: *Anthropic Bound on the Cosmological Constant*. Phys. Rev. Lett. **59**, 2607-2610 (1987).
- [26] F. Denef, M. R. Douglas and S. Kachru: *Physics of String Flux Compactifications*. Ann. Rev. Nucl. Part. Sci. **57** (2007) 119. arXiv:hep-th/0701050
- [27] F. Denef: *Les Houches Lectures on Constructing String Vacua*. arXiv:0803.1194 [hep-th]

- [28] S. B. Giddings, S. Kachru and J. Polchinski: *Hierarchies from fluxes in string compactifications*. Phys. Rev. D **66**: 106006 (2002). [arXiv:hep-th/0105097](#)
- [29] S. Kachru, R. Kallosh, A. Linde and S. Trivedi: *de Sitter vacua in string theory*. Phys. Rev. D **68**: 046005 (2003). [arXiv:hep-th/0301240](#)
- [30] S. Kachru, R. Kallosh, A. Linde, J. Maldacena, L. McAllister and S. Trivedi: *Towards inflation in string theory*. JCAP **0310**: 013 (2006). [arXiv:hep-th/0308055](#)
- [31] A. R. Frey, M. Lippert and B. Williams, *The Fall of stringy de Sitter*, Phys. Rev. D **68** (2003) 046008 [[hep-th/0305018](#)].
- [32] C. Asensio and A. Segui: *Applications of an exact counting formula in the Bousso-Polchinski Landscape*. Phys.Rev.D82:123532,2010. [arXiv:1003.6011](#) [[hep-th](#)]
- [33] P. G. O. Freund and M. A. Rubin: *Dynamics of Dimensional Reduction*. Phys. Lett. B **97** (1980) 233.
- [34] S. Randjbar-Daemi, A. Salam and J. A. Strathdee: *Spontaneous Compactification in Six-Dimensional Einstein-Maxwell Theory*. Nucl. Phys. B **214** (1983) 491.
- [35] M. R. Douglas and S. Kachru: *Flux compactifications*. Rev. Mod. Phys. **79**: 733-796 (2007). [arXiv:hep-th/0610102](#)
- [36] J. J. Blanco-Pillado, D. Schwartz-Perlov and A. Vilenkin: *Quantum tunneling in flux compactifications*. JCAP **0912**: 006 (2009). [arXiv:0904.3106](#) [[hep-th](#)]
- [37] M. J. Duff, B. E. W. Nilsson and C. N. Pope: *The Criterion For Vacuum Stability In Kaluza-klein Supergravity*, Phys. Lett. B **139** (1984) 154.
- [38] M. Berkooz and S. -J. Rey: *Nonsupersymmetric stable vacua of M theory*, JHEP **9901**, 014 (1999) [Phys. Lett. B **449**, 68 (1999)] [[hep-th/9807200](#)].
- [39] O. DeWolfe, D. Z. Freedman, S. S. Gubser, G. T. Horowitz and I. Mitra: *Stability of AdS(p) x M(q) compactifications without supersymmetry*, Phys. Rev. D **65**, 064033 (2002) [[hep-th/0105047](#)].
- [40] R. Kantowski and R. K. Sachs: *Some Spatially Homogeneous Anisotropic Relativistic Cosmological Models* . J. Math. Phys. **7** (3), 443 (1966).
- [41] A. Linde: *Inflation and quantum cosmology*, p. 624 in *300 years of gravitation*, S. W. Hawking and W. Israel (eds.), CUP, ISBN 0 521 34312 7.
- [42] S. M. Carroll, M. C. Johnson and L. Randall: *Dynamical compactification from de Sitter space*. JHEP **0911** (2009) 094, [arXiv:0904.3115](#) [[hep-th](#)]
- [43] P. K. Townsend and M. N. R. Wohlfarth: *Accelerating cosmologies from compactification*. Phys. Rev. Lett. **91** (2003) 061302, [arXiv:hep-th/0303097](#)

- [44] R. Emparan and J. Garriga: *A Note on accelerating cosmologies from compactifications and S branes*. JHEP **0305** (2003) 028, [arXiv:hep-th/0304124](#)
- [45] N. Ohta: *Accelerating cosmologies from S-branes*. Phys. Rev. Lett. **91** (2003) 061303, [arXiv:hep-th/0303238](#)
- [46] N. Ohta: *A Study of accelerating cosmologies from superstring / M theories*. Prog. Theor. Phys. **110** (2003) 269, [arXiv:hep-th/0304172](#)
- [47] C. -M. Chen, P. -M. Ho, I. P. Neupane, N. Ohta and J. E. Wang: *Hyperbolic space cosmologies*. JHEP **0310** (2003) 058, [arXiv:hep-th/0306291](#)
- [48] C. -M. Chen, P. -M. Ho, I. P. Neupane, N. Ohta and J. E. Wang: *Addendum to 'Hyperbolic space cosmologies'*. JHEP **0611** (2006) 044, [arXiv:hep-th/0609043](#)
- [49] R Development Core Team: *R: A language and environment for statistical computing*. R Foundation for Statistical Computing, Vienna, Austria. ISBN 3-900051-07-0 (2007). <http://www.R-project.org>
- [50] C. Asensio and A. Segui: *A geometric-probabilistic method for counting low-lying states in the Bousso-Polchinski Landscape*. Phys. Rev. D **80**: 043515 (2009). [arXiv:0812.3247 \[hep-th\]](#)
- [51] C. Asensio and A. Segui: *Counting states in the Bousso-Polchinski Landscape*, 99-110 in M. Asorey, J. V. García Esteve, M. F. Rañada and J. Sesma (Editors): *Mathematical Physics and Field Theory – Julio Abad, in Memoriam*, Prentas Universitarias de Zaragoza, ISBN 978-84-92774-04-3 (2009). [arXiv:0903.1947 \[hep-th\]](#)
- [52] J. D. Brown and C. Teitelboim: *Dynamical neutralization of the cosmological constant*. Phys. Lett. **B195**, 177 (1987).
- [53] J. D. Brown and C. Teitelboim: *Neutralization of the cosmological constant by membrane creation*. Nucl. Phys. **B297**, 787-836 (1988).
- [54] R. Bousso and I. Yang: *Landscape predictions from cosmological vacuum selection*. Phys. Rev. D **75**: 123520 (2007). [arXiv:hep-th/0703206](#)
- [55] D. Schwartz-Perlov and A. Vilenkin: *Probabilities in the Bousso-Polchinski multiverse*. JCAP **0606**: 010 (2006). [arXiv:hep-th/0601162](#)
- [56] J. P. Conlon, R. Kallosh, A. D. Linde and F. Quevedo: *Volume Modulus Inflation and the Gravitino Mass Problem*, JCAP **0809** (2008) 011 [[arXiv:0806.0809 \[hep-th\]](#)].
- [57] J. M. Maldacena and C. Nuñez: *Supergravity description of field theories on curved manifolds and a no go theorem*. Int. J. Mod. Phys. A **16** (2001) 822. [arXiv:hep-th/0007018](#)